JOURNAL OF CAVE AND KARST STUDIES

June 2018
Volume 80, Number 2
ISSN 1090-6924
A Publication of the National Speleological Society

DEDICATED TO THE ADVANCEMENT OF SCIENCE, EDUCATION, EXPLORATION, AND CONSERVATION

Published By
The National Speleological Society

http://caves.org/pub/journal

Office
6001 Pulaski Pike NW
Huntsville, AL 35810 USA
Tel:256-852-1300
nss@caves.org

The *Journal of Cave and Karst Studies* , ISSN 1090-6924, CPM Number #40065056, is a multi-disciplinary, refereed journal published four times a year by the National Speleological Society. The *Journal* is available by open access on its website, or check the website for current print subscription rates. Back issues are available from the NSS office.

POSTMASTER: send address changes to the National Speleological Society Office listed above.

The Journal of Cave and Karst Studies is covered by the following ISI Thomson Services Science Citation Index Expanded, ISI Alerting Services, and Current Contents/Physical, Chemical, and Earth Sciences.

Front cover: Cave entrance in weathered shale, Wyoming. See article by Medville in this issue.

A. Queffelec, P.I Bertran, T. Bos, and L. Lemée. Mineralogical and organic study of bat and chough guano: implications for guano identification in ancient context. *Journal of Cave and Karst Studies*, v. 80, no. 2, p. 1-17. DOI: 10.4311/2017ES0102

MINERALOGICAL AND ORGANIC STUDY OF BAT AND CHOUGH GUANO: IMPLICATIONS FOR GUANO IDENTIFICATION IN ANCIENT CONTEXT

Alain Queffelec[1,C], Pascal Bertran[1,2], Teddy Bos[3], and Laurent Lemée[4]

Abstract

The mineralogical and geochemical evolution of cave guano deposits in France has been investigated in detail. Two test pits were excavated in guano mounds from insectivorous bats and one in a guano mound from omnivorous choughs. Both bats and choughs are thought to be among the main accumulators of guano during the Pleistocene in southwest France. Thin section analysis, mineralogical identification and quantification, geochemical analysis, organic matter characterization through pyrolysis and thermochemolysis coupled to gas-chromatography**,** were conducted to better understand the evolution of guano in caves and to identify the underlying factors. Bat guano undergoes mineralization through loss of organic matter and precipitation of phosphate and sulfate minerals. The neoformed minerals include gypsum, ardealite, brushite, francoanellite, hydroxylapatite, monetite, newberyite, and taranakite, and vary according to the local availability of chemical elements released by the alteration of detrital minerals due to acidic solutions. Chough guano**,** located at higher altitude in a periglacial environment, does not show similar mineral formation. Organic geochemical analysis indicates strong differences between guano. Abundant hydrocarbons derived from insect cuticles were the dominant feature in bat guano, whereas a mostly vegetal origin typifies chough guano. Geochemical analysis points to an especially high content of copper and zinc in bat guanos, a few hundreds of µg/g and thousands of µg/g, respectively. Both organic matter analysis and geochemistry may help identification of bat guano in archeological contexts**,** where phosphate minerals can originate from multiple sources.

Introduction

Sediments in karstic caves often contain large amounts of phosphate minerals that have been exploited and used as fertilizer for centuries. Excrement (guano) from cave animals, especially bats, has long been designated as the primary source of phosphate accumulation in caves (Hutchinson, 1950; Hill and Forti, 1997). Detailed mineralogical inventories have been made and a large diversity of mineral species have been identified worldwide in caves (Bridge, 1973; Balenzano et al., 1976; Fiore and Laviano, 1991; Onac et al., 2001; Karkanas et al., 2002; Onac et al., 2005, 2009; Dumitraş et al., 2008; Puşcaş et al., 2014; Wurster et al., 2015). Some of these studies focused on Paleolithic sites from Western Europe and the Near East, where phosphates form diffuse concentrations in the sediments (such as macro or microscopic nodules), or occur as stratiform units of varying thickness and hardness. In contrast, only a few actualistic studies deal with guano alteration and the redistribution of alteration products within the sediment, which leads to the formation of authigenic minerals (Shahack-Gross et al., 2004; Wurster et al., 2015). A detailed understanding of these processes is, however, of paramount importance for the study of cave sites and for the evaluation of the alteration of archeological artifacts due to the percolation of phosphate and sulfate solutions. Phosphate dynamics may also impact the isotopic and palynological record preserved in guano-rich sediments used for paleoenvironmental studies (Mizutani et al., 1992; Carrión et al., 2006; Bird et al., 2007; Wurster et al., 2008; Geantă et al., 2012; Forray et al., 2015; Royer et al., 2017).

Insofar as bats are currently the main accumulators of phosphate in caves, and since their geographical distribution covers almost all terrestrial environments (Parker et al., 1997), this study focuses on the analysis of bat guano and its diagenesis in limestone context. A comparison is made with guano of choughs, which are another potential phosphate accumulator in caves. The analysis combines micromorphology, mineralogy and chemistry in an attempt to better understand the degradation of guano in caves located in southwest France, in a humid temperate climate (bat guano), or in a high-altitude periglacial area (chough guano). This multiproxy analysis allows us to propose new criteria from geochemistry and organic matter composition for the identification of bat guano origin of authigenic minerals in the fossil record, in addition to the sole mineralogy used so far.

Geological Setting of the Selected Sites

La Fage and Rancogne caves (Fig. 1) are both located at low altitude (300 and 88 m above sea level, respectively) in Mesozoic (Bajocian) oolitic limestones in the Aquitaine Basin, France (Lefavrais-Raymond et al., 1976; Le Pochat et al., 1986) (mean annual air temperature = 12 °C, mean annual precipitation ≈ 877 mm y^{-1}). La Fage Cave, which yielded

[1]Université de Bordeaux, PACEA–UMR CNRS 5199, avenue Geoffroy Saint-Hilaire, 33615 Pessac, France
[2]Inrap, 140 avenue du Maréchal Leclerc, 33130 Bègles, France
[3]Service Archéologique – Toulouse Métropole, 37 chemin Lapujade 31200 Toulouse, France
[4]Université de Poitiers, IC2MP - UMR CNRS 7285, Poitiers, France
[C]Corresponding Author: alain.queffelec@bordeaux.fr

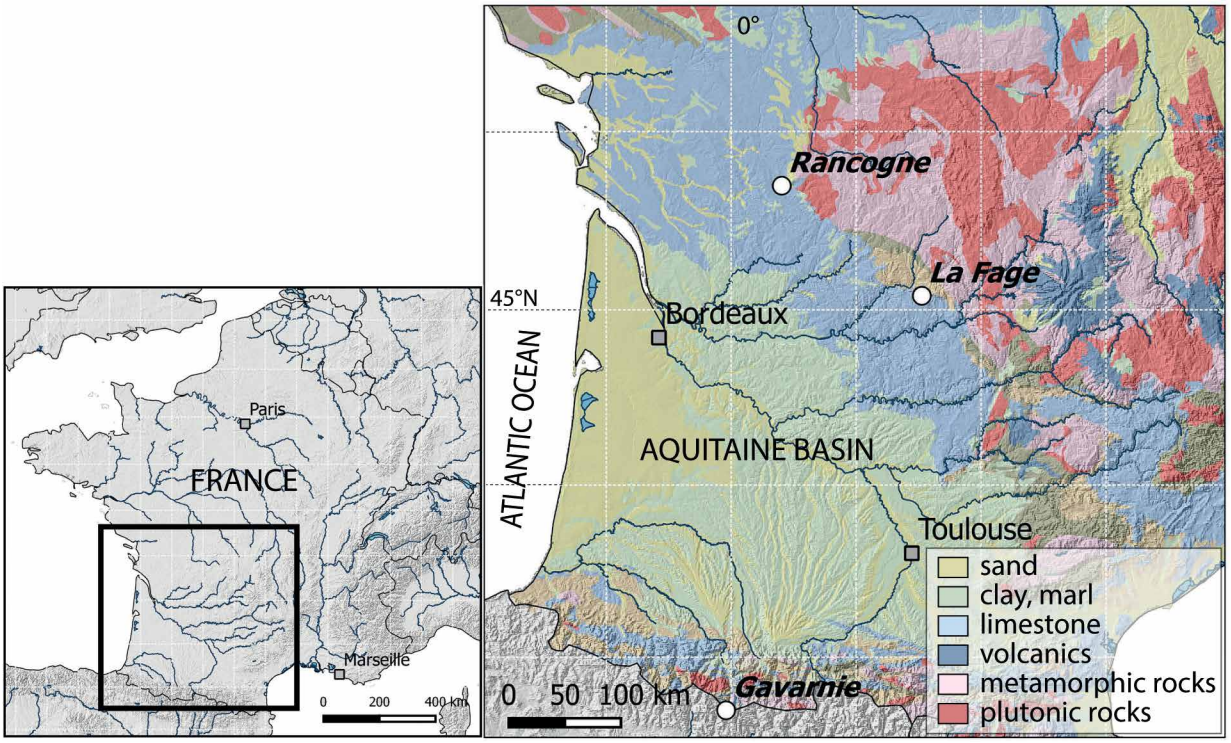

Figure 1. Location of the studied sites.

Middle Pleistocene paleontological remains (Beaulieu et al., 1973), presently shelters a large and multispecies colony of bats. The studied cross section, located ca. 100 m from the entrance, was dug to the limestone substrate in a still active, 70 cm thick guano mound (Fig. 2a). In Rancogne Cave, the sampled test pit was also made in an active guano mound (Fig. 2b). Sedimentation in this site is still influenced by the floods of the Tardoire River, as testified by blankets of alluvial silt in the karst conduit and input of detrital sediment in the guano piles. However, these floods are not strong enough or frequent enough to destroy the guano mounds. Intense biological activity took place at the surface of the mound, which was covered by larvae of dung-feeding insects. Bats from both caves are insectivorous species, mostly *Minopterus schreibersii*.

Gavarnie Cave is located in the central Pyrenees (Fig. 1), approximately 2900 m above sea level, and opens in a wall of dolomitized limestone (mean annual air temperature = 0 °C, mean annual precipitation ≈ 1800 mm y^{-1}). Chough (*Pyrrhocorax graculus*) is a small, social corvid currently found only in mountainous areas, but which was present at much lower altitude during the Pleistocene (Laroulandie, 2004). Its diet consists mainly of insects (Coleoptera, Ortho-

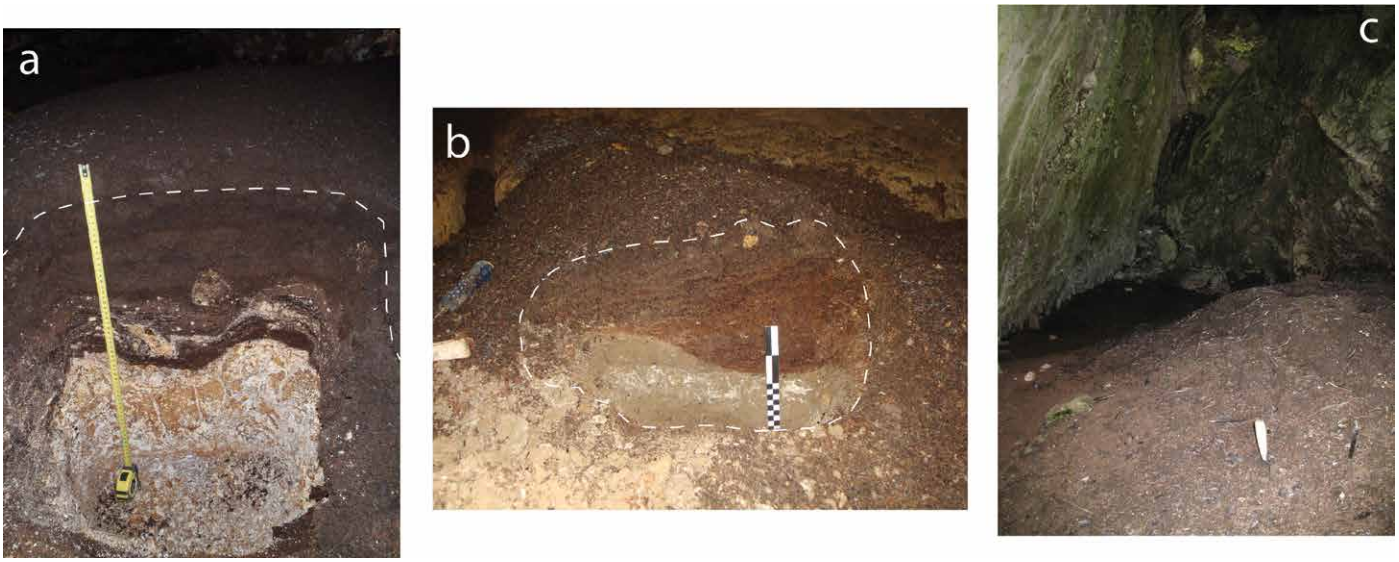

Figure 2. Three guano mounds: (a) La Fage Cave (bat guano), scale is 60 cm long; (b) Rancogne Cave (bat guano), scale bar is 20 cm long; (c) Gavarnie Cave (chough guano); trowel is 20 cm long. The top of the pit is indicated by the dashed line.

ptera and Diptera) and berries (Dendaletche, 1997; Géroudet, 2010). The guano accumulation, 1.5 m thick, is located a dozen meters from the cave entrance, and guano is mainly composed of vegetal debris and feather remains (Fig. 2c). Except in the upper 30 cm of the mound, abundant lenses of segregation ice were observed within the organic accumulation. Since the field observations were made in September, at the end of the summer, ice obviously indicates that the mound remained perennially frozen. A cold trap-like behavior of the cave, due to its descending configuration (cold heavy air rapidly enters the cave in winter, in contrast to warm air in summer), is thought to be responsible for this micro-environment.

Methods

Sections were cleaned and described in detail. Blocks of undisturbed sediment were sampled for micromorphological study. The thin sections (up to 7 × 13 cm) were prepared after drying and impregnation of the samples with a polyester resin, following Guilloré's method (1980). Observation was conducted with a Leica DM2500P petrographic microscope and the LAS V4 software.

The mineralogical composition of the sediment was studied by X-ray diffraction on ground samples in a silicon, calibrated PANalytical X'Pert diffractometer, using the Kα 1 of a copper anticathode operated at 40 kV and 40 mA. Thirty minutes of measurement for each sample allowed for the spectra to be collected from 8° to 80° (2 theta) with a resolution of 0.02°. Mineralogical identification was made by comparison with the JCPDS-ICDD database using the DIFFRACPLUS Eva software. The TOPAS software, based on Rietveld's (Rietveld, 1969) method, allowed quantification of the different mineral phases. Quantification was performed only on samples containing low amounts of short-range ordered material and only for crystalline phases.

The pH was measured following Baize's (Baize, 2000) method on a suspension of 2 g of sediment in 10 g of water, using a pH-meter, calibrated with buffer solutions at pH 4 and pH 7.

The Total Organic Carbon (TOC) and sulfur (S) content was measured by pyrolysis (1500 °C) coupled with infrared spectrometry using a Leco CS-125 analyzer, after hydrochloric acid treatment to remove the carbonates. In addition, the organic matter content was obtained from the dried sample by calcination at 650 °C for 4 h. The Loss-On-Ignition (LOI) is the loss of sample mass during the process.

Semi-quantitative, geochemical analysis was made by Energy Dispersive X-Ray Fluorescence (ED-XRF) and compared with the XRD results. The lack of specific calibration of the machine for this kind of organic-, sulfur- and/or phosphate-rich samples did not allow a fully quantitative approach. Therefore, the values must be taken as approximate and were complemented by the observation of spectra. The analyses were performed in 60 seconds on powdered samples with a Spectro X-SORT instrument, equipped with a tungsten (W) X-ray tube, run at 40 kV and 0.01 mA.

The organic matter was characterized at the molecular scale using on-line pyrolysis and thermochemolysis. The crushed sample was placed in a stainless-steel cup. Pyrolysis took place at 600 °C for one minute in a Frontier Lab (EGA PY 3030D) pyrolyzer equipped with an AS-1020E auto sampler and directly coupled to a quadrupolar Shimadzu QP2010 Ultra GC/MS. The pyrolysis products were sent directly to the GC/MS in a stream of helium. Direct coupling prevents the loss of volatile compounds or the possible degradation of the pyrolysis products. The GC separations were conducted in a fused silica, capillary column (BPX 5 (SGE), 5% Phenyl siloxane, 30 m length, 0.25 mm i.d. (0.25 µm film thickness), and helium 5.5 (Messer), 99,9995% purity as carrier gas. The injector was set to 250 °C with a split of 100/1. The column temperature was programmed from 60 °C to 300 °C at 5 °C min^{-1} and held at 300 °C for 15 min. The ionization was produced by electron impact (70 eV), the data were recorded in full scan mode, the source temperature was 220 °C, and the transfer line was set to 280 °C. The pyrolysis or thermochemolysis products were identified on the basis of their GC retention times, and by comparison of their mass spectra with analytical standards (phenol and toluene from Sigma-Aldrich; aliphatic hydrocarbon kit, fatty acid methyl esters standards and bacterial fatty acids from Supelco) and library data (NIST). Thermochemolysis was done using tetramethyl ammonium hydroxide (TMAH) as alkylating agent. 0.5 mg of sample was mixed with 5 µL of TMAH methanolic solution 50/50 (v/v) in methanol and then placed in an inox cup in the sampler. The analysis was then conducted as for pyrolysis.

Results

Stratigraphy and Mineralogy

La Fage Cave

Four stratigraphic units were distinguished above the oolitic limestone. These are, from top to bottom (Fig. 3):

1. Unit 1 – Crudely bedded, brownish black (7,5YR 2/2), 20 cm thick, recent guano. It is characterized in thin section by tangled, organic debris (Fig. 4a), among which some insect fragments can be identified. Clay nodules and quartz grains indicate weak, detrital inputs during guano deposition. Despite its young age, this level contains a limestone fragment partially replaced by hydroxylapatite (Fig. 4b). Small radial aggregates of needle-shaped crystals are visible (Figs. 4c and 4d), and may correspond to the newberyite identified by X-ray

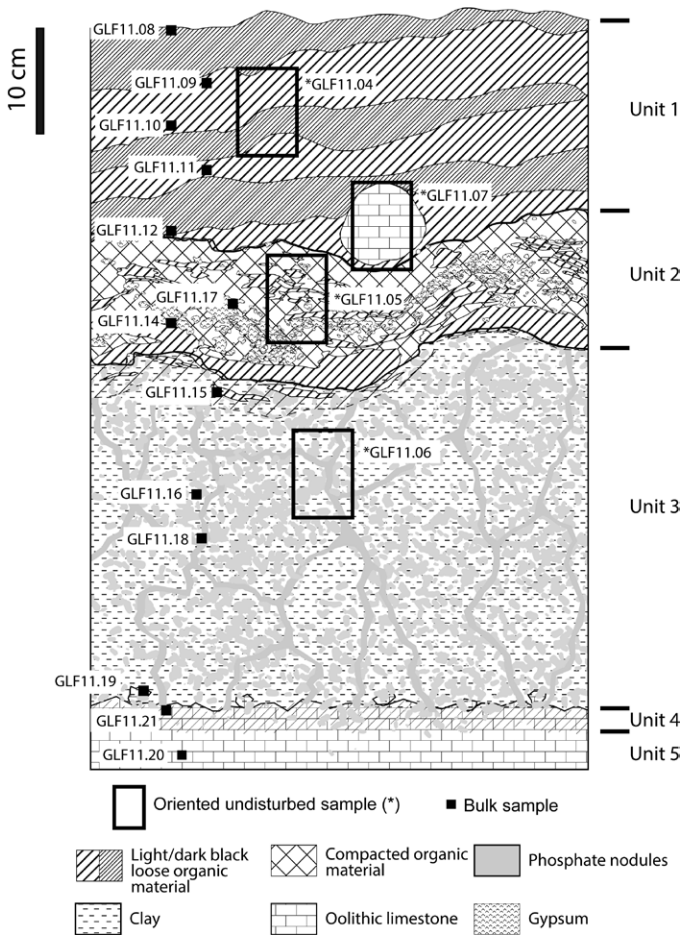

Figure 3. Stratigraphy of the guano mound in La Fage Cave and sample locations.

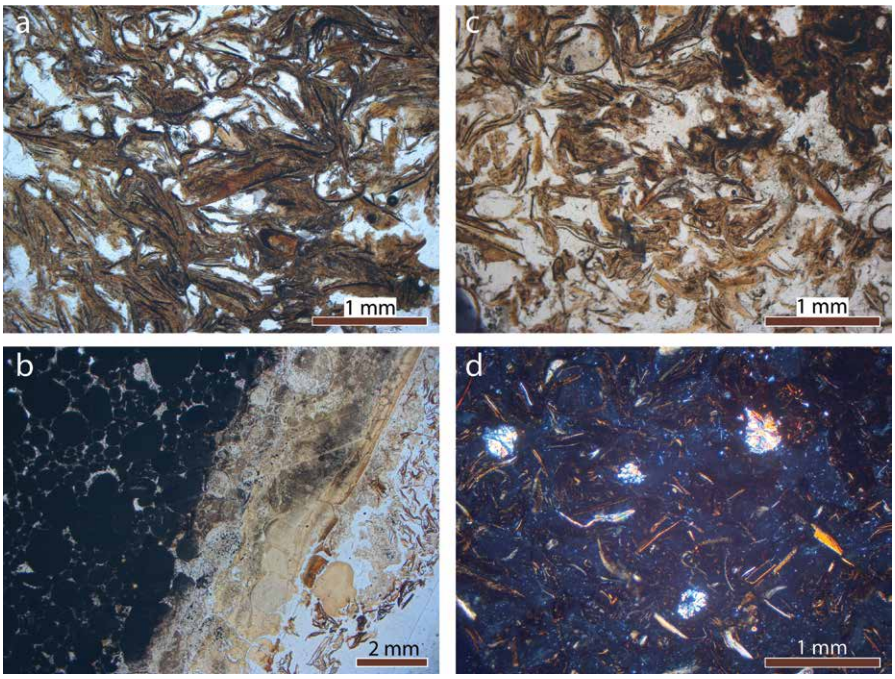

Figure 4. Microphotographs of La Fage Cave unit 1 **:** (a) Tangled organic debris, mainly insect fragments PPL; (b) Oolitic limestone (left) fragment partially pseudomorphosed by hydroxylapatite (right), PPL; (c) Phosphate spherulites scattered in organic debris, PPL; (d) Idem, XPL.

diffraction (Fig. 6a and Table 1). The dominant mineral in this unit is brushite, even if the highly amorphous, organic content of the sample (Table 2) prevented us from satisfying Rietveld quantification. The low mineral content makes it difficult to measure the major light elements such as silicon (Si) or phosphorus (P), but potassium (K) (and rubidium (Rb) as a substitute) from feldspar or clay is detected, as is iron (Fe) (Table 3). The main trace elements are copper (Cu) and zinc (Zn), with exceptionally high concentrations, several hundreds and thousands of µg/g respectively.

2. Unit 2 – 10 cm thick, organic level with discontinuous horizontal bedding, indicated by alternating brownish black (10YR 2/2) and pale yellow (2,5Y 8/4), nodular soft beds. Thin section observation reveals that this level is composed of an organic matrix with some debris still recognizable (Fig. 6a) and authigenic minerals. The neoformed minerals are either microcrystalline phosphate grains forming homogeneous areas, or rhombic, larger crystals (Fig. 6b). Gypsum is the main mineralogical phase present in this level (Fig. 5b, Table 2), which is consistent with the high sulfur (S) content measured by combustion (Table 3). Higher guano mineralization, as indicated by the decrease in TOC, allows more elements to be identified by ED-XRF (Table 3). The contents in Cu and Zn remain markedly high.
3. Unit 3 – 30 cm thick, strong brown (7,5YR 5/8) massive clay. The desiccation cracks are filled with pale yellow (2,5Y 8/4) masses of authigenic minerals. Isolated nodules are also visible within the clay. In thin section, the fillings are formed by coalescent, microcrystalline phosphate nodules. X-ray diffraction allows identification of taranakite as the principal component (Fig. 5c and Table 2). Accordingly, geochemical data show high P and K contents. Trace elements typically associated with clay are also in higher amounts at the top part of the unit, where kaolinite is the most abundant mineral. Cu and Zn concentrations decrease in this unit.
4. Unit 4 – A yellow crust formed by pseudomorphic replacement of calcite by phosphate, developed at the top of the limestone. It preserved the limestone microstructure (as for the altered limestone fragment in Unit 1, Fig. 4b) and is mainly composed of hydroxylapatite and taranakite (Fig. 5d and Table 2). ED-XRF data show higher calcium (Ca, as a constituent of hydroxylapatite) content than in Unit 3. Cu and especially Zn are present in notably high proportions (Table 3) for this phosphate crust.

Table 1. List of the minerals identified by X-ray diffraction.

Group	Mineral	Abbr.a	Chemical formulae
Carbonates			
	Calcite	Cal	$CaCO_3$
Sulfates			
	Gypsum	Gp	$CaSO_4{\cdot}2H_2O$
Phosphates			
	Ardealite	Ar	$Ca_2(PO_3OH)(SO_4){\cdot}4H_2O$
	Brushite	B	$Ca(PO_3OH){\cdot}2H_2O$
	Francoanellite	F	$K_3Al_5(PO_4)_2(PO_3OH)_6{\cdot}12H_2O$
	Hydroxylapatite	H	$Ca_5(PO_4)_3(OH)$
	Monetite	M	$Ca(PO_3OH)$
	Newberyite	N	$Mg(PO_3OH){\cdot}3H_2O$
	Taranakite	T	$K_3Al_5(PO_3OH)_6(PO_4)_2{\cdot}18H_2O$
Silicates			
	Kaolinite	Kln	$Al_2Si_2O_5(OH)_4$
	K-Feldspar	KFs	$K(AlSi_3O_8)$
	Albite	Ab	$Na(AlSi_3O_8)$
	Montmorillonite	Mnt	$(Na,Ca)_{0.3}(Al,Mg)_2Si_4O_{10}(OH)_2{\cdot}n(H_2O)$
	Muscovite	Ms	$KAl_2(Si_3Al)O_{10}(OH)_2$
Oxides			
	Quartz	Qz	SiO_2

[a] Abbr. = Abbreviation

5. Unit 5 – The bedrock sampled just below the crust reveals that it has been altered by acidic percolations. Although mainly composed of calcite, gypsum occurs in significant amounts (Table 2) and the concentration of Cu and Zn remains high.

Units 1 to 4 are weakly calcareous, despite the geological environment, with pH ranging between 4.6 and 5.4 (Table 3).

Rancogne Cave

From top to bottom, the sequence comprises the following units (Fig. 7):

1. Unit 1 – 12 cm thick, brownish black (7,5YR 2.5/2) layer of fresh guano, showing alternating dark and light-colored beds. This unit is mainly composed of macro debris from insect cuticles. Small lenses of microcrystalline, pale-yellow phosphates are observed in thin section (Figs. 8a and 8b), and are composed of brushite and monetite (Fig. 9a). Some centimeter-thick phosphate nodules are also visible at the base of the unit, forming crude beds. The pH in this organic layer is remarkably low with values close to 4.0 (Table 3).
2. Unit 2 – Massive, dark brown (7.5YR 3/3) organic layer, mainly composed of compacted organic debris, as shown by the especially high TOC content (Table 3). Close

Table 2. Mineralogy of all bulk samples (see Table 1 for abbreviations).

				Phosphates										Clays				
Sample	Site	Unit	Depth	H	T	Ar	F	B	N	M	Gp	Cal	Qz	Mnt	Kln	Ms	KFs	Ab
GLF 11.08	La Fage	1	0					3	52					16			29	
GLF 11.09	La Fage	1	5					6	63					15			16	
GLF 11.10	La Fage	1	10						Brushite, K-Feldspar, Clays identified									
GLF 11.11	La Fage	1	15						Brushite, K-Feldspar, Clays identified									
GLF 11.12	La Fage	1	20						Brushite, K-Feldspar, Clays identified									
GLF 11.17	La Fage	2	28								100							
GLF 11.14	La Fage	2	30		26						33				13		28	
GLF 11.15	La Fage	3	35		56						12				9		23	
GLF 11.16	La Fage	3	45		43						18				19		20	
GLF 11.18	La Fage	3	48		100													
GLF 11.19	La Fage	3	60			1					18	80						
GLF 11.21	La Fage	4	63	73	12						15							
GLF 11.20	La Fage	5	65								13	87						
RAN 11.06	Rancogne	1	5					65		35								
RAN 11.07	Rancogne	2	15	10			24						66					
RAN 11.08	Rancogne	3	18		11								48			20		20
RAN 11.04	Rancogne	3	20		7								36			36	16	6
RAN 11.10	Rancogne	3	25		10								50			20		20
RAN 11.11	Rancogne	3	26		32								38			10		20
GAV 08.01	Gavarnie	Top	5						Dolomite, Quartz, Calcite, Clays identified									
GAV 08.02	Gavarnie	Base	20						Dolomite, Quartz, Calcite, Clays identified									

Notes: see Table 1 for abbreviations

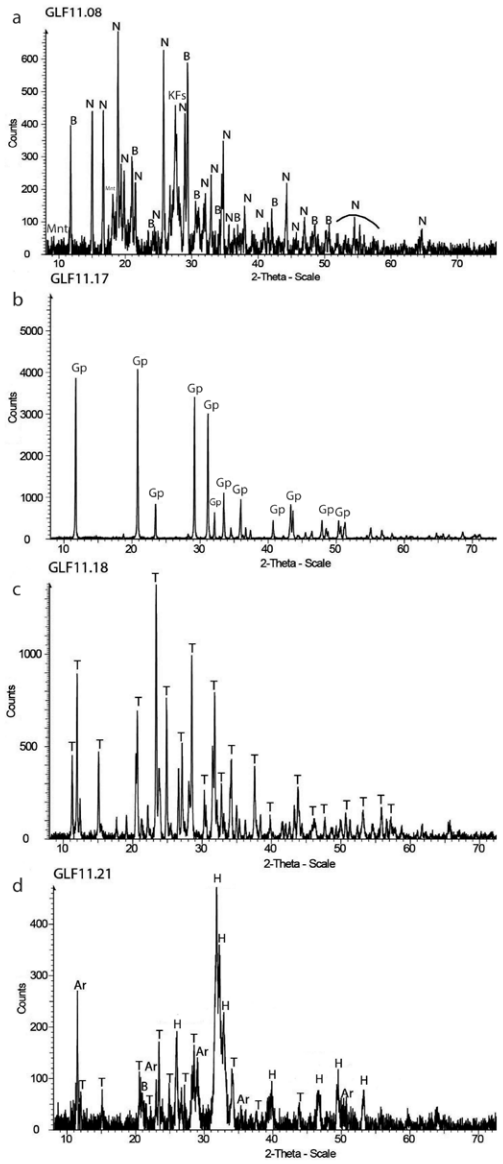

Figure 5. X-ray diffractograms of La Fage cave samples. (a) Sample GLF 11.08; (b) Sample GLF 11.17; (c) Sample GLF 11.18; (d) Sample GLF 11.21. See Table 1 for abbreviations.

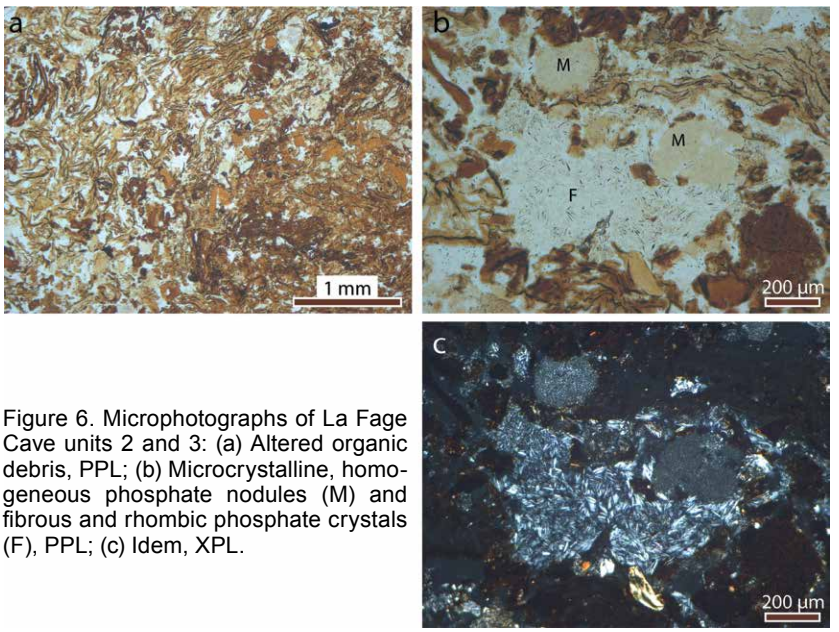

Figure 6. Microphotographs of La Fage Cave units 2 and 3: (a) Altered organic debris, PPL; (b) Microcrystalline, homogeneous phosphate nodules (M) and fibrous and rhombic phosphate crystals (F), PPL; (c) Idem, XPL.

to the substratum, homogeneous, microcrystalline phosphate accumulations fill the cracks (Fig. 8c). The thickness of this unit is highly variable and ranges between 1 cm and 15 cm. The minerals identified by XRD include quartz, francoanellite and hydroxylapatite (Fig. 9b). The pH is higher than in the overlying layer, but still remains acidic (ca. 5.2).

3. Unit 3 – Bright brown (10YR 6/6), bedded alluvial silts, which form the substrate. The amount of phosphate minerals changes significantly from one bed to another. Bed b, which is the coarsest, contains much more authigenic minerals than beds a and c (Figs. 8d and 8e). They are organized in small, yellowish nodules, identified as taranakite (Fig. 9c). The pH is particularly low with values around 5.

Zn concentration is high and decreases down the sequence from several thousands to a few hundreds of ppm. Cu is also in concentrations above normal values (i.e. typical of cave sediments). High Rb, Sr, and Zr amounts reflect the detrital component of the unit.

Gavarnie Cave

The cross-section made in the mound of chough guano (Fig. 10) reveals a rather loose accumulation of organic fragments with rough bedding, marked by the alternation of centimeter-thick, dark and light beds. This alternation may be the result of seasonal variations in the activity of the bird community or in their diet. Two samples were collected in the section, and these show a total lack of authigenic minerals. Only minerals coming from the surrounding rock walls were found (Table 2). The TOC content increases three-fold from top to bottom, whereas the carbonate content decreases, indicating progressive decalcification. The pH remains almost neutral in both samples with a slight decrease in the deepest sample (Table 3). It is noteworthy that in this guano, Cu and Zn do not reach high concentrations and P is not detected in ED-XRF.

Organic Matter Characterization

Pyrolysis at 600 °C

The analysis showed important dissimilarities between bat and chough guano mounds (Table 4 and Fig. 11). The pyrolysis products of bat guano are almost exclusively composed of a series of unsaturated and saturated hydrocarbons ranging from C9 to C28 (Fig. 11a). These n-alkene/n-alkane doublets are generally produced by the pyrolysis of polymers or biopolymers made of long alkyl chains, by radical cleavage of carbon-carbon bonds (Tegelaar et al., 1989). Alkenes/alkanes doublets can also result from acid decarboxylation or alcohol dehydration, by random cleavage of carbon chains (Quénéa et al., 2006). Indeed, the probability to obtain an alkane or an alkene via the homolytic scission of

Table 3. Chemical composition of all bulk samples.

Sample	Site	Unit	Depth (cm)	pH	TOC (%)	LOI (%)	CaCO3 (%)	S (%)	C total (%)	Si (%)	P (%)	K (%)	Ca (%)	V (µg/g)	Fe (µg/g)	Cu (µg/g)	Zn (µg/g)	Rb (µg/g)	Sr (µg/g)	Zr (µg/g)
GLF 11.08	La Fage	1	0	5.3	30	87	1	1.7	30	< LOD	< LOD	1.598	0.6996	< LOD	0.05545	213	2548	11.5	7.3	< LOD
GLF 11.09	La Fage	1	5	5.4	30	86	0	1.5	30	< LOD	< LOD	1.395	1.807	< LOD	0.08432	269	4478	13.5	11.8	7.8
GLF 11.10	La Fage	1	10	4.7	35	90	1	1.3	35	< LOD	3.28	5.309	1.626	< LOD	0.3203	1355	4121	14.8	7.6	< LOD
GLF 11.11	La Fage	1	15	4.8	37	92	1	1.7	37	< LOD	3.95	4.708	1.71	< LOD	0.3176	1419	3598	10.8	< LOD	< LOD
GLF 11.12	La Fage	1	20	4.8	38	93	0.5	1.7	38	< LOD	< LOD	0.8052	0.6068	< LOD	0.0899	332.4	2309	10.2	< LOD	8.4
GLF 11.17	La Fage	2	28	...	...	...	...	...	...	0.79	2a	0.4372	18.62	< LOD	0.12	545.6	285.9	< LOD	< LOD	104.6
GLF 11.14	La Fage	2	30	4.6	13	48	0.5	3.3	13	4.61	5.19	2.767	2.424	< LOD	2.618	1632	1717	41.4	37.6	118.4
GLF 11.15	La Fage	3	35	5.0	1	25	0	0.4	1	8.26	9.86	5.103	0.2147	43.9	4.323	307.5	605.1	53.8	42.5	209.7
GLF 11.16	La Fage	3	45	5.2	0.5	21	0	0.3	0.5	14.59	4.28	4.087	0.1936	91.3	5.526	299.2	406	71.6	73.1	240.6
GLF 11.18	La Fage	3	48	...	...	...	...	...	...	2.04	14.7	6.872	0.2138	< LOD	2.099	217.7	160.8	23	< LOD	140.1
GLF 11.19	La Fage	3	60	...	...	...	...	...	...	4	6a	0.7439	63.86	< LOD	0.6559	720	3603	15.6	43.2	397.2
GLF 11.21	La Fage	4	63	5.0	...	...	...	...	...	2.5	9.696	1.487	22.53	52.2	0.5816	436	6427	11	44.2	196.9
GLF 11.20	La Fage	5	65	...	...	...	...	...	...	3.96	6a	0.6657	86.56	< LOD	0.1741	1026	4456	< LOD	152.9	506.7
RAN 11.06	Rancogne	1	5	4.0	25	72	1	1.6	25	< LOD	< LOD	0.8651	4.784	< LOD	0.1322	315.8	3386	9.8	9.5	8.4
RAN 11.07	Rancogne	2	15	5.2	34	92	0.5	1.0	34	1.8	< LOD	1.175	2.738	< LOD	0.8305	1318	1039	49.1	79.7	218.9
RAN 11.08	Rancogne	3	18	5.0	1	9	0	0.1	1.5	23.18	< LOD	2.881	0.6522	45.2	3.162	213.1	400.6	169.1	94.1	425.8
RAN 11.04	Rancogne	3	20	5.0	1	5	0	0.1	1	20.95	< LOD	2.868	0.4632	74.7	5.044	160.3	553.7	186.8	59.4	391.8
RAN 11.10	Rancogne	3	25	5.3	2	12	0	0.2	2	23.24	< LOD	2.904	0.7394	< LOD	3.218	234.7	471.7	158.9	85.1	414.1
RAN 11.11	Rancogne	3	26	...	...	...	...	...	...	18.02	2.88	3.741	0.5194	28.1	2.454	235.3	295.9	140.6	73.5	339.1
GAV 08.01	Gavarnie	Top	5	7.0	10	60	8	0.2	11	5.38	< LOD	0.5335	10.75	< LOD	0.8309	51.6	113	30.5	91	90.6
GAV 08.02	Gavarnie	Base	20	6.8	31	87	1	0.8	32	2.46	< LOD	0.3695	7.197	< LOD	0.7004	111.8	133.9	23.1	91.8	78.4

Notes: TOC = Total Organic Carbon, LOI = Loss On Ignition, < LOD = under the limit of detection

[a] Values strongly influenced by Ca escape lines because of interaction with the silicon detector as observed on the spectra. The expected values are probably much lower.

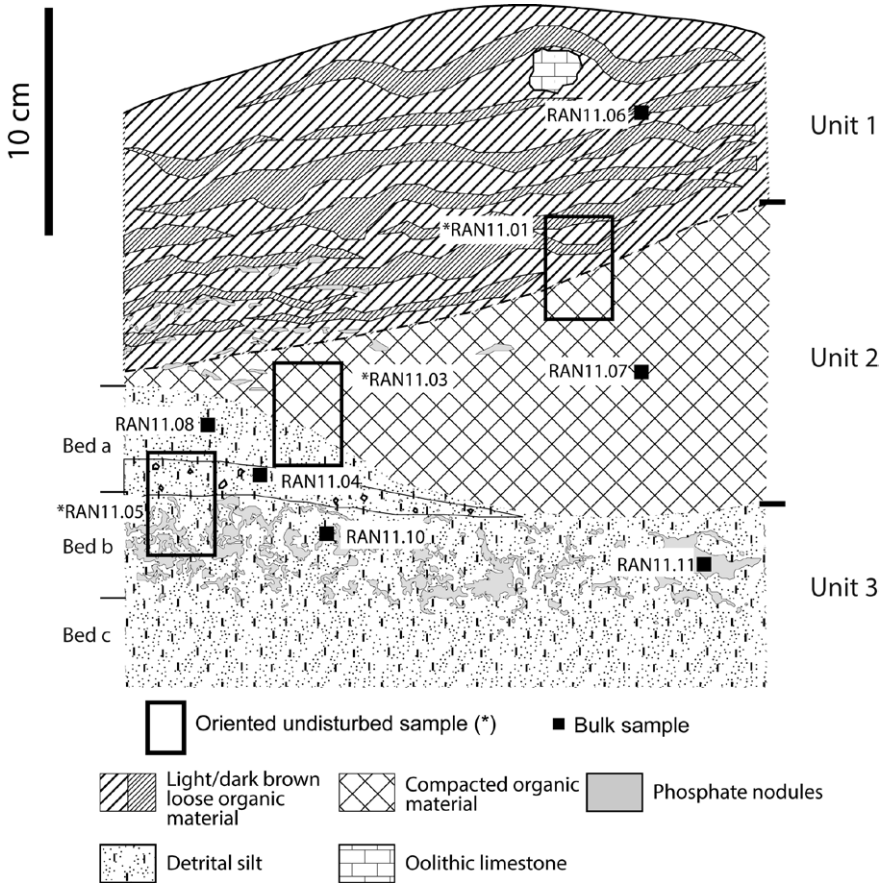

Figure 7. Stratigraphy of the guano mound in Rancogne Cave and sample locations.

an alkyl chain is the same, thus resulting in a doublet on the chromatogram. This hypothesis is supported by the total lack of such alkane/alkene series within the products of pyrolysis at lower temperature (200 °C). This demonstrates indeed that these doublets are not present on the sample in natural state, but are only observed when created by pyrolysis at 600 °C. The short-chained alkanes/alkenes, coming from the cleavage of long chains, may indicate the importance of insect cuticles. Indeed, hydrocarbons are important components of the cuticular lipids of many insects. These lipids are essentially composed of long, odd numbered, carbon chain (generally from C21 to C33) hydrocarbons (Blomquist, 2010) and branched alkanes (Kolattukudy, 1976). The aliphatic biopolymer, characterized by the alkane/alkene doublets, can be produced by a diagenetic polymerization of cuticular waxes and internal body lipids (Stankiewicz et al., 1998).

In mass spectrometry, the m/z 57 fragment is diagnostic of alkyl chains. This molecular ion is used to selectively detect alkanes from a complex sample.

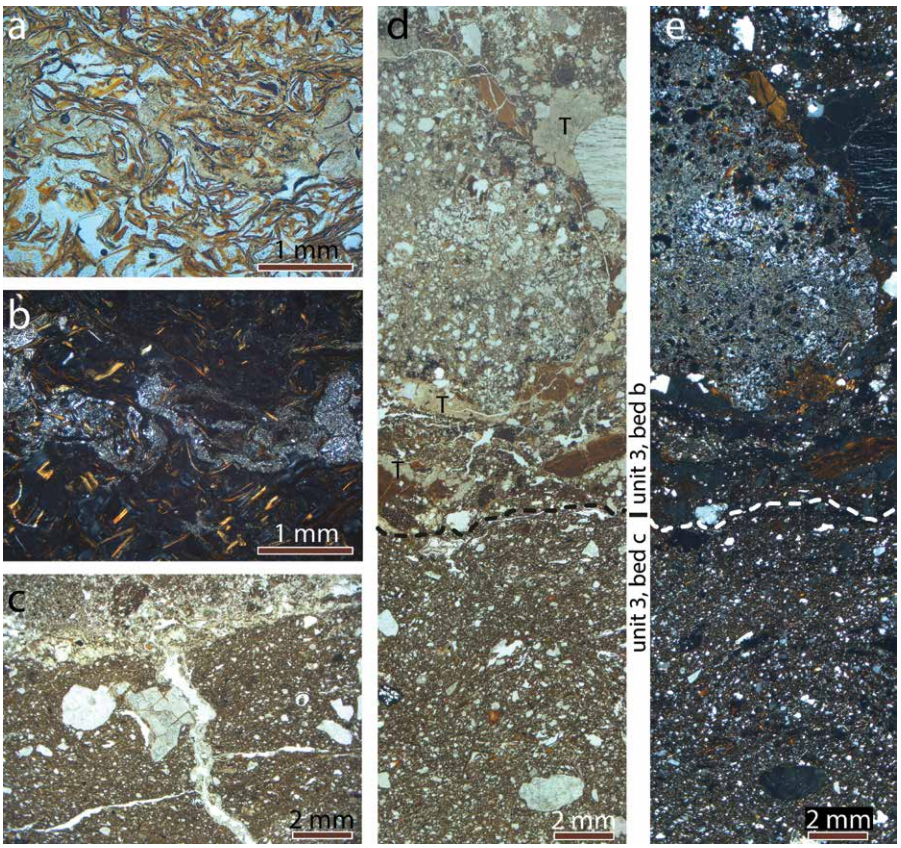

Figure 8. Microphotographs of Rancogne Cave samples: (a) Microcrystalline phosphate lens in organic debris, PPL; (b) Idem, XPL; (c) Microcrystalline and homogeneous phosphate lens partially filling a crack in the silty sediment, PPL; (d) Yellowish phosphate nodule of taranakite (T) and its distribution in the beds b and c, unit 3, PPL; (e) Idem, XPL.

The comparison between the total ion current (Fig. 11a), representing all the detected compounds, and the m/z 57 ion extract (Fig. 11b) clearly shows that hydrocarbons are the main products of the pyrolysis at 600°C. The 57 ion extracts from the two samples reflect notably similar distributions in alkanes.

The pyrolysis of chough guano is far more complex (Fig. 11c). The peaks marked with L, C, N correspond, respectively, to pyrolysis products derived from lignin, cellulose and proteins/chitin. Some alkenes (marked n:1) can be distinguished as trace compounds.

Thermochemolysis (TMAH pyrolysis 600 °C)

Pyrolysis at 600 °C in the presence of tetramethylammonium hydroxide, as alkylating reagent, makes it possible for the detection of polar compounds such as fatty acids, that tend to be degraded by classical pyrolysis (del Río and Hatcher, 1998) cuticles and a suberin. Thermochemolysis is complementary to pyrolysis, and improves the detection of fatty acids, whereas the hydrocarbons are minored.

Fatty acids can be selectively detected in mass spectrometry, using the m/z 74 fragment as a diagnostic ion, resulting from the classical McLafferty's rearrangement (McLafferty, 1959). The comparison of the total ion current (TIC), obtained by thermochemolysis of bat guano (Fig. 12a) and the m/z 74 ion extract (Fig. 12b), shows that fatty acids are the major constituents obtained by thermochemolysis. They are mainly composed of long, even chained compounds usually interpreted to be of higher plant origin (Kolattukudy, 1976). However, lignin is almost absent from the pyrolysis analysis and long-chain fatty acids have also been observed in fungi (Řezanka and Mareš, 1987; Řezanka, 1989).

The distribution of fatty acids in chough guano is displaced toward the short-chained compounds (Fig. 13). Unlike bat guano, fatty acids are not the

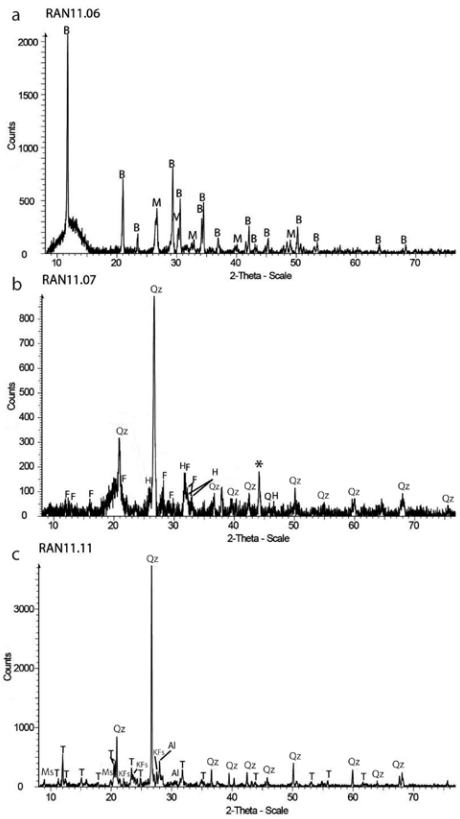

Figure 9. X-ray diffractograms of Rancogne cave samples: (a) Sample RAN 11.06; (b) Sample RAN 11.07; (c) Sample RAN 11.11. See Table 1 for abbreviations. (*) is for the diffraction peak of sample holder that diffracted with organic-rich sample.

Figure 10. Gavarnie Cave test-pit. The scale bar is 20 cm long.

main constituents and other compounds (hydroxyl acids, diacids) are also present (Table 5).

Discussion

The La Fage Cave section allows observation and study of a complete sequence documenting the evolution of insectivorous bat guano in a calcareous context, under humid, temperate climate (Fig. 14).

The first stage of guano decomposition is accompanied by the formation of newberyite, a mineral present only in the top part of the accumulation. This magnesium phosphate may form directly from phosphate solutions. Magnesium is naturally present in small amounts in guano (Perrenoud, 1993), but has probably been brought mainly by water flowing through dolomitized limestone (Martini and Kavalieris, 1976), which crops out in the upstream part of the karst system (Lefavrais-Raymond et al., 1976). According to Hutchinson (1950) and Hill and Forti (1997), newberyite may have struvite (an unstable magnesium and ammonium phosphate) as a precursor, and may result from its transformation by loss of soluble ammonia, and by dehydration (Boistelle et al., 1983). This mineral, identified in the Grotte XVI sediments, is proposed by Karkanas et al. (2002) as an evidence for bat guano origin of phosphate-rich sediments. The mineral crystallized in recent guano into small, scattered and radial nodules, only visible under the microscope.

Several centimeters below the newberyite-rich layer in Unit 1, the only phosphate mineral identified is brushite. This phosphate, especially common in caves (Fiore and Laviano, 1991; Hill and Forti, 1997; Marincea et al., 2004) forms from solutions provided by the decomposition of guano in a humid environment and under acidic conditions (pH less than 6) (Hill and Forti, 1997).

In Unit 2, which corresponds to older and more degraded guano, brushite disappears and gypsum becomes largely dominant, in association with taranakite, an aluminum phosphate. Organic matter degradation increases and, as a consequence, the sediment becomes more acidic because of bacteria-induced production of sulfuric acid (Li et al., 2008; Paul, 2007). The origin of the sulfur used by these bacteria can be from bat guano (Hosono et al., 2006). The presence of sulfuric acid seems to be the main factor involved in gypsum formation (Rinaudo and Abbona, 1988; Hill and Forti, 1997; Shahack-Gross et al., 2004; Dumitraş et al., 2008; Engel et al., 2004). In the La Fage test-pit, this is correlated with the lowest pH values, which are close to 4.6. The loose arrangement of the organic material allows for the authigenic minerals to form in the voids. Therefore, no signs of sediment disturbance due to crystallization were observed.

Percolation appears to be the main factor that explains the stratigraphic distribution of secondary minerals. Higher affinity of SO_4^{2-} to Ca^{2+}, when compared with PO_4^{3-}, results in the progressive depletion in SO_4^{2-} and Ca^{2+} of the solutions, in the preferential precipitation of gypsum, in the upper part of the sequence (guano layers), and the presence of phosphates only in the underlying clay layer. Clay alteration, due to acidic, phosphate-rich solutions, releases Al and K, leading to the crystallization of taranakite. This aluminum phosphate is frequently encountered in caves (Sakae and Sudo, 1975; Fiore and Laviano, 1991; Marincea et al., 2002; Onac and Vereş, 2003; Puşcaş et al., 2014). It is a marker of humid environment and its crystallization needs acidic solutions (Puşcaş et al., 2014). In La Fage Cave, taranakite is largely predominant in clay and forms millimeter- to centimeter-thick fillings of desiccation cracks, giving way to a network of phosphatized veins. Francoanellite, a mineral similar to taranakite with less structural water, is present in small amounts and may reflect partial drying of the deposit (Onac and Vereş, 2003). Taranakite, as other aluminum phosphates, is assumed to be stable and is part of the common mineral association usually described in archeolog-

Table 4. Pyrolysis products and their probable origin for both guano samples.

Ret.Time[a]	Bats	Chough	Origin/class of compound
1.993		Propanal	cellulose
2.193		Amino-pentanol	nitrogen containing compound
2.287		Hydrazine, butenyl-	nitrogen containing compound
2.363		Butanoic acid	
3.553		1H-Pyrrole, methyl-	nitrogen containing compound
3.743		Pyridine	nitrogen containing compound
4.007		Toluene	lignin
4.493		Hydroxymethyl-furane	cellulose
4.790		Furfural	cellulose
5.157		Furfural	cellulose
5.427	Methyl pyrrole	Methyl pyrrole	nitrogen containing compound
6.5	Nonene (C9 :1)		alkene
6.59	styrene		lignin
6.75	Nonane (C9)		alkane
7.413		Cyclopentanedione	cellulose
8.443		methyl furancarboxaldehyde	cellulose
8.990	Phenol	Phenol	lignin
9.297	Decene (C10 :1)	Decene	alkene
9.5	Decane (C10)		alkane
10.357		Methyl cyclopentanedione	cellulose
11.0	indene		nitrogen containing compound
11.230		2-methyl- Phenol	lignin
11.890		4-methyl- Phenol	lignin
12.360	Undecene (C11 :1)	Undecene	alkene
12.6	Undecane (C11)		alkane
15.440		Menthol, O-isobutenyryl-	lignin
15.7	Dodecane (C12)		alkane
16.343		dihydro Benzofuran	lignin
18.587		Indole	nitrogen containing compound
	Dodecanal (Ald C12)		aldehyde
	Tridecene (C13 :1)		alkene
19.057		Hydroxy-methylacetophenone	lignin
	tetradecene (C14 :1)		alkene
	Dodecanone (ket C12)		ketone
	Tetradecane (C14)		alkane
21.237		1H-Indole, methyl-	nitrogen containing compound
22.863		Phenol, methoxy-(propenyl)	lignin
23.917	Pentadecene (C15 :1)	Pentadecene	alkene
	Pentadecanal (Ald C15)		aldehyde
	Hexadecene (C16 :1)		alkene
	Methyl nonenone		ketone
	heptadecene (C17 :1)		alkene
	Heptadecane (C17)		alkane
	Octadecene (C18 :1)		alkene
	Nonadecene (C19 :1)		alkene
	Eicosene (C20 :1)		alkene
	Uncosene (C21 :1)		Alkene
	Docosene (C22 :1)		Alkene
	Tricosene (C23 :1)		Alkene
	Tetracosene (C24 :1)		Alkene
	Pentacosene (C25 :1)		Alkene
	Hexacosene (C26 :1)		Alkene
	Octcosene (C28 :1)		alkene
53.473		Hentriacontane (C31)	alkane
53.907		Stigmastan-3,5-diene	steroide
57.337		pentatriacontane (C35)	alcane

[a] Ret. Time = retention time on the chromatogram.

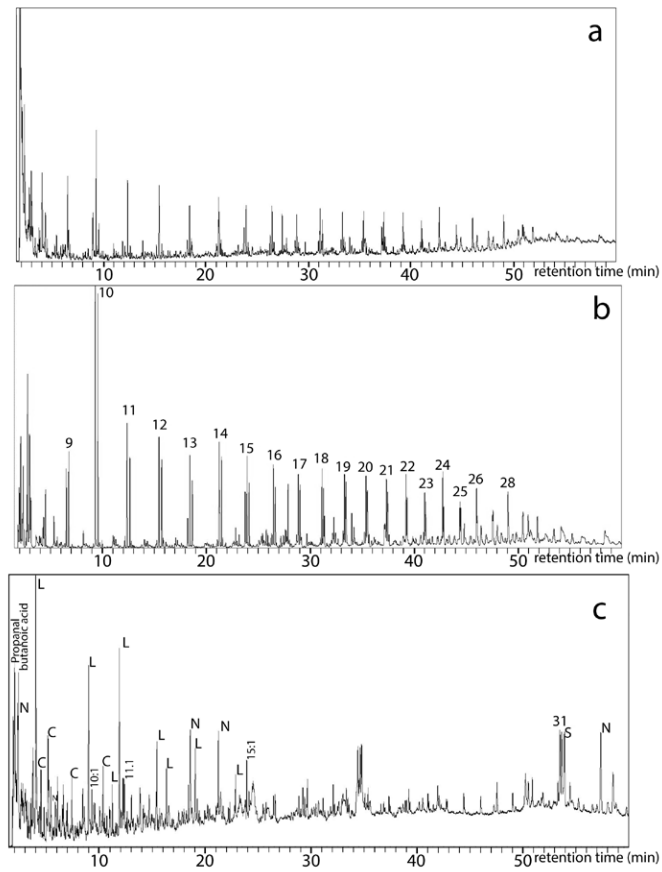

Figure 11. Pyrolysis products obtained at 600 **°C (**Py-GC/MS). (a) Total ion current of bat guano; (b) Ion extract (m/z 57) of bat guano; (c) Total ion current of chough guano. L = lignin, C = cellulose, N = nitrogen containing compounds, n = alkane with n carbon atoms.

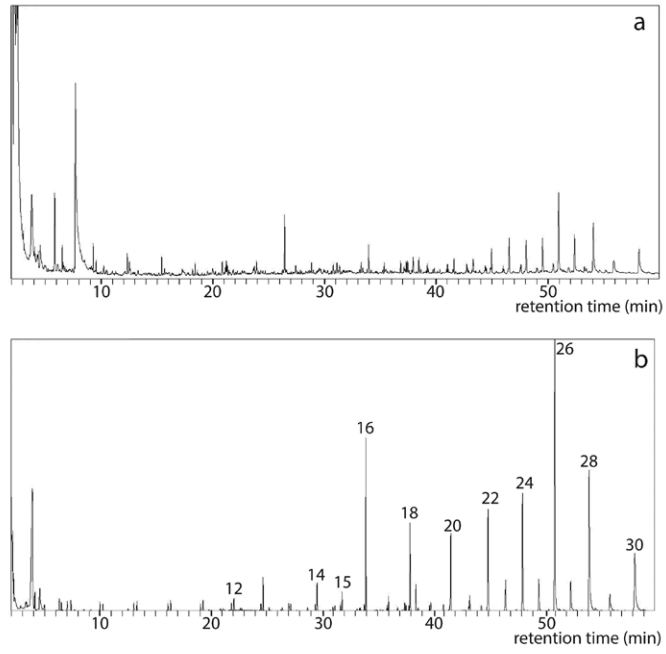

Figure 12. Thermochemolysis (TMAH) products of bat guano. (a) Total ion current (b) Ion extract (m/z 74).

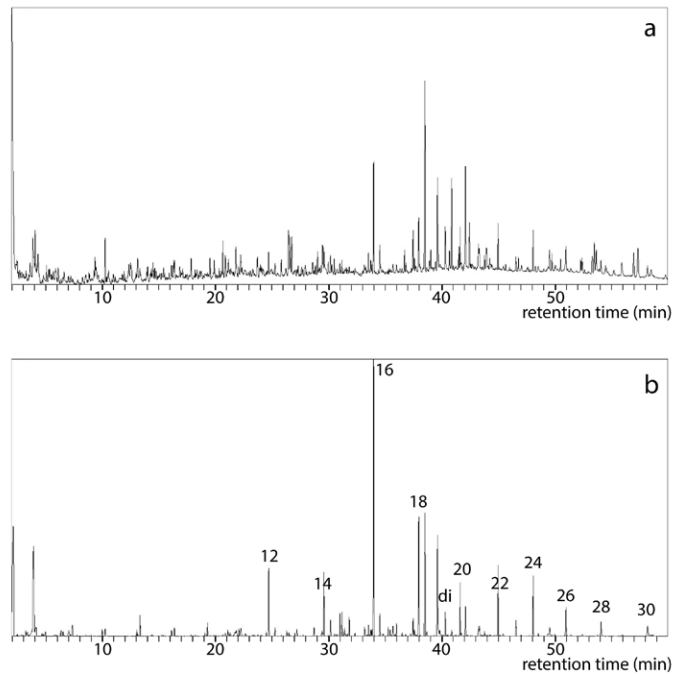

Figure 13. Thermochemolysis (TMAH) products of chough guano. (a) Total ion current; (b) Ion extract (m/z 74).

ical contexts, along with hydroxylapatite, notably in the Levant and Greece (Hill and Forti, 1997; Karkanas et al., 2000; Weiner et al., 2002). However, it has to be noted that taranakite is absent, to our knowledge, in all Pleistocene sites investigated in southwest France (Bertran, 1999; Karkanas et al., 2002; Ajas et al., 2013). Because of the accumulation of abundant limestone debris released by frost wedging of the walls during the glacial periods, basic conditions probably prevailed most of the time in cave sediments. This process is tentatively assumed to be the main factor involved in the poor preservation of taranakite.

Deeper into the sequence, an alteration crust formed at the top of the limestone by pseudomorphic replacement of calcite by hydroxylapatite. Limestone dissolution by acidic solutions released Ca^{2+} ions that favored the formation of hydroxylapatite. Such an evolution is documented in numerous caves (Hutchinson, 1950; Goldberg and Nathan, 1975; Martini and Kavalieris, 1976; Courty et al., 1989; Perrenoud, 1993; Hill and Forti, 1997; Ajas et al., 2013; Wurster et al., 2015). Thinner crusts with ardealite, brushite and hydroxylapatite developed also around limestone blocks scattered in Unit 3. This association has already been described in the archeological sites of Kebara and Tabun in the Near East by Goldberg and Nathan (1975). Karkanas et al. (2000) and Shahack-Gross et al. (2004) suggested that this association reflects a chain of mineral reactions, which are strongly dependent on the geochemical micro-environments around the blocks.

In Rancogne Cave (Fig. 15), the transformation of guano is disturbed by river floods. Units 1 (fresh guano), 2 (old guano) and 3 (alluvial silts) are separated by unconformi-

Table 5. Thermochemolysis products and their probable origin for both guano samples.

Ret.Time[a]	Bats	Chough	Origin/class of compound
5.825	Dimethyl phosphite		phosphate
6.517	Nonene (C9 :1)		hydrocarbon
7.767	trimethyl phosphate		phosphate
9.283	Decene (C10 :1)		hydrocarbon
9.55	Decane (C10)		hydrocarbon
10.242		methoxy methyl benzene	
12.342	Undecene (C11 :1)		hydrocarbon
12.525	methyl benzoate		lignin
12.617	Undecane (C11)		hydrocarbon
15.417	Dodecene (C12 :1)		hydrocarbon
15.675	Dodecane (C12)		hydrocarbon
17.8		methyl indole	
18.183	Methyl dodecene		hydrocarbon
18.392	Tridecene (C13 :1)		hydrocarbon
18.625	Tridecane (C13)		hydrocarbon
19.983	N-methyl Pyrrolidone-methyl carboxylate		sugar
19.525	Furan-3-carboxaldehyde, 2-methoxy-2,3-dihydro-		sugar
20.6		trimethoxy benzene	
20.833	methoxy methyl Benzoate	methoxy methyl Benzoate	lignin
21.142	phenyl methyl propenoate		lignin
21.217	Tetradecene (C14 :1)		hydrocarbon
21.283	Dodecanone (ket C12)		cetone
21.425	Tetradecane (C14)		hydrocarbon
21.8		trimethoxy toluene	
22.2	Dimethyl-tetrahydro-pyrimidinone		sugar
23.625	dimethoxy benzaldehyde		lignin
23.717	Methyl tetradecene		hydrocarbon
23.892	Pentadecene (C15 :1)		hydrocarbon
24.1	Pentadecane (C15)		hydrocarbon
24.683	methyl dodecanoate (C12Me)		acid
25.8		Dimethoxyacetophenone	
26.417	dimethoxy methyl benzoate	dimethoxy methyl benzoate	lignin
27.425	methyl nonenone		cetone
28.833	Heptadecane (C17)		hydrocarbon
29.5		methyl tetradecanoate (C14Me)	
30.783	hydroxy methoxy trimethyl methyl benzoate		lignin
31.108	Octadecene (C18 :1)		hydrocarbon
33.283	Nonadecene (C19 :1)		hydrocarbon
33.7		methyl hexadecenoate (C16:1Me)	
33.942	methyl hexadecanoate	methyl hexadecanoate (C16Me)	acid
35.342	Eicosene (C20 :1)		hydrocarbon
35.983	methyl heptadecanoate		acid
37.317	Uncosene (C21 :1)		hydrocarbon
37.442	methyl octadecenoate	methyl octadecenoate (C18:1Me)	acid
37.942	methyl octadecanoate	methyl octadecanoate (C18Me)	acid
38.5	methyl nonadecenoate	methyl nonadecenoate (C19Me)	acid
39.6		Methyl hydroxy hexadecanoate	
40.28		dimethyl hexadecanedioate	
41.6	methyl eicosanoate (C20Me)	methyl eicosanoate (C20Me)	acid
43.25		methyl uncosenoate (C21Me)	
43.3	Tetracosene (C24)		hydrocarbon
44.95	methyldocosanoate (C22Me)		acid
46.542		methyl methyldocosanoate (C22Me)	
48.058	methyl tetracosanoate (C24Me)	methyl tetracosanoate (C24Me)	acid
50.958	methyl Hexacosanoate	methyl Hexacosanoate (C26Me)	acid
53.45		Hentriacontane	
54.058	Methyl octacosanoate	Methyl octacosanoate (C28Me)	acid
55.175		Sitosterol	
55.892	Dotriacontene (C32)		hydrocarbon
56.917		Cholesten-3-ol, acetate	
57.3		Pentatriacontane (C35)	
58.175	Methyl triacontanoate (C33)	Methyl triacontanoate (C30Me)	acid

[a] Ret. Time = retention time on the chromatogram.

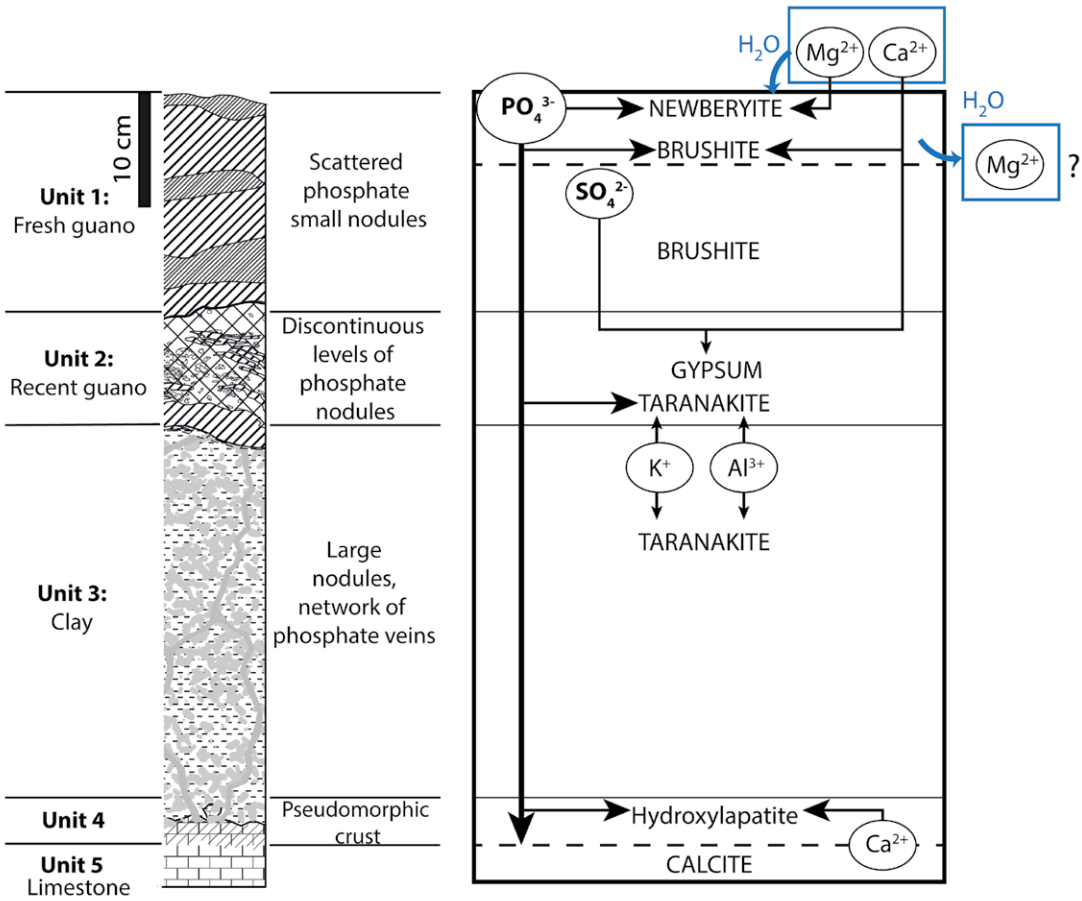

Figure 14. Schematic interpretation of the mineralogical evolution of La Fage Cave guano.

ties that are due to flow erosion. Unit 1 is similar to the upper unit in La Fage Cave, except for the lack of newberyite, which may reflect smaller amounts of Mg^{2+} ions provided by the host limestone. Monetite partially replaces brushite, possibly because sampling was done at the end of the dry season and the guano could have suffered some dehydration. Unit 2 corresponds to older guano mixed with detrital sediment. The lack of gypsum is assumed to result either

Figure 15. Schematic interpretation of the mineralogical evolution of Rancogne Cave guano.

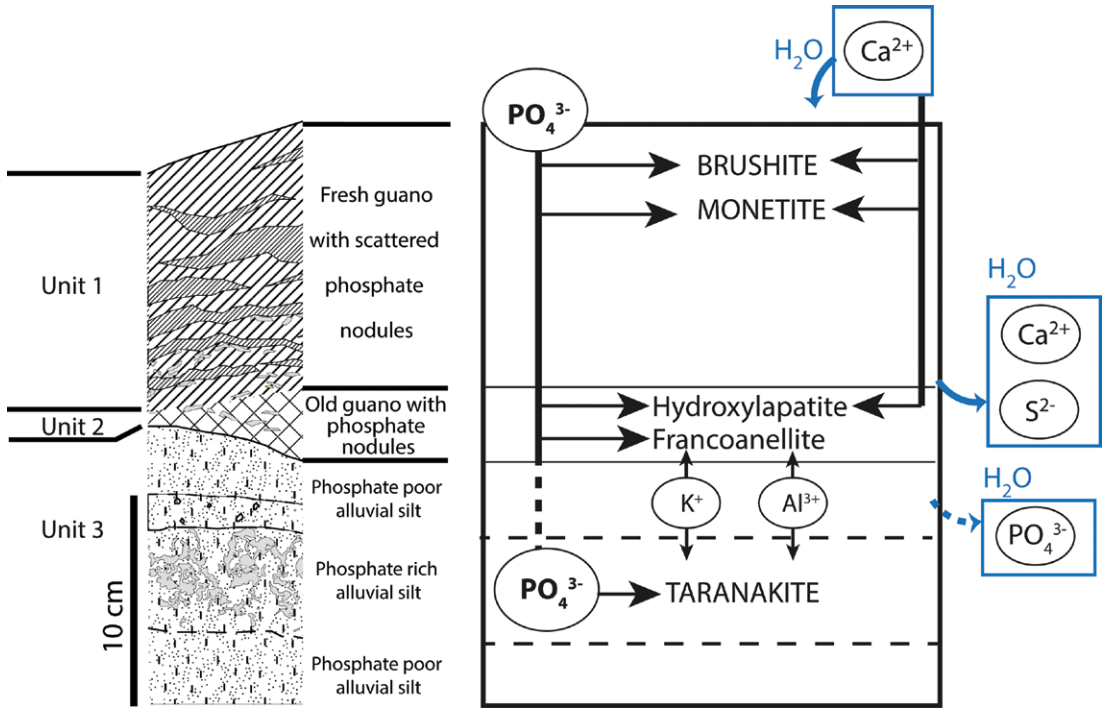

from dilution of the acidic solutions percolating through the guano mound, which prevented gypsum formation, or from subsequent dissolution of the crystals. Simultaneously, more stable minerals, such as hydroxylapatite and francoanellite, concentrated in degraded guano. Francoanellite is an uncommon mineral similar to taranakite, both in chemistry and structure (Table I). It has been reported in some caves (Balenzano et al., 1976; Marincea et al., 2012; Onac and Vereş, 2003; Queffelec et al., 2011) in close relationship to taranakite in clay sediments (Onac and Vereş, 2003), and its chemistry involves ions provided by the dissolution of clay minerals. As already noted above for monetite, sampling at the end of the dry season may explain the presence of this rare mineral instead of taranakite, the more hydrated mineral of the same phosphate group. The low amount of authigenic minerals in the underlying silty unit also suggests that the concentration in phosphate and sulfate ions remained low. Taranakite, which is poorly soluble in water, subsisted despite repeated flooding.

The guano sequence of Gavarnie Cave did not undergo similar phosphate accumulation. Possible factors involved are the periglacial climate that prevents organic matter degradation and the low availability of water (most water formed segregation ice in the deposits), that restricted ion redistribution within the guano mound. Another possible factor involved is that the choughs produce only limited amounts of phosphorus- and sulfur-rich compounds because of their dominantly herbivorous diet, when compared to the insectivorous bats. However, it has to be noted that frugivorous bats also produce guano, and degradation leads to the formation of abundant of phosphate minerals in subtropical and tropical contexts (Shahack-Gross et al., 2004; Queffelec et al., 2011, Royer et al., 2017).

Geochemical analysis reveals especially high Cu and Zn concentrations in bat guano both in La Fage and Rancogne caves. Hundreds of ppm μg g^{-1} of Cu and thousands of ppm of Zn have already been measured in recent bat guano (Fenolio et al., 2006; Zukal et al., 2015), as well as in an archeological context at Gorham's Cave (Monge et al., 2015). In this site, high Cu and Zn concentrations have been interpreted as being of anthropogenic origin (i.e. pollution). However, long-lasting bat settlement of the cave (Rodríguez-Vidal et al., 2014), rather, suggests that Cu and Zn is derived from bat guano. A recent study in southeast Asia (Wurster et al., 2015) also showed similar enrichment in transition metals in recent and ancient cave guano. Additionally, a guano-induced origin of Zn-rich phosphates in a Bahamian cave has been proposed by Onac et al. (2009). The fact that these sediments from bat-inhabited, worldwide caves show remarkably high Cu and Zn concentrations makes it extremely unlikely that this could be due to recent pollution of the sites. The values measured in La Fage and Rancogne caves, both in fresh guano and in the underlying sediments, exceed by far the highest values measured in European soils and Quaternary sediments (De Vos et al., 2006). Cu values have been found to be lower than 260 μg g^{-1} in soils, 300 μg g^{-1} in humus, and 500 μg g^{-1} in modern floodplain sediments (De Vos et al., 2006). Therefore, values in excess of 1000 μg g^{-1} in units 1 and 5 in La Fage Cave and Unit 2 in Rancogne Cave have to be interpreted as resulting from local enrichment, due to the accumulation of bat guano. Zn also reaches the highest values recorded in Europe, which range from 1860 ug g^{-1} (soils) to 3060 μg g^{-1} (humus), while means are only 76 μg g^{-1} and 100 μg g^{-1}, respectively. Zn reaches 1478 μg g^{-1} in floodplain sediments located near the Pierrefitte Zn-Pb ore deposit in the French Pyrenees (De Vos et al., 2006). As for Cu, Zn values in excess of 4000 μg g^{-1} in both La Fage and Rancogne caves have to be attributed to bat guano enrichment. It is also noteworthy that the highest values were measured in fresh guano (unit 1 of both sites) and in unit 4 of La Fage Cave, which is almost exclusively composed of authigenic minerals. In the first case, few minerals may act as Cu and Zn accumulators, and these elements are probably adsorbed on the organic matter, while in the second case they may be integrated in the authigenic minerals.

The analysis of organic matter by pyrolysis and thermochemolysis show noticeable differences between the two types of guano. On the one hand, the entomological origin of bat guano is demonstrated by the presence of alkenes/alkanes doublets, coming from the pyrolysis of aliphatic biopolymers that are characteristic of insect cuticles. Chough guano, on the other hand, does not contain similar hydrocarbons, and its plant origin has been confirmed by the presence of abundant lignin and cellulosic components. As revealed by thermochemolysis, fatty acid abundance also differs. Fatty acids in bat guano may derive from plant remains, or more likely, from fungal development within the mound. Long-chain fatty acids, similar to the ones detected in the bat guano, have indeed been detected already in *Mycelia sterilia* (Stahl and Klug, 1996), a fungus identified on bat guano in Puerto Rico (Nieves-Rivera et al., 2009). The potential of this method to identify molecular compounds from bat excrements has to be underlined. Indeed, organic molecules from chitin, cellulose, and lignin have demonstrated as resistant to biodegradation through time (Stankiewicz et al., 1997, 1998). These may be used as markers for identifying bat guano in the archeological record and help distinguish potential sources of phosphate accumulation, whereas phosphate mineralogy alone does not provide clear indications.

Conclusion

The study of recent guano in caves allows better understanding of the main stages of its degradation and mineralization in a temperate, humid context. It also provides the opportunity to compare guano from bats and from choughs, another potential contributor to organic matter deposition in caves. The deposition, degradation and chemical evolution of a mound of bat guano leads to massive production of phosphorous and sulfur compounds that react with local cat-

ions to produce specific minerals. This study demonstrates the ubiquity of brushite and hydroxylapatite in calcareous contexts and the presence of taranakite or francoanellite when clay interacts with the acidic solutions. The formation of newberyite depends on the availability of magnesium ions provided by the host rocks. Water availability also plays a key role in guano degradation by the soil microfauna, in the degree of hydration of the authigenic minerals formed, and in their sediment preservation. Bat guano was found to contain large amounts of phosphate accumulation. In the investigated cave, chough guano did not lead to the production of neoformed minerals, perhaps mainly because of local conditions such as cold temperature and poor water availability (mostly frozen). The diversified and low trophic-level diet of the choughs may also be involved in the lower production of phosphates.

The early degradation stages of bat guano have little potential for preservation in the fossil record of southwest France since the main authigenic minerals are soluble or unstable over long periods in humid environments. In addition, gypsum may derive from sources other than guano, particularly in arid or coastal environments. Hydroxylapatite is common in archeological sites and may also come from other sources such as bones or coprolites. Newberyite and taranakite, which are less frequent, can be used as proxies for acidic solutions interacting with minerals in karstic sediments. These phosphate minerals, however, are almost absent in the archeological record from southwest France. This may reflect their instability in calcareous contexts that remained dominantly alkaline over the long term. However, since newberyite has been identified in Grotte XVI (Karkanas et al., 2002), thus testifying to its ability to be preserved in regional caves at least locally, the lack of such minerals may alternatively indicate that bat guano was not the main source of phosphate accumulation in most sites.

In contrast, this study suggests strongly that both the composition of organic matter and the content in transition metals may provide useful arguments for identifying the phosphate sources. In particular, aliphatic biopolymers, typical of insect cuticles, can be identified using pyrolysis on recent bat guano. Since these compounds are known to be resistant over time, they may potentially be identified in Pleistocene cave sediments. Cu and Zn concentrations have shown to be unusually high both in bat guano and in the underlying sediments containing neoformed minerals. Similar concentrations of Cu and Zn do not occur naturally in the study region or in other parts of southwest France, and obviously come from guano.

ACKNOWLEDGMENTS

We are grateful to Vincent Nicolas, Catherine Rouveron, Danielle Doucet and her husband for allowing us to sample the La Fage and Rancogne caves. We also acknowledge Eric Lebraud (UPR 9058 ICMCB) for XRD analysis, Nadia Cantin (UMR 5060 IRAMAT-CRP2A) for the TOPAS access, Dominique Poirier and Henri Etcheber (UMR 5805 EPOC) for pH and the LECO analyses. This study was partly conducted in the Collective Research Program “Caves of Guadeloupe: geological, paleontological and archaeological studies” funded by the Regional Service of Archaeology, the Guadeloupe Regional Council and the DEAL of Guadeloupe as an realistic approach for better understanding Caribbean guano deposits. This research was also supported by the LaScArBx research program (ANR-10-LABX-52). Four anonymous reviewers are thanked for their thorough comments on previous versions of this manuscript. These comments have helped to markedly improve it.

References

Ajas, A., Bertran, P., Lemée, L., and Queffelec, A., 2013, Stratigraphy and Palaeopedology of the Palaeolithic Cave Site of Combe-Saunière, Southwest France: Geoarchaeology, p. 1–18, http://doi:10.1002/gea.21451.

Baize, D., 2000, Guide des analyses en pédologie: 2e édition, revue et augmentée: Editions Quae.

Balenzano, F., Dell’Anna, L., and Di Pierro, M., 1976, Francoanellite, H6K3Al5(PO4)8·13H2O, a new mineral from the caves of Castelagna, Puglia, southern Italy: Neues Jahrbuch für Mineralogie Abhandlungen, p. 49–57.

Beaulieu, J.-L., Debard, E., Guérin, C., Jammot, D., Petter, F., Renault, P., and Vilain, R., 1973, Le gisement paléontologique pléistocène des Abîmes de la Fage à Noailles (Corrèze): Lyon, Nouvelles Archives du Museum d’Histoire Naturelle de Lyon.

Bertran, P., 1999, Dynamique des dépôts de la grotte Bourgeois-Delaunay (La Chaise-de-Vouthon, Charente) : apport de la micromorphologie / Depositional processes in the Bourgeois-Delaunay Cave (La Chaise-de-Vouthon, Charente, France): micromorphological approach: Paléo, v. 11, p. 9–18, http://doi:10.3406/pal.1999.1168.

Bird, M.I., Boobyer, E.M., Bryant, C., Lewis, H.A., Paz, V., and Stephens, W.E., 2007, A long record of environmental change from bat guano deposits in Makangit Cave, Palawan, Philippines: Earth and Environmental Science Transactions of The Royal Society of Edinburgh, v. 98, p. 59–69, http://doi:10.1017/S1755691007000059.

Blomquist, G.J., 2010, Structure and analysis of insect hydrocarbons, *in* Insect hydrocarbons: Biology, biochemistry, and chemical ecology, New York, Blomquist & Bagnères, p. 19–34.

Boistelle, R., Abbona, F., and Madsen, H.L., 1983, On the transformation of struvite into newberyite in aqueous systems: Physics and Chemistry of minerals, v. 9, p. 216–222.

Bridge, P.J., 1973, Guano minerals from Murra-el-elevyn Cave, Western Australia: Mineralogical Magazine, v. 39, p. 467–469.

Carrión, J.S., Scott, L., and Marais, E., 2006, Environmental implications of pollen spectra in bat droppings from southeastern Spain and potential for palaeoenvironmental reconstructions: Review of Palaeobotany and Palynology, v. 140, p. 175–186, http://doi:10.1016/j.revpalbo.2006.03.007.

Courty, M.A., Goldberg, P., and MacPhail, R., 1989, Soils and micromorphology in archaeology: Cambridge.

De Vos, W., Tarvainen, T., Salminen, R., Reeder, S., De Vivo, B., Lima, A., and others, 2006, Geochemical atlas of Europe. Part 2. Interpretation

of geochemical maps, additional tables, figures, maps, and related publications: Geological Survey of Finland, v. 2.
Dendaletche, C., 1997, Les Pyrénées. La vie sauvage en montagne et celle des hommes: Paris, Delachaux and Niestlé, La bibliothèque du naturaliste, 335 p.
Dumitraş, D.-G., Marincea, S., Bilal, E., and Hatert, F., 2008, Apatite-(CaOH) in the fossil bat guano deposit from the "dry" Cioclovina cave, Şureanu Mountains, Romania: The Canadian Mineralogist, v. 46, p. 431–445, http://doi:10.3749/canmin.46.2.431.
Engel, A.S., Stern, L.A., and Bennett, P.C., 2004, Microbial contributions to cave formation: New insights into sulfuric acid speleogenesis: Geology, v. 32, p. 369–372, http://doi:10.1130/G20288.1.
Fenolio, D.B., Graening, G.O., Collier, B.A., and Stout, J.F., 2006, Coprophagy in a cave-adapted salamander; the importance of bat guano examined through nutritional and stable isotope analyses: Proceedings of the Royal Society B: Biological Sciences, v. 273, p. 439–443, http://doi:10.1098/rspb.2005.3341.
Fiore, S., and Laviano, R., 1991, Brushite, hydroxylapatite, and taranakite from Apulian caves (southern Italy): New mineralogical data: American Mineralogist, v. 76, p. 1722–1727.
Forray, F.L., Onac, B.P., Tanţău, I., Wynn, J.G., Tămaş, T., Coroiu, I., and Giurgiu, A.M., 2015, A Late Holocene environmental history of a bat guano deposit from Romania: an isotopic, pollen and microcharcoal study: Quaternary Science Reviews, v. 127, p. 141–154, http://doi:10.1016/j.quascirev.2015.05.022.
Geantă, A., Tanţău, I., Tămaş, T., and Johnston, V.E., 2012, Palaeoenvironmental information from the palynology of an 800-year-old bat guano deposit from Măgurici Cave, NW Transylvania (Romania): Review of Palaeobotany and Palynology, v. 174, p. 57–66, http://doi:10.1016/j.revpalbo.2011.12.009.
Géroudet, P., 2010, Les passereaux d'Europe Tome 2 - de la bouscarle aux bruants: Paris, Delachaux and Niestlé, 512 p.
Goldberg, P., and Nathan, Y., 1975, The phosphate mineralogy of et-Tabun cave, Mount Carmel, Israel: Mineralogical Magazine, v. 40, p. 253–258.
Guilloré, P., 1980, Méthode de fabrication mécanique et en série des lames minces: Institut National Agronomique, Paris-Grignon, France.
Hill, C.A., and Forti, P., 1997, Cave minerals of the world: Huntsville, Alabama, 464 p.
Hosono, T., Uchida, E., Suda, C., Ueno, A., and Nakagawa, T., 2006, Salt weathering of sandstone at the Angkor monuments, Cambodia: identification of the origins of salts using sulfur and strontium isotopes: Journal of Archaeological Science, v. 33, p. 1541–1551, http://doi:10.1016/j.jas.2006.01.018.
Hutchinson, G.E., 1950, The biogeochemistry of vertebrate excretion: New-York, Survey of existing knowledge of biogeochemistry 3, v. 96, 554 p.
Karkanas, P., Bar-Yosef, O., Goldberg, P., and Weiner, S., 2000, Diagenesis in Prehistoric Caves: the Use of Minerals that Form In Situ to Assess the Completeness of the Archaeological Record: Journal of Archaeological Science, v. 27, p. 915–929, http://doi:10.1006/jasc.1999.0506.
Karkanas, P., Rigaud, J.-P., Simek, J.F., Albert, R.M., and Weiner, S., 2002, Ash Bones and Guano: a Study of the Minerals and Phytoliths in the Sediments of Grotte XVI, Dordogne, France: Journal of Archaeological Science, v. 29, p. 721–732, http://doi:10.1006/jasc.2001.0742.
Kolattukudy, P.E., 1976, Chemistry and biochemistry of natural waxes: Elsevier Scientific Pub. Co.
Laroulandie, V., 2004, Exploitation des ressources aviaires durant le Paléolithique en France: bilan critique et perspectives, *in* J.-P. Brugal, J. Desse (dir.), Petits Animaux et Sociétés Humaines. Du complément alimentaire aux ressources utilitaires. Actes des XXIVe rencontres internationales d'archéologie et d'histoire, Antibes, 23-25 Octobre 2003, APDCA, p. 163–172.
Lefavrais-Raymond, A., Boissonas, J., Talbert, J.-C., Feys, R., Raynal, J.-P., David, L., Bonfils, P., and Barruol, J., 1976, Notice explicative de la feuille Brive-la-Gaillarde à 1/50.000è.
Li, X., Arai, H., Shimoda, I., Kuraishi, H., and Katayama, Y., 2008, Enumeration of Sulfur-Oxidizing Microorganisms on Deteriorating Stone of the Angkor Monuments, Cambodia: Microbes and Environments, v. 23, p. 293–298, http://doi:10.1264/jsme2.ME08521.
Marincea, Ş., Dumitraş, D.G., Diaconu, G., and Fransolet, A.-M., 2012, Mineralogical data on the bat guano deposit from Gura Ponicovei cave (Almaj Mountains, Romania): Romanian Journal of Earth Science.
Marincea, S., Dumitras, D.-G., Dianocu, G., and Bilal, E., 2004, Hydroxylapatite, brushite and ardealite in the bat guano deposit form Pestera Mare de la Meresti, Persani Mountains, Romania: Neues Jahrbuch für Mineralogie - Monatshefte, v. 10, p. 464–488.
Marincea, S., Dumitras, D., and Gibert, R., 2002, Tinsleyite in the "dry" Cioclovina Cave (Sureanu Mountains, Romania): the second occurrence: European Journal of Mineralogy, v. 14, p. 157–164, http://doi:10.1127/0935-1221/2002/0014-0157.
Martini, J.E., and Kavalieris, I., 1976, Mineralogy of Transvaal cave formations: South African Speleological Association Bulletin, v. 17, p. 11–12.
McLafferty, F.W., 1959, Mass spectrometric analysis. Molecular rearrangements: Analytical Chemistry, v. 31, p. 82–87.
Mizutani, H., McFarlane, D.A., and Kabaya, Y., 1992, Carbon and Nitrogen Isotopic Signatures of Bat Guanos as Record of Past Environments: Journal of the Mass Spectrometry Society of Japan, v. 40, p. 67–82, http://doi:10.5702/massspec.40.67.
Monge, G., Jimenez-Espejo, F.J., García-Alix, A., Martínez-Ruiz, F., Mattielli, N., Finlayson, C., Ohkouchi, N., Sánchez, M.C., de Castro, J.M.B., Blasco, R., Rosell, J., Carrión, J., Rodríguez-Vidal, J., and Finlayson, G., 2015, Earliest evidence of pollution by heavy metals in archaeological sites: Scientific Reports, v. 5, http://doi:10.1038/srep14252.
Nieves-Rivera, Á., Santos-Flores, C., Dugan, F., and Miller, T., 2009, Guanophilic fungi in three caves of southwestern Puerto Rico: International Journal of Speleology, v. 38, p. 61–70, http://doi:10.5038/1827-806X.38.1.7.
Onac, B.P., Ettinger, K., Kearns, J., and Balasz, I.I., 2005, A modern, guano-related occurrence of foggite, CaAl(PO4)(OH)2·H2O and churchite-(Y), YPO4·2H2O in Cioclovina Cave, Romania: Mineralogy and Petrology, v. 85, p. 291–302, http://doi:10.1007/s00710-005-0106-4.
Onac, B.P., Mylroie, J.E., and White, W.B., 2001, Mineralogy of cave deposits on San Salvador Island, Bahamas: Carbonates and Evaporites, v. 16, p. 8–16, http://doi:10.1007/BF03176222.
Onac, B.P., Sumrall, J., Mylroie, J.E., and Kearns, J., 2009, Cave Minerals of San Salvador Island, Bahamas: University of South Florida Tampa Library.
Onac, B.P., and Vereş, D.Ş., 2003, Sequence of secondary phosphates deposition in a karst environment: evidence from Măgurici Cave (Romania): European Journal of Mineralogy, v. 15, p. 741–745, http://doi:10.1127/0935-1221/2003/0015-0741.
Parker, D.I., Lawhead, B.E., and Cook, J.A., 1997, Distributional Limits of Bats in Alaska: Arctic, v. 50, p. 256–265.
Paul, E.A., 2007, Soil microbiology, ecology, and biochemistry: San Diego, California, USA, Academic Press.
Perrenoud, C., 1993, Origine et mise en place des paragenèses phosphatées de remplissages karstiques quaternaires. Etude micromorphologique des sédiments de la Caune de l'Arago (Tautavel, Pyrénées-Orientales) et de la Baume Bonne (Quinson, Alpes-de-Haute-Provence) [PhD dissertation]: Paris.
Puşcaş, C.M., Kristaly, F., Stremţan, C.C., Onac, B.P., and Effenberger, H.S., 2014, Stability of cave phosphates: Case study from Liliecilor Cave (Trascău Mountains, Romania): Neues Jahrbuch f??r Mineralogie - Abhandlungen: Journal of Mineralogy and Geoche, v. 191, p. 157–168,

http://doi:10.1127/0077-7757/2014/0254.

Queffelec, A., Lenoble, A., and Lebraud, E., 2011, Remplissage des cavités de Guadeloupe : caractérisation par diffraction des rayons X pour une meilleure connaissance des environnements passés, *in* 9ème colloque Rayons X et Matière, Tours, http://doi:10.13140/RG.2.2.12635.98084.

Quénéa, K., Derenne, S., González-Vila, F.J., González-Pérez, J.A., Mariotti, A., and Largeau, C., 2006, Double-shot pyrolysis of the non-hydrolysable organic fraction isolated from a sandy forest soil (Landes de Gascogne, South-West France): Comparison with classical Curie point pyrolysis: Journal of Analytical and Applied Pyrolysis, v. 76, p. 271–279, http://doi:10.1016/j.jaap.2005.12.007.

Řezanka, T., 1989, Very-long-chain fatty acids from the animal and plant kingdoms: Progress in Lipid Research, v. 28, p. 147–187, http://doi:10.1016/0163-7827(89)90011-8.

Řezanka, T., and Mareš, P., 1987, Unusual and very long-chain fatty acids produced by Basidiomycetes: Journal of Chromatography A, v. 409, p. 390–395, http://doi:10.1016/S0021-9673(01)86818-7.

Rietveld, H., 1969, A profile refinement method for nuclear and magnetic structures: Journal of applied Crystallography, v. 2, p. 65–71.

Rinaudo, C., and Abbona, F., 1988, A contribution to the study of the crystal chemistry of calcium sulfate phosphate hydrate: Mineralogical and Petrographica Acta, v. 31, p. 95–105.

del Río, J.C., and Hatcher, P.G., 1998, Analysis of aliphatic biopolymers using thermochemolysis with tetramethylammonium hydroxide (TMAH) and gas chromatography–mass spectrometry: Organic Geochemistry, v. 29, p. 1441–1451, http://doi:10.1016/S0146-6380(98)00070-9.

Rodríguez-Vidal, J., d'Errico, F., Pacheco, F.G., Blasco, R., Rosell, J., Jennings, R.P., Queffelec, A., Finlayson, G., Fa, D.A., López, J.M.G., Carrión, J.S., Negro, J.J., Finlayson, S., Cáceres, L.M., et al., 2014, A rock engraving made by Neanderthals in Gibraltar: Proceedings of the National Academy of Sciences, v. 111, p. 13301–13306, http://doi:10.1073/pnas.1411529111.

Royer, A., Malaizé, B., Lécuyer, C., Queffelec, A., Charlier, K., Caley, T., and Lenoble, A., 2017, A high-resolution temporal record of environmental changes in the Eastern Caribbean (Guadeloupe) from 40 to 10 ka BP: Quaternary Science Reviews, v. 155, p. 198–212, http://doi:10.1016/j.quascirev.2016.11.010.

Sakae, T., and Sudo, T., 1975, Taranakite from the Oniwo-Iwaya cave at Hiroshima Prefecture, Japan: a new occurence: American Mineralogist, v. 60, p. 331–334.

Shahack-Gross, R., Berna, F., Karkanas, P., and Weiner, S., 2004, Bat guano and preservation of archaeological remains in cave sites: Journal of Archaeological Science, v. 31, p. 1259–1272, http://doi:10.1016/j.jas.2004.02.004.

Stahl, P.D., and Klug, M.J., 1996, Characterization and differentiation of filamentous fungi based on fatty acid composition: Applied and Environmental Microbiology, v. 62, p. 4136–4146.

Stankiewicz, B.A., Briggs, D.E.G., Evershed, R.P., Flannery, M.B., and Wuttke, M., 1997, Preservation of Chitin in 25-Million-Year-Old Fossils: Science, v. 276, p. 1541–1543, http://doi:10.1126/science.276.5318.1541.

Stankiewicz, B.A., Poinar, H.N., Briggs, D.E.G., Evershed, R.P., and Poinar, G.O., 1998, Chemical preservation of plants and insects in natural resins: Proceedings of the Royal Society B: Biological Sciences, v. 265, p. 641–647.

Tegelaar, E.W., De Leeuw, J.W., and Holloway, P.J., 1989, Some mechanisms of flash pyrolysis of naturally occurring higher plant polyesters: Journal of Analytical and Applied Pyrolysis, v. 15, p. 289–295.

Weiner, S., Goldberg, P., and Bar-Yosef, O., 2002, Three-dimensional distribution of minerals in the sediments of Hayonim Cave, Israel: diagenetic processes and archaeological implications: Journal of Archaeological Science, v. 29, p. 1289–1308.

Whitney, D.L., and Evans, B.W., 2010, Abbreviations for names of rock-forming minerals: American mineralogist, v. 95, p. 185–187.

Wurster, C.M., Munksgaard, N., Zwart, C., and Bird, M., 2015, The biogeochemistry of insectivorous cave guano: a case study from insular Southeast Asia: Biogeochemistry, v. 124, p. 163–175, http://doi:10.1007/s10533-015-0089-0.

Wurster, C.M., Patterson, W.P., McFarlane, D.A., Wassenaar, L.I., Hobson, K.A., Athfield, N.B., and Bird, M.I., 2008, Stable carbon and hydrogen isotopes from bat guano in the Grand Canyon, USA, reveal Younger Dryas and 8.2 ka events: Geology, v. 36, p. 683–686, http://doi:10.1130/G24938A.1.

Zukal, J., Pikula, J., and Bandouchova, H., 2015, Bats as bioindicators of heavy metal pollution: history and prospect: Mammalian Biology - Zeitschrift für Säugetierkunde, v. 80, p. 220–227, http://doi:10.1016/j.mambio.2015.01.001.

D. Medville. Speleogenesis of caves in a cretaceous shale: Bighorn Basin, Wyoming. *Journal of Cave and Karst Studies*, v. 80, no. 2, p. 1-15.
DOI: 10.4311/2017ES0121

SPELEOGENESIS OF CAVES IN A CRETACEOUS SHALE: BIGHORN BASIN, WYOMING

Douglas M. Medville[1]

Abstract

Blind valleys, aligned dolines, and openings leading to 50 to 70 m long, linear caves, developed entirely within the lower Cretaceous Cody Shale, are found along the west flank of a 150 m high and 7 km long ridge on the eastern side of the Bighorn Basin in north-central Wyoming. Precipitation events on a swelling soil allow water and oxygen to reach the shale a few meters below the surface and to react with pyrite in the shale. Microbially-assisted oxidation of the pyrite, possibly by *Acidithiobacillus ferrooxidans*, produces sulfuric acid that reacts with calcite in the shale, resulting in gypsum fracture fillings, observed as 2 to 4 cm thick beds on cave walls and sub-mm-diameter deposits within shale beds. Evidence for pyrite oxidation is provided by the presence of a ferric oxyhydroxide (goethite) as a by-product, visible as brown fillings on cave walls, confirmed by XRD. Stable sulfur isotope analysis, using gypsum samples taken from fracture fillings in the caves, was conducted with negative values for $\delta^{34}S$ obtained (versus positive values for marine sulfate), providing additional evidence for pyrite as the source of sulfur in the gypsum. This was confirmed by SEM imaging of shale samples. These samples showed gypsum inclusions in the shale, biofilm-coated, framboidal pyrite pseudomorphs, and iron oxyhydroxide residue remaining on the framboidal surfaces, evidence for pyrite oxidation. The 2× molar-volume increase, resulting from calcite re-crystallization to gypsum and subsequent growth of gypsum crystals, leads to fracturing and separation of individual shale beds, reducing the structural integrity of the shale. Dissociated shale beds along passage walls and rubble slopes of decomposed shale beneath the walls are evidence of shale decomposition. Subsequent dissolution of gypsum by meteoric water moving through beds and fractures in the shale results in the creation of small, localized voids. When wetted, the shale decomposes into micron-scale particles that are removed by episodic water flowing downslope. Sapping occurs at the places where sediment-laden water emerges, creating openings that progress headward. As material is removed on a grain-by-grain basis by corrasion, the small voids coalesce into more integrated spaces, ultimately permitting human entry.

Geological Setting

The Bighorn Basin is a large, intermontane basin in north-central Wyoming and south-central Montana, encompassing an area of nearly 27,000 km^2 and bounded by the Bighorn Mountains to the east, the Absaroka Mountains to the west, and the Owl Creek mountains to the south. Anticlines and synclines encircle the basin, with numerous faults and anticlines found along the basin's eastern shoulder, these containing several small oil fields. The center of the basin is composed of Tertiary (Eocene and Paleocene) sediments, while the surrounding shoulder of the basin consists mostly of Cretaceous and Jurassic rock. The area is semi-arid with mean annual rainfall and snowfall of 17.5 cm and 46 cm, respectively.

A pseudokarst surface containing dolines, blind valleys, and caves is developed on a 150 m high, 7 km long ridge on the 78 to 83 Ma late Cretaceous Cody Shale. The area is on U.S. Bureau of Land Management property and is 10 km SE of Greybull, Wyo., in the eastern part of the Bighorn Basin (Fig. 1). Structurally, the area is in a small syncline, between the Torchlight Dome anticline to the west and the Lamb anticline to the east; local dip is 2° to 5° ESE as shown in Figure 2 (Pierce, 1948).

Locally, the Cody Shale is about 1150 m thick and consists of marine shale, sandstone, and siltstone. The unnamed lower member of the Cody Shale is about 360 m thick and consists of a dark gray to black, thin-bedded, marine shale, composed of "gray to black shale, calcareous shale, and bentonite, with minor amounts of siltstone and sandstone that were deposited in an offshore environment" (Finn, 2013). Based on the structure contours in Figure 3, drawn on the base of the Cody Shale, the area containing caves is in non-calcareous shales about 100 m above the base of the Cody Shale.

Soils on the cave ridge are classified as U.S. Department of Agriculture (USDA) soil map unit 371AD, Greybull-Persayo complex, 0−30% slope. The soil is described as "side slope residuum weathered from shale," consisting of a silty, clay loam for 23 to 28 cm depth to paralithic bedrock beneath (USDA, 2017). The description of the underlying bedrock as paralithic is consistent with the observed nature of wall material seen in the caves: partially weathered and requiring only a moderate force to be broken into smaller fragments.

While a majority of the dolines and blind valleys are sediment choked, 19 enterable caves, up to 70 m long, have been observed in nine of 17 drainage basins examined. The caves are found in dolines (Fig. 4) and at the ends of

[1]10701 Pinewalk Way, Highlands Ranch CO 80130, medville@centurylink.net

Figure 1. Shale cave study area location.

and are not shelters are unusual since dissolution of shale by carbonic or sulfuric acid does not take place in the absence of carbonates. Palmer (2007) states: "Shale does not dissolve perceptibly, but it erodes easily. Its main contribution to speleology is to form shelter caves capped by more resistant rocks." The presence of linear cave passages extending into darkness for distances of up to 70 m (Figs. 6 and 7) appears to be unusual and resulted in this investigation.

Methods

Bulk mineral analysis of cave wall material was conducted using a Pananalytical X'Pert Pro X-Ray Diffraction (XRD) diffractometer for powder XRD analysis. Continuous scans over a 40-minute period were carried out between 6° and 69° 2θ positions with a step size of 0.017°. Counting peaks provided a semi-quantitative measure of mineral components in the sam-

blind valleys (Fig. 5). Maps of two of the longer caves are shown in Figures 6 and 7. The caves are linear, contain stream channels in their floors, and are characterized by gypsum-streaked and gypsum-wedged shale walls. Linear rubble piles, composed of broken and decomposed shale, are found beneath the passage walls.

The caves are developed entirely within the shale, and they have bedrock walls and ceilings covered, in part, by a thin veneer of decomposed shale (clay) as shown in Figure 8. In this image, the arched gray strip across the ceiling is the shale, exposed by removal of the clay coating. Figure 9 illustrates the entrance passage of another cave showing a rubble floor and triangular cross-section.

Enterable caves in non-calcareous shale that contain stream channels in their floors

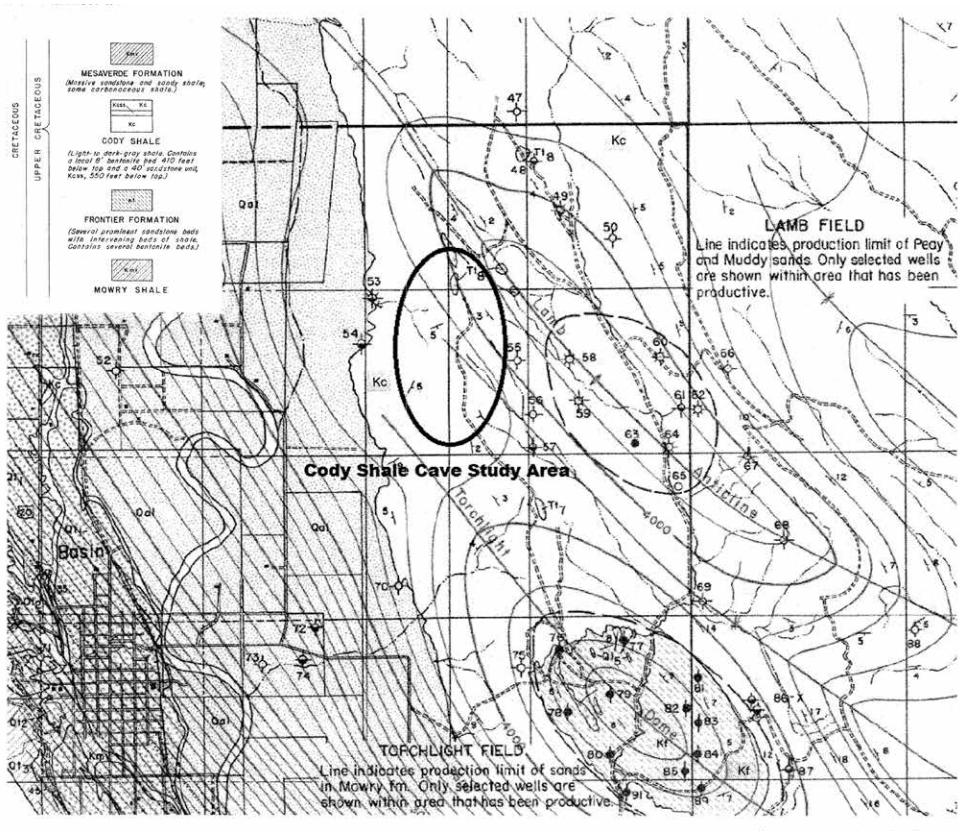

Figure 2. Structure contour map of study area. Contours on base of Cody Shale/top of the Frontier Formation.

Figure 3. Cody Shale pseudokarst east of Basin, Wyoming.

Figure 4. Cave entrance in doline on weathered Cody Shale.

ples with peak intensities, which were used to determine the relative mineral proportions.

Scanning electron microscopy (SEM), using a Tescan Vega 3 SEM coupled with an IXRF Systems silicon drift X-ray detector (XRD) for elemental analysis, was applied to examine gypsum, framboidal pyrite pseudomorphs, and biofilms found on the shale at 5μm−10μm scales. X-ray counting peaks on Energy Dispersive Spectroscopy (EDX), results were consistent with those seen in XRD diffractograms for minerals of interest: gypsum and goethite. Stable sulfur isotope measurements were conducted using a Costech Instruments Elemental Analyzer (CHNS-O ECS 4010) coupled to an Isochrom Continuous Flow Stable Isotope Ratio Mass spectrometer. $\delta^{34}S$ results, with respect to the Canyon Diablo Troilite meteorite standard, were reported in per mil (‰) units.

Process Initiation

As noted, the surface above the caves contains blind valleys, entrances, pits, and dolines. These features are the same as those found in karst terranes, but the processes involved differ: corrasional removal of study area material versus carbonate rock dissolution.

Soil samples were taken at cave entrances and from the cave floor and sent to the Soil Testing Laboratory at Colorado State University. These samples were analyzed for three measures of the soil propensity to swell, and by inference, to allow surface water to move downward reaching the unweathered shale. Tests were conducted to determine the exchangeable sodium percentage (ESP), the sodium adsorption ratio (SAR), and the soil's cation exchange capacity (CEC), a measure of the ability of wetted cations, adsorbed on clay surfaces, to be exchanged with other cations.

ESP (i.e., the percentage of cations that are sodium) was 8.4%, lower than the 15% expected for sodic soils (Parker and Higgins, 1990). SAR, defined as $Na/[0.5(Ca+Na)]^{1/2}$, another measure of sodicity, is an indicator of the soil's susceptibility to develop pipes. For the samples tested, SAR was 7.3 meq/L, slightly higher than the minimum of 5.0 meq/L expected for soils subjected to piping failure (Parker and Higgins, 1990). Finally, CEC, determined by measuring the ratio of each cation quantity to that cation's equivalent weight, summing the ratios, and converting the result to meq/100g, was 17.6. The range of CECs for sodium montmorillonite is 60 to 150 meq/100g (Carroll, 1959; Soil Quality Organization, 2017), substantially higher than the mean CEC for the soil samples tested, since the montmo-

Figure 5. Entrance at the lower end of a blind valley.

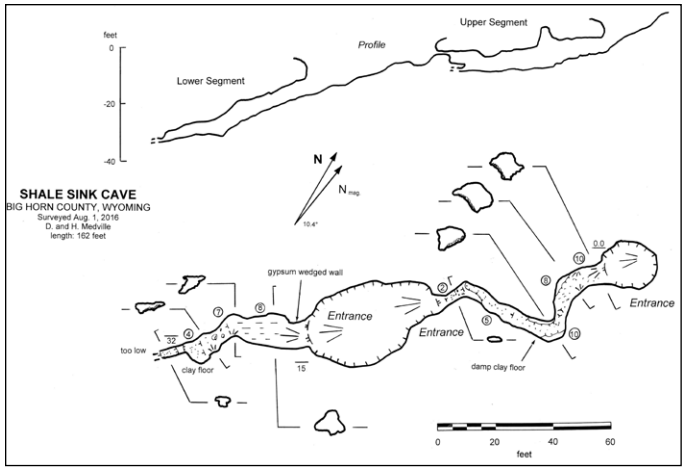

Figure 6. Segmented cave in shale.

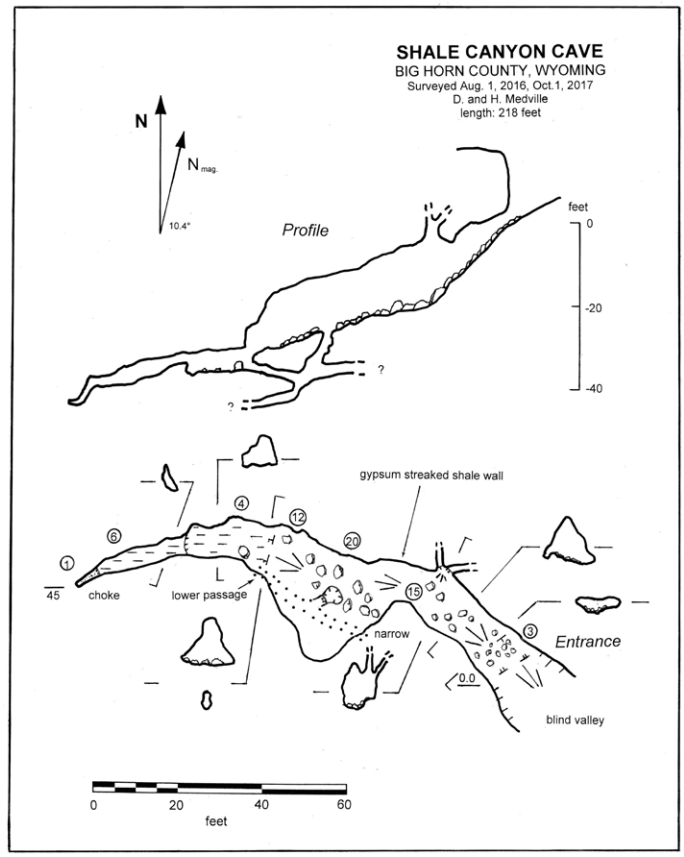

Figure 7. Cave below blind valley.

Figure 8. Ceiling of a cave in the Cody Shale showing exposed shale.

rillonite content of the eroded shale at cave entrances is only on the order of 15 % to 20 %. Consequently, the CEC for this material should be correspondingly lower than for soils having a higher concentration of montmorillonite. For samples of the Cretaceous Mancos Shale in western Colorado that contain similar quantities (20 to 40 meq/100g) of smectite-family clays, "the cation exchange capacity of weathered Mancos Shale samples ranged from 13.14 to 25.15 meq/g" (U.S. Department of Energy, 2011), consistent with the 17.6 meq/100g value obtained for the eroded Cody Shale sample.

The tests indicate that the weathered Cody Shale on the surface above the caves has a modest swell potential since the mean montmorillonite content in the two shale samples from cave walls was only 17 %. However, this is an amount sufficient to allow soil swell/shrink cycles to take place and to produce the landforms observed. The resulting openings provide a means for oxygen to reach the shale. Water can also reach the shale through normal fluvial processes (erosion and deepening of gullies) and via inter-pore vertical movement through the regolith. Downward diffusion of reactive O_2, carried in solution by water moving through the unsaturated zone in the shale, results in the oxidation of pyrite in the shale.

Figure 9. Passage cross-section showing rubble floor.

Table 1. Composition of wall material in shale caves.

Location	Quartz, %	Muscovite, %	Montmorillonite and Kaolinite, %
Shale Sink Cave, upper segment	35	41	21
Shale Sink Cave, lower segment	44	37	17
Shale Canyon Cave	34	42	20

Shale Composition

Samples of the wall material were taken in three of the caves and sent to the New Mexico Bureau of Geology for a bulk mineral analysis using powder X-Ray diffraction. The composition of the wall samples is shown in Table 1.

The composition for the samples is nearly the same: predominantly quartz and muscovite (mica) with moderate quantities of montmorillonite and kaolinite. Remaining material consisted of minor quantities of dolomite and gypsum (1 % to 3 % of each). Calcite, if present, was below detection limits of 2 % by weight. Sodium montmorillonite, a swelling, smectite-family clay in the shales sampled, is the primary constituent of bentonite, a swelling clay that is mined locally from beds in the Cody Shale. The presence of montmorillonite in the shale is consistent with the pseudokarst surface observed above the caves: desiccation cracks, a popcorn-like surface on the soil, small pits, dolines, and blind valleys as illustrated in Figures 4 and 5.

Pyrite Oxidation

A variety of well-documented, pyrite weathering pathways exist (Penner, et al., 1972; Hoover, et al., 2004). Under aerobic conditions, the chemolithoautotrophic bacterium *A. ferrooxidans* uses pyrite (FeS_2) as an electron donor and oxidizes it into ferric iron and sulfuric acid. This takes place in two steps as per reactions (1) and (2) below.

Oxidation of iron sulfide to ferrous sulfate and sulfuric acid:

$$2FeS_2 + 2H_2O + 7O_2 \rightarrow 2FeSO_4 + 2H_2SO_4 \quad (1),$$

followed by conversion from ferrous to ferric sulfate, where the bacteria increase the ferrous oxidation rate by five to six orders of magnitude “and thereby makes pyrite oxidation a rapid self-perpetuating process” (Nordstrom, 1982)

Figure 10. Tan beds containing goethite in cave wall. Length of scale bar is 15 cm.

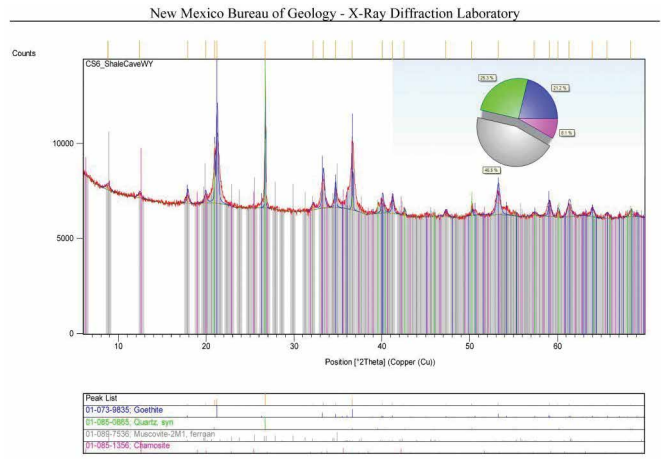

Figure 11. Diffractogram for goethite-containing cave wall material.

$$4FeSO_4 + O_2 + 2H_2SO_4 \rightarrow 2Fe_2(SO_4)_3 + 2H_2O \quad (2).$$

For low pH (e.g., ≤ 3) this is followed by the reaction of ferric sulfate with additional, unreacted pyrite, to yield additional ferrous sulfate and sulfuric acid:

$$7Fe_2(SO_4)_3 + FeS_2 + 8H_2O \rightarrow 15FeSO_4 + 8H_2SO_4 \quad (3).$$

As the pH increases above 3, solids will precipitate and the reaction is

$$Fe_2(SO_4)_3 + 6H_2O \rightarrow 2Fe(OH)_3 + 3H_2SO_4 \quad (4),$$

yielding ferric hydroxide and sulfuric acid.[2] The dehydration of the ferric hydroxide yields goethite, a solid ferric oxyhydroxide, resulting from the oxidation of iron-rich sulfide minerals,

$$Fe(OH)_3 \rightarrow FeO(OH) + H_2O \quad (5).$$

A summary reaction for pyrite oxidation, skipping the intermediate steps, with goethite and sulfuric acid as reaction products, is given in Taylor and Eggleton, (2001):

$$4FeS_2 + 15O_2 + 10H_2O \rightarrow 4FeO(OH) + 8H_2SO_4 \quad (6).$$

Macroscopic evidence for goethite as a reaction product is provided by thin stringers and small masses of a yellow-tan material, observed on the shale cave walls, as illustrated in Fig. 10. X-Ray diffraction of a sample of this material indicates that a majority (71 %) of the material is quartz and muscovite (mica), and a substantial component (21.2 %) is goethite (Fig. 11). The 2θ peaks at 21°, 33°, 36°, and 41° are those seen in diffractograms for pure goethite (RRUFF database, 2017).

A graphic summary of the overall sequence of reactions for microbially-assisted pyrite oxidation, resulting in sulfate ions and goethite, is shown in Figure 12, and is reproduced from figure 3 in Nordstrom (1982) with the reaction pathway highlighted. Nordstrom describes this figure as "the grand sequence of reactants, products, and catalysts for pyrite oxidation." Note that in 2000, *T. ferrooxidans,* referred to in Figure 12, was reclassified as *Acidithiobaccillus ferrooxidans* (Kelly and Wood, 2000) and the *A. ferrooxidans* genus/species terminology is used in this paper.

Conversion to Gypsum

Sulfuric acid resulting from pyrite oxidation will react with calcite in the shale to produce gypsum, water, and CO2, with one mole of calcite being replaced by one mole of gypsum:

$$CaCO_3 + H2SO_4 + 2H_2O \rightarrow CaSO_4 \cdot 2H_2O + H_2O + CO_2 \quad (7).$$

Evidence for pyrite-derived gypsum deposition in the Cody Shale caves is provided by the presence of numerous fibrous, gypsum fracture fillings, 1 to 3 cm thick, observed on cave walls (Fig. 13). This is consistent with the obser-

[2]Other reactions that yield sulfuric acid, sulfate ions, and ferric hydroxide from pyrite oxidation are:
$4FeS_2 + 14H_2O + 15O_2 \rightarrow 4Fe(OH)_3 + 16H^+ + 8SO_4^+$
$FeS_2 + 15/4O_2 + 7/2H_2O \rightarrow Fe(OH)_3 + 2H_2SO_4$

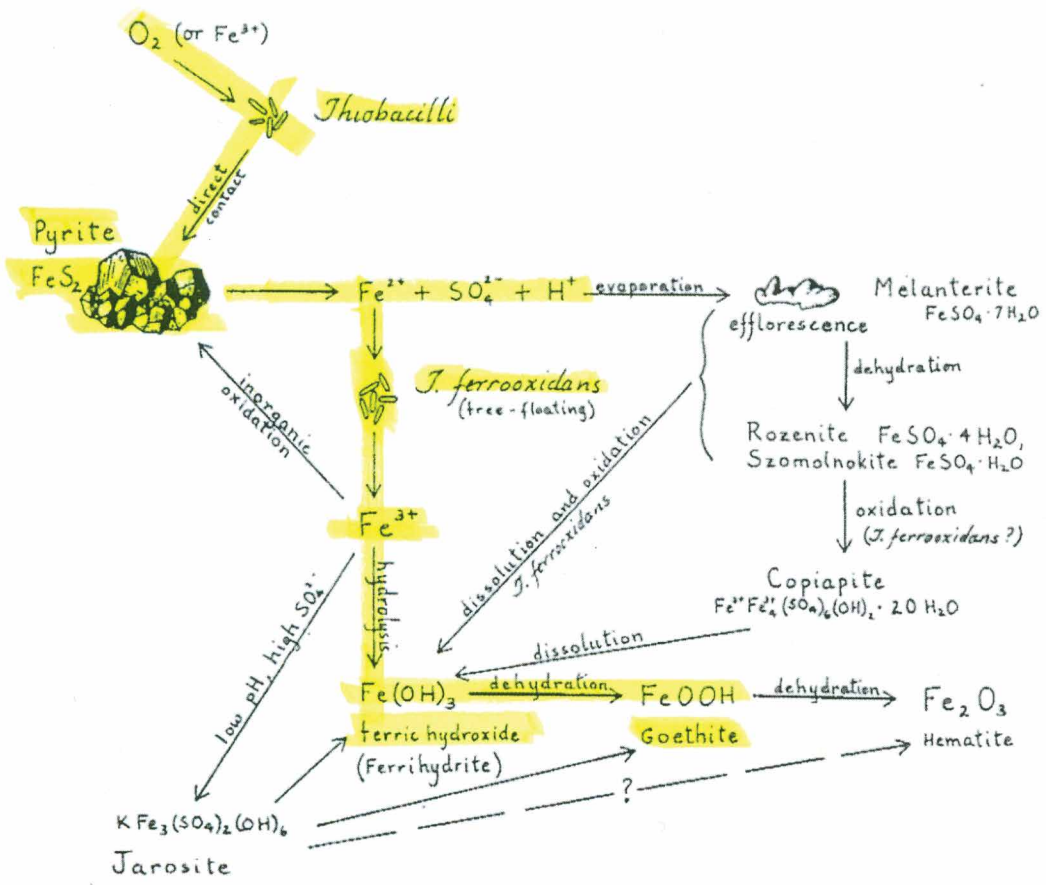

Fig. 3. The overall sequence of mineral reactions for pyrite oxidation showing the relationships between oxidizing agents, catalysts, and mineral products.

Figure 12. Summary of pyrite oxidation reactions (from Nordstrom, 1982).

Figure 13. Gypsum fracture fillings in passage wall.

vation that pyrite oxidation is local, and that the resulting gypsum commonly concentrates along certain beds or bedding-plane partings (Palmer, 2007).

The concentrated gypsum fracture fillings observed between layers in the shale, i.e., crystallization in bedding plane partings, as illustrated in Figures 13 and 14, is consistent with a pyrite oxidation source of sulfate ions, resulting in replacement of calcite by gypsum. Other evidence for pyrite as a source, e.g., halos of gypsum around oxidized pyrite grains and staining of the gypsum by iron oxides, has not been observed, however.

The source of the sulfur in the gypsum can be determined via stable sulfur isotope analysis by computing the deviation of the $^{34}S/^{32}S$ isotope ratio from the standard ratio of 0.045005, obtained from troilite in the Canyon Diablo meteorite (Thode, 1991).

$$\delta^{34}S = 1000 \times [(^{34}S/^{32}S)_{sample} / (^{34}S/^{32}S)_{standard} - 1]‰ \quad (8)$$

Three potential sources of sulfur exist:

Figure 14. Shale wall (left) with gypsum-wedged shale (right). Height and width are about 1 m.

Figure 15. Shale containing gypsum fracture fillings and goethite laminations.

(a) H2S from petroleum. The area containing the caves is 3 km NW of an active oil and gas field (Torchlight Dome). However, production is from Cretaceous sands, 152 m to 305 m (500 ft to 1000 ft) below the caves, with no H2S reported (Lupton, 1916). If petroleum is the source of the sulfur, $\delta^{34}S$ deviations on the order of 0 to +30 ‰ may be expected.

(b) Gypsum precipitated from sea water during deposition of the Cody Shale; i.e., ancient marine gypsum. Seawater sulfate from the Cretaceous is enriched in ^{34}S with respect to the standard. Positive $\delta^{34}S$ values of 19.0 ‰ to 19.5 ‰ were reported for Cretaceous seawater at ≈80 Ma (Paytan, A. et al., 2011); i.e., at the midpoint of the 78 to 83 Ma age range for the Cody Shale.

(c) Gypsum derived from pyrite. This gypsum will be light in ^{34}S with negative $\delta^{34}S$ values expected. For example, White (2015) states that deviations on the order of −1 to −5 "are in the range expected if the sulfur in the gypsum is derived from the oxidation of pyrite." Also, highly negative $\delta^{34}S$, compared to

Figure 16. Gypsum inclusions on shale surface, 1 mm background grid.

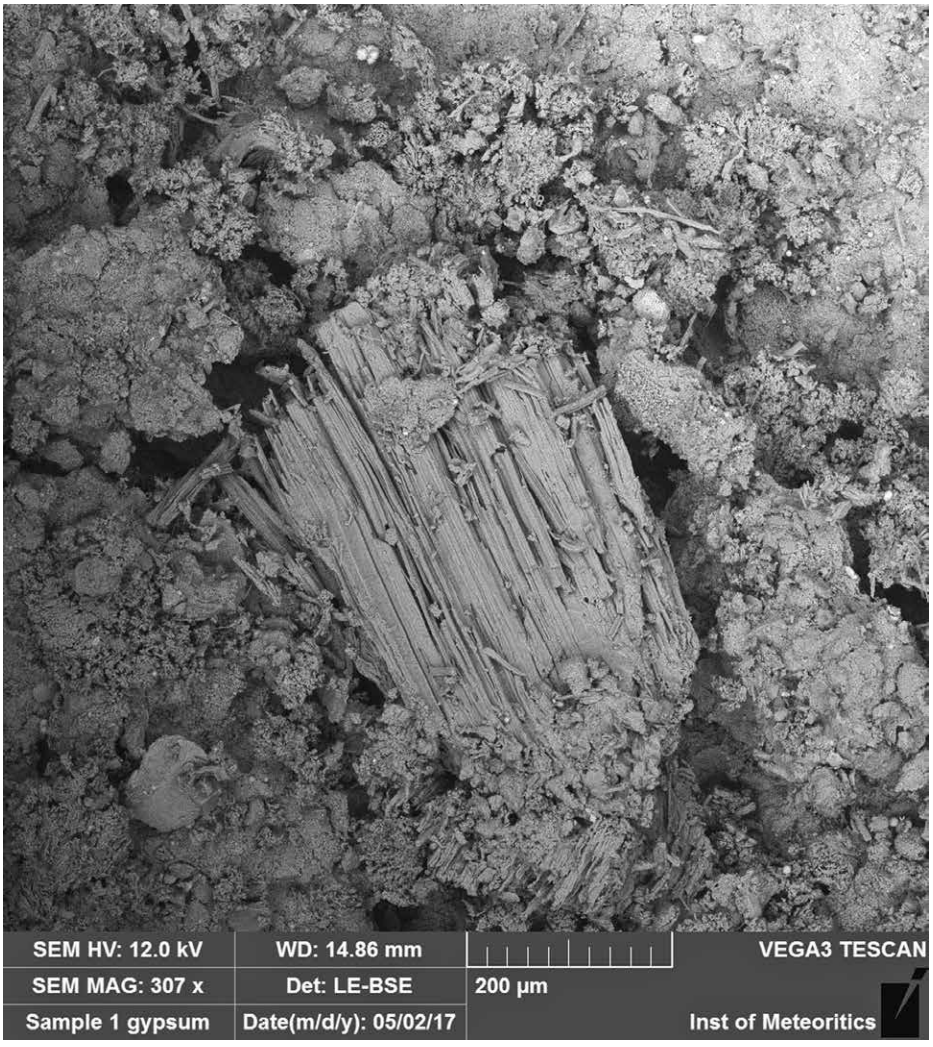

Figure 17. SEM image of gypsum on shale.

Permian-age gypsum beds in Carlsbad Cavern, is cited as evidence for the sulfur not being derived from marine gypsum (Palmer, 2007).

To determine the origin of the sulfur in the gypsum, samples were removed from fracture fillings in the walls of two caves, about 0.5 km apart. The samples were finely ground, and 50 mg of each sample was sent to the Environmental Isotope Laboratory at the University of Waterloo in Ontario, Canada for sulfur isotope analysis. Measured $\delta^{34}S$ values of −12.65 ‰ for one sample and −8.11 ‰ for the other were obtained, supporting the hypothesis that the sulfur in the gypsum samples was derived from pyrite. Pyrite was not detected in the shale or clay (eroded shale) samples analyzed via XRD. It either exists, but the quantities are below the limits of detection (1 % by weight), or, for the samples taken, all of the pyrite has been oxidized and is no longer present.

The hypothesis that all of the pyrite, and also all of the calcite in the shale, has been depleted is supported in a paper that analyzed the influence of weathering on pyrite oxidation and carbonate dissolution of a Silurian Shale in Pennsylvania as a function of depth beneath the regolith (Brantley, et al., 2013). Based on drill borings, the study proposed that the observed absence of carbonates and pyrite in fractured shale above the water table was a result of pyrite oxidation and carbonate dissolution reaction fronts in the shale by CO_2-charged fluids and H_2SO_4. The paper concluded that "Pyrite and carbonate depletion go to 100 % completion because the mineral abundances are generally low and the reactions fast relative to physical erosion of material; in contrast, clay mineral depletion is not complete at the land surface because clays are abundant and weathering rates are slow." This conclusion is consistent with the lack of detectable quantities of both pyrite and calcite in the shale wall samples taken for XRD analysis. However, the possibility exists that pyrite oxidation alteration products (i.e., pseudomorphs) may still exist in

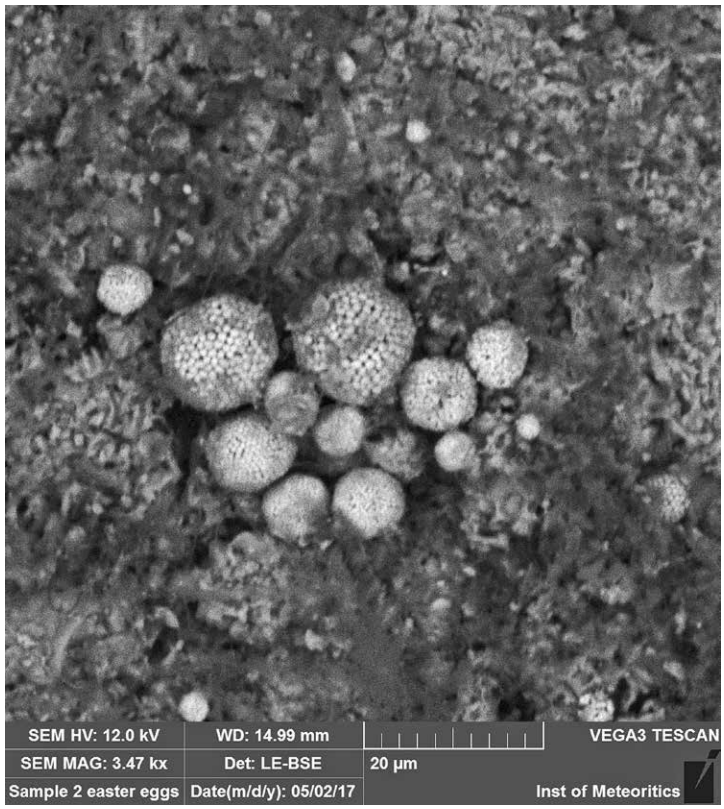

Figure 18. Framboidal pyrite pseudomorphs on shale surface.

the shale.

Microbial Influence on Pyrite Depletion and Replacement

To determine whether any pyrite or its reaction products still exist, samples of shale, observed to contain sub-mm scale, round, white inclusions, hypothesized to be starburst gypsum, were taken from the passage walls (Fig. 16) and separated into individual shale platelets.

The shale samples were analyzed at the Electron Microprobe and Scanning Electron Microscope Laboratories at the University of New Mexico using SEM imaging of the samples, coupled with energy dispersive spectroscopy (EDS) to identify the elemental composition of the constituents. As expected, the white inclusions were identified as gypsum (Fig. 17), with high-counting peaks for O, S, and Ca observed on the EDS results. In addition, framboidal pyrite pseudomorphs were also observed (Fig. 18). Results of the analysis of the elemental composition of the pseudomorphs, using EDS, are shown in Figure 19 with high-counting peaks for O and Fe, consistent with bacteria metabolizing the sulfur in the pyrite. The Fe is present as an oxyhydroxide, most likely goethite: FeO(OH), consistent with the brown deposits observed on passage walls (Fig. 10) and confirmed by XRD.

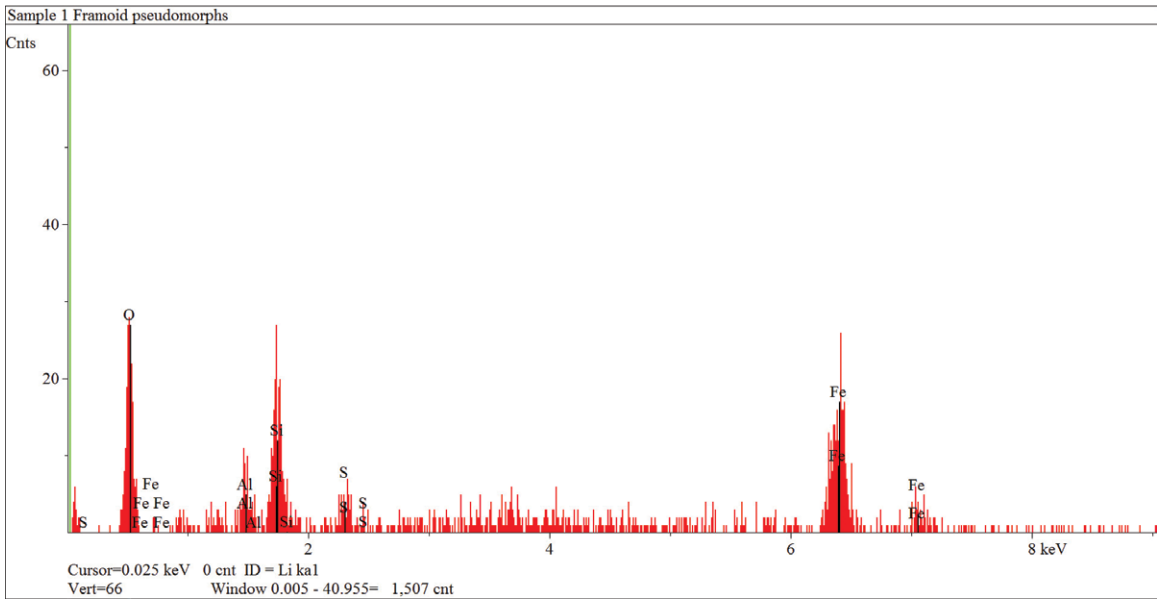

Figure 19. EDS counting peaks for framboidal pseudomorphs.

Many of the framboids are enclosed within material interpreted as an active biofilm, with bacterial stringers visible, as shown in Figures 20 and 21. Biofilm that coats pyrite has been described as "oxidizing bacteria attached to the pyrite surface in a matrix of extracellular, polymeric substances produced by the bacteria" (Crundwell, 1996). The biofilm observed via SEM matches that description and consists of "sub-micrometer cocci, smooth filaments, and chains of segmented bacteria" (Spilde, M., personal communication). If the biofilm is composed of *A. ferrooxidans*, then this is consistent with the observation that this bacteria oxidizes pyrite crystals by direct contact with the pyrite surface (Beck and Brown, 1968). To summarize, the SEM images provide support for the hypothesis that bacterially-assisted oxidation of pyrite in the shale has taken place.

Cave Development

As described above, the presence of smectite-family swelling clays enhances the transport of oxygen and surface water through the regolith to unweathered, fractured shale a few meters below. The resulting oxidation of pyrite

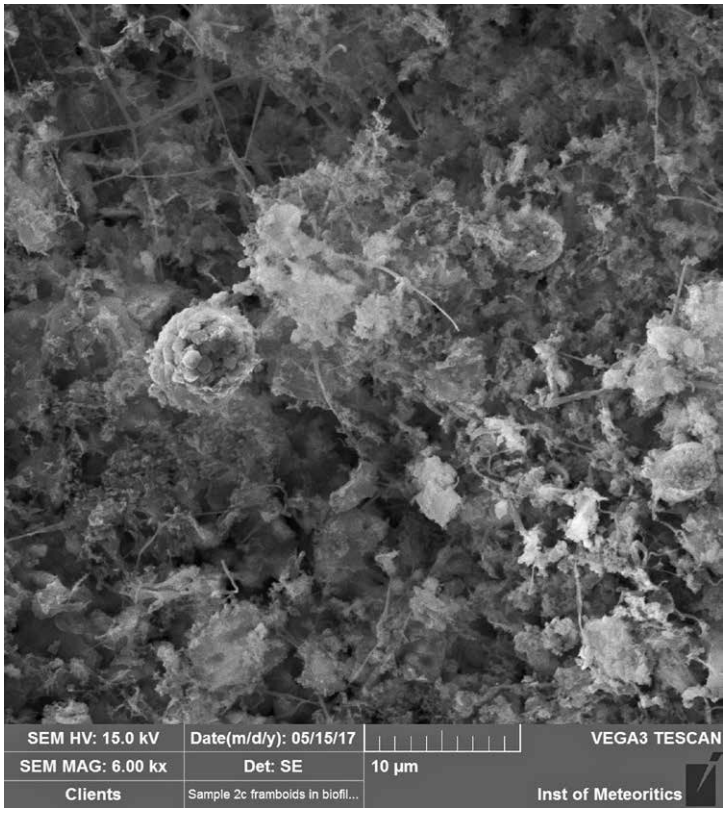

Figure 20. Framboidal pseudomorphs enclosed in biofilm with stringers.

in the shale leads to gypsum deposition and subsequent wedging apart of the shale beds. The conversion of calcite in the shale to gypsum results in a volume increase by a factor of about two (White and White, 2003, Penner et al., 1972), since the molar volume of gypsum, 74.14 cc/mol, is about twice that of calcite, 36.90 cc/mol[3].

Penner et al. (1972) states: "Although the volume increases by a factor of two, of greater importance is the force associated with the growth of gypsum crystals. Under ideal circumstances, this force can be extremely high ... resulting in much greater heave than would occur with simple volume expansion during formation." As the shale beds are forced apart, the secondary porosity of the shale increases, along with a loss of structural integrity, resulting from the separation of individual beds (Figs. 14 and 15). This process of heaving and fracturing of shale beds by gypsum, deposited along bedding and fracture planes, is described for the Cretaceous Mancos Shale in western Colorado (White and Greenman, 2008). A similar process is observed in the Cody Shale caves, formed in partially weathered, paralithic bedrock, where loose angular fragments and small blocks of shale, containing gypsum interbeds, can be removed from the wall by hand or with a rock hammer. These fragments form rubble slopes beneath the passage walls (Fig. 22).

Gypsum dissolution, leading to surface subsidence, has been documented in a variety of settings. For example, in Colorado, soil slumping, due to the dissolution of gypsum in the Pennsylvanian Eagle Valley evaporates, is described in White and Greenman, (2008): "dissolution of soluble soil constituents results in soil-mass loss and settlement of the ground surface." In a study conducted in Derbyshire, England, it was concluded that "chemical alteration of shale involving oxidation of pyrite, leaching of carbonates by sulphuric acid, formation of iron hydroxide minerals, and leaching of cations from clay minerals, is a rapid process that led to the collapse of a shale embankment" (Pye and Miller, 1990).

In the San Juan Basin, New Mexico, sandstone soil slumping in filled clastic pipes that result in down-dropped beds (in pipes up to 9 m in diameter) are described in Hunter, R.E. et. al. (1992). They state that the down-dropped beds "can form by localized dissolution of an evaporite body formed by solution collapse," and conclude: "we doubt that mechanisms other than solution-induced collapse could have created the space

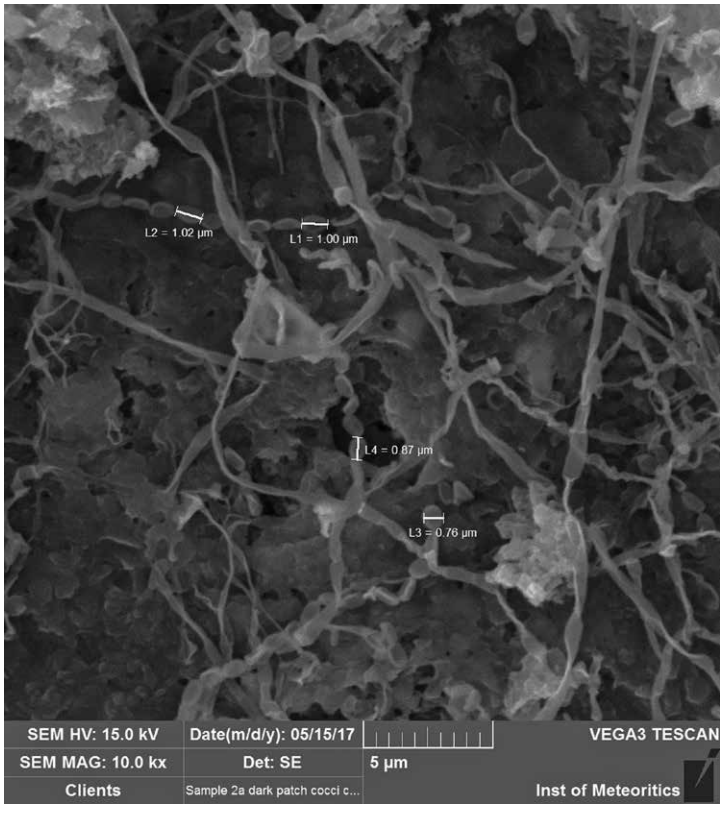

Figure 21. Cocci on bacterial stringers within biofilm.

[3]The molar volume of $CaSO_4 \cdot 2H_2O$ = 172 g/mol/2.32 g/cc = 74.137 cc/mol; 1 cc = .01349 mol. The molar volume of $CaCO_3$ = 100g/mol/2.71 g/cc = 36.9 cc/mol; 1cc = 0.0271 mol. One cc of $CaCO_3$ converts to (0.0271/0.01349) = 2.009 cc of $CaSO_4 \cdot 2H_2O$. In (Palmer, 2007, p. 335), a similar calculation is carried out for the conversion of pyrite to gypsum. The molar mass of FeS2 = 120 g/mol and the density of FeS2 = 5 g/cc; thus 1 cc of FeS2 = 0.04167 mol. Since one cubic centimeter of gypsum ≈ 0.01349 mol and one mole of pyrite converts to two moles of $CaSO_4 \cdot 2H_2O$, the conversion factor is 2 × (0.04167/.01349) = 6.178 (i.e., 1 cc of FeS_2 converts to 6.178 cc $CaSO_4 \cdot 2H_2O$).

Figure 22. Cave passage illustrating arched ceiling, damp cave floor and lateral rubble slope.

necessary for down dropping in the pipes."

None of these examples, however, describe conditions that are the same as observed in the Cody Shale caves in Wyoming, nor do they describe processes that led to the development of enterable cavities. However, it is argued that they are similar enough to provide some support for the sequence suggested in this paper. The closest analogue to what is observed in the Cody Shale caves is found in a report by White and Greenman, (2004) describing the development of openings in the Cretaceous Mancos Shale in western Colorado. The text states of that report states:

> "fractures in claystone have been infilled with crystalline gypsum. The Mancos Shale was deposited in a deep-water, reduced environment and contains significant amounts of disseminated pyrite. Within the weathered zone, oxidation of pyrite creates sulfuric acid that reacts with available calcite in the shale to form gypsum. The gypsum tends to crystallize along bedding and fracture planes in the shale. The volume change when calcite recrystallizes to gypsum and during further growth of gypsum crystals can heave the claystone, physically fracturing, splitting, and jacking it apart. Subsequent wetting of this 'jacked' claystone can result in the dissolution of the gypsum, micropiping erosion, and creation of subsurface voids... Water from rainfall and snowmelt dissolves the gypsum in the shale, creating small voids, removing the broken/heaved shale fragments via corrasion."

A similar process appears to be taking place in the Cody Shale caves. Following the separation of shale beds from gypsum wedging, secondary porosity increases, allowing vadose water to flow through the spaces between the disassociated shale. When the water reaches an outlet point down-gradient on the hillside, sapping takes place with corrasional removal of particles and gradual opening of a void. As water continues to remove material, this void progresses headward with a proto-passage opening in an upstream direction, similar to passage enlargement in soil piping caves. Parker (1990) described this as "seepage-face erosion":

> "water begins to seep from the bed at the point of highest permeability or lowest elevation in the face of the slope. As water leaves the slope, it carries away disaggregated and dispersed silt particles in suspension. This action initially creates a small orifice for the developing pipe in the cliff face."

Micron-scale clay particles, quartz grains, and other clastics are washed out by precipitation events. Given sufficient precipitation, this can take place fairly rapidly, resulting in a passage containing shale walls and ceiling, and a sediment floor consisting of a mix of clay, quartz, goethite, and other material. The shale walls tend to slough off as a result of continued gypsum wedging, leaving lateral ridges of broken shale paralleling the passages. Cantilevered ceiling blocks fall to the floor with the ceilings gradually stoping upward toward the center of the passage until structural stability is reached with

an arched ceiling remaining, as shown in Figure 22. As water flows intermittently through the passage, a wetted, floor channel develops, also shown in Figure 22. A 0.3 m deep test pit, dug in a channelized floor (Fig. 23), revealed a transition from a bedrock wall to a damp matrix, most likely resulting from the disaggregation of spalling-shale wall material, as well as surface material washed in by precipitation events. The floor material, determined via XRD, consisted of 76 percent quartz, 6 percent gypsum, and a mix of chamosite and albite.

Figure 23. Test pit in cave passage floor showing transition from bedrock wall to damp, firm material.

Clay particles were absent, perhaps indicating that material in the one- to five-micron range had been removed by flowing water, leaving larger particles to settle in the floor. In a paper on sediment transport in limestone caves, White and White (1968) write that "when very small particles in the clay and silt size-range are in suspension, it takes a long time for the material to fall out, and the load can be transported a long way before the water clears." A general relationship between the horizontal transport of material per unit of fall, expressed in feet per feet, and channel velocity, in feet per second for various grain sizes, is given in Figure 8 of that paper. Using that figure, for a conservative velocity of 0.03048 m/s (0.1 ft/s) and a grain size of 1 μm, typical of clay particles, the horizontal transport distance is somewhat over 305 m/m of fall (1000 ft/ft of fall. This is sufficient for particles to remain in suspension for the distances observed between sink points and resurgences, typically on the order of tens of meters (hundreds of feet).

Cave Evolution

The processes described above take place over time but the rate at which caves develop and enlarge is not known. Two scenarios can be given:

1. The caves develop and enlarge quickly, but intermittently. Intense precipitation events, while infrequent, do occur. When this happens, sufficient water can move through the caves in short time periods to quickly enlarge proto-passages through wall scouring and corrasional removal of material, similar to suffosional soil piping cave processes. When immersed in water, the shale rapidly decomposes into clay particles. Gypsum-fractured shale in an environment where passages or proto-passages are immersed in storm waters should also decompose, allowing passages to rapidly enlarge. These events are interspersed with much longer time periods of low precipitation, when little or no passage enlargement may take place.
2. The caves develop slowly, but continuously. Small, but relatively higher frequency precipitation events and snowmelt result in soils and shale remaining seasonally damp with shale decomposition taking place on a semi-continuous basis. Over time, small quantities of floor and wall material are removed at a low but continuous rate.

Either one, or more likely, a combination of both scenarios may account for the development of the caves.

Age of the Caves

Determining or estimating a minimum age for the Cody Shale caves presents challenges not present when dating caves in carbonate rocks or in basalts. Commonly used methods include dating using $^{230}Th/^{234}U$ decay, dating using $^{40}K/^{40}Ar$ or $^{40}Ar/^{39}Ar$ ratios, cosmogenic dating using autochtonous quartz pebbles in or beneath passage floors, and carbon-14 dating. In the absence of calcite speleothems, gypsum crusts, a source of potassium, quartz pebbles, and organic material in the caves, these quantitative methods cannot be used.

Qualitatively, the caves appear to be old in terms of their life cycle. The caves are found in small surface catchments; typically 0.5 to 2.5 ha in area (mean basin size = 1.4 ha). Considering the small catchment areas and low annual precipitation of 22 cm water equivalent per year, insufficient quantities of water move through the caves to allow corrasion-induced passage enlargement or even to remove material currently being spalled from passage walls. Based on limited observations to date, the cave entrances appear to be gradually infilling with surface material resulting from soil slumps. Possibly as a result of a lack of flowing water in the caves, entrances are not being washed open. Also, all of the caves contain passages that either end downstream in rubble chokes or become too narrow to follow; none of the caves contain lower entrances where water resurges even though sediment-choked rise points are seen. Given the current static environment in which the caves are found, it can be speculated that the caves may have developed in a wetter, perhaps post-Pleistocene periglacial environment; however, there is no evidence to support this. Unless datable material can be found in the caves, it will not be possible to quantitatively estimate their minimum ages.

Process Summary

The following sequence is proposed to explain the presence of caves in, and related landforms on, the Cody Shale.

1. Rainfall and snowmelt move downward through soil and reach the top of unweathered shale a few meters below. Some soil swell/shrink properties associated with the presence of swelling clays, such as montmorillonite, also assist water and oxygen movement downward by forming desiccation cracks, which eventually enlarge to produce small dolines. Water then moves through the shale below via joints, faults, and bedding partings.
2. Water and oxygen react with disseminated pyrite in the shale, resulting in formation of H_2SO_4 and leaving a ferric oxyhydroxide residue as concentrated fillings on cave passage walls, and as a coating on framboidal pyrite pseudomorphs. Essentially, all of the pyrite in the shale is depleted.
3. The H_2SO_4 and acidic meteoric water react with calcite in the shale, depleting the calcite and producing gypsum fracture fillings that wedge the shale beds apart and structurally weaken them.
4. As the shale beds separate because of gypsum-induced wedging, small, open voids are created, allowing additional water to contact the shale. Corrasional processes remove fine particles (about 2×10^{-3} mm diameter), on a grain by grain basis, enlarging the voids.
5. As a result of the removal of material, slumping occurs on the surface, allowing a more localized flow of surface water and additional oxygen to reach the fractured shale below, enhancing the process. As vadose water moves through the fragmented shale, the local hydraulic gradient permits water to flow downhill to a discharge point, where sapping takes place. At this point, a proto-passage develops with gradual headward enlargement due to corrasional removal of material. This allows larger and more continuous voids to develop until integrated passages remain.
6. Continued surface slumping from upward stoping of the ceiling, and removal of material below, results in isolated, hillside dolines developing that intersect the voids and allow additional surface water to reach the shale.

Conclusions

The proposed sequence of events leading to the development of the caves observed in the Cody Shale is based on known processes for surface weathering of clay soils, pyrite oxidation, gypsum deposition, shale heaving resulting from replacement of pyrite by gypsum, and granular removal of broken shale and clay particles by corrasional processes. Although all of these processes commonly occur, caves that develop as a result have not been reported and require an unusual set of circumstances (e.g., a swelling soil, sufficient pyrite and calcite in the shale, fracturing of the shale allowing oxygen to circulate, a hydraulic gradient sufficient for material to be removed and a discharge point). If these conditions are met, then as outlined in this paper, enterable caves can result.

Acknowledgments

The work described in this paper was supported by analyses conducted at several laboratories. The soil analyses were carried out by the Soil, Water, and Plant Testing Laboratory at Colorado State University. X-Ray diffraction analyses and diffractograms were conducted by the XRD laboratory at the New Mexico Bureau of Geology and Mineral Resources in Soccoro, New Mexico. Virgil Lueth, laboratory manager, provided valuable insights in conversations about the XRD results. Richard Heemskerk at the Environmental Isotope Laboratory, Department of Earth and Environmental

Science, University of Waterloo in Ontario, Canada, did the stable sulfur isotope analysis of the gypsum samples collected in caves. Scanning electron microscopy and energy dispersive spectroscopy of shale samples was conducted by Michael Spilde, manager of the Electron Microprobe and Scanning Electron Microscope labs at the University of New Mexico in Albuquerque, N.M. The images obtained provided evidence for the role of microbes in oxidizing pyrite; Mike's observations and insights were especially helpful. Review comments and suggestions made after reading earlier drafts of this paper were provided by William B. White, Arthur Palmer, John Mylroie, and Ed LaRock. These comments and e-mail exchanges provided valuable feedback and guidance. Finally, comments and support in the field was provided by Hazel Medville without whose help, the data and photographs needed to support this work could not have been obtained.

References

Beck, J.V. and Brown, G.D., 1968, Direct sulfide oxidation in the solubilization of sulfide ores by *Thiobacillus ferrooxidans*, Journal of Bacteriology, v. 96, p. 1433-1434.

Brantley, S.L., Hollerin, M.E., Jin, L., and Bazilevskaya, B., 2013, Probing deep weathering in the Shale Hills Critical Zone Observatory, Pennsylvania (USA): the hypothesis of nested chemical reaction fronts in the subsurface: Earth Surface Processes and Landforms, v. 38, no. 11, p. 1280-1298. https://doi.org/10.1002/esp.3415.

Carroll, D., 1959, Ion exchange *in* Clays and Other Minerals, GSA Bulletin, v. 7, no. 6, p. 749−779. https://doi.org/10.1130/0016-7606(1959)70[749:IEICAO]2.0.CO;2

Crundwell, F., 1996, The formation of biofilms of iron-oxidizing bacteria on Pyrite *in* Minerals in Engineering, v. 9, no. 10, p. 1081−1089.

Finn, T.M., 2013, Lower Cody Shale (Niobrara equivalent) in the Bighorn Basin, Wyoming and Montana: thickness, distribution, and source rock potential. U.S. Geological Survey Scientific Investigations Report 2013, 5138, 32 p.

Granger, D.E. and Fabel, D., 2005, Cosmogenic isotope dating *in* Culver, D.C. and White, W.B. (eds.), Encyclopedia of Caves, Elsevier Academic Press, London, p. 137−141.

Hunter, R.E., Gelfenbaum, G., and Rubin, D.M., 1992, Clastic pipes of probable solution-collapse origin in Jurassic rocks of the Southern San Juan Basin, New Mexico. U.S. Geological Survey Bulletin 1808-L, 19p.

Hoover, S.E., Wang, M.C. and Dempsey, B., 2004, Structural damage induced by pyritic shale, Fifth International Conference on Case Histories in Geotechnical Engineering Paper 7.02, p. 1−7.

Kelly, D.P. and Wood, A.P, 2000, Reclassification of some species of *Thiobacillus* to the newly- designated genera *Acidithiobacillus* gen. nov., *Halothiobacillus* gen. nov. and *Thermithiobacillus* gen. nov. *in* International Journal of Systematic and Evolutionary Microbiology 50: 511−516. https://doi.org/10.1099/00207713-50-2-511.

Lupton, C.T., 1916, Oil and gas near Basin, Big Horn County, Wyoming. Geological Society of America Bulletin 621, p. 157−190.

Nordstrom, D.K., 1982, Aqueous pyrite oxidation and the consequent formation of secondary iron minerals. Chapter 3 *in* Acid Sulfate Weathering, Soil Science Society of America, p. 56−77.

Palmer, A.N., 2007, Cave Geology. Cave Books, Dayton, Ohio.

Parker, G.G. and Higgins, C.C., 1990, Piping and pseudokarst in drylands *in* Higgins, C.G. and Coates, D.R. (eds.), Geological Society of America Special Paper 252, Groundwater Geomorphology: The Role of Subsurface Water in Earth-Surface Processes and Landforms, p. 77−110. https://doi.org/10.1130/SPE252-p77.

Paytan, A., Gray, E.T., Ma, Z., Erhardt, A., and Faul, K., 2011, Application of sulphur isotopes for stratigraphic correlation. Isotopes in Environmental and Health Studies. p. 1−12.

Penner, E. and Eden, W.J., 1972, CBD-152, Expansion of pyritic shales. Canadian Building Digest, Division of Building Research, National Research Council Canada, 6 p.

Pierce, W.G., 1948, Geologic and structure contour map of the Basin-Greybull area, Big Horn County, Wyoming. U.S.G.S. Oil and Gas Investigation Map OM-77, scale 1:48000, one sheet.

Pye, K. and Miller, J.A., 1990, Chemical and biochemical weathering of pyritic mudstones in a shale embankment *in* Quarterly Journal of Engineering Geology and Hydrogeology, v. 23, p. 365−382.

RRUFF Database, 2017, http://rruff.info/goethite/display=default/R050142.

Soil Quality Organization website, Australia, 2017, Cations and Cation Exchange Capacity Factsheet. http://www.soilquality.org.au/factsheets/cation-exchange-capacity.

Taylor, G. and Eggleton, R.A., 2001, *In situ* weathering profiles *in* Regolith Geology and Morphology, Chapter 11, p. 191−218, John Wiley and Sons, New York.

Thode, H.G., 1991, Sulphur isotopes in nature and the environment: an overview *in* H.R. Krouse and V.A. Grinenko, (eds.), Soluble Isotopes in the Assessment of Natural and Anthropogenic Sulphur in the Environment. John Wiley and Sons, Chichester. p. 1−26.

U.S. Department of Agriculture, Natural Resources Conservation Service, Web Soil Survey, Published Soil Survey for Wyoming, Bighorn County area, 2017. https://www.nrcs.usda.gov/wps/portal/nrcs/surveylist/soils/survey/state?stateId=WY.

U.S. Department of Energy, Environmental Sciences Laboratory, 2011, Natural contamination from the Mancos Shale, Report ESL-RPT-2011-01, p. 46−47.

White, E.L. and White, W.B., 1968, Dynamics of sediment transport in limestone caves *in* Bulletin of the National Speleological Society. v. 30, no. 4, p. 115−129.

White, J.L. and Greenman, C., 2008, Collapsible soils in Colorado. Colorado Geological Survey Publication EG-14, 108 p.

White, W.B. (ed.), 2015, The Caves of Burnsville Cove, Virginia, Springer, New York, p. 436−437. https://doi.org/10.1007/978-3-319-14391-0.

White, W.B. and White, E.L., 2003, Gypsum wedging and cavern breakdown: Studies in the Mammoth Cave System, Kentucky *in* Journal of Cave and Karst Studies, v. 65, no. 1, p. 43−52.

A. Marrón-Becerra, M. Hermoso-Salazar and V. Solis-Weiss. *Hyalella maya*, a new hyalellidae species (crustacea: amphipoda) from a cenote in the Yucatan Peninsula, Mexico. *Journal of Cave and Karst Studies*, v. 80, no. 2, p. 1-11. DOI: 10.4311/2017LSC0115

HYALELLA MAYA, A NEW HYALELLIDAE SPECIES (CRUSTACEA: AMPHIPODA) FROM A CENOTE IN THE YUCATAN PENINSULA, MEXICO

Aurora Marrón-Becerra[1], Margarita Hermoso-Salazar[2] and Vivianne Solís-Weiss[3,C]

Abstract

Hyalella maya n. sp. from a sinkhole (cenote) in Quintana Roo, Mexico, is described herein, based on morphological characters. It is the third species recorded in Mexico and the second species of *Hyalella* found in the Aktun-Ha sinkhole. It can be distinguished from its closest species, *Hyalella azteca* from Veracruz, by the shape of the palp of maxilla 1, the number of setae in the posterior margin of the basis, the relative palm length and the truncate process of gnathopod 2 in males, the number of setae in the lobe of the basis of pereopod 7, and the shape and setation of the telson. Those characters have been found to be useful for species distinction in the complex by González and Watling (2002). The main differences between *Hyalella cenotensis* and *Hyalella maya* n. sp. are: the presence of eyes, the number of articles in the flagellum in antennae 1 and 2, the relative length of antennae to the total body length, the relative length of the rami in uropod 3 to the peduncle length, and the number of setae in the telson.

Introduction

Up to now, about 70 species of the genus *Hyalella* have been described, with approximately 60 species distributed in South America (Horton and Lowry, 2013) and 12 species in North America, Central America and the Caribbean (Fig.1, Table 1). These last are: *Hyalella azteca* (De Saussure, 1858); *H. faxoni* (Stebbing, 1903); *H. texana* (Stevenson and Peden, 1973); *H. montezuma* (Cole and Watkins, 1977); *H. caribbeana* (Bousfield, 1996); *H. longicornis* (Bousfield, 1996); *H. muerta* (Baldinger, Shepard and Threloff, 2000); *H. sandra* (Baldinger, Shepard and Threloff, 2000); *H. meraspinosa* (Baldinger, 2004); *H. cenotensis* (Marrón-Becerra, Hermoso-Salazar and Solís-Weiss, 2014); *H. spinicauda* (Soucek and Lazo-Wasem, et al., 2015) and *H. wellborni* (Soucek and Lazo-Wasem, et al., 2015). The *Hyalella azteca* complex is considered to be present only in North America, Central America and the Caribbean, with no records from South America (González and Watling, 2001; 2002; González, 2003; González and Watling, 2003a-d). There are now around 40 "provisional" species included in the *H. azteca* complex: 33 in the U.S. (Witt et al., 2006) and seven in Canada (Hogg et al., 1998; Witt and Hebert, 2000). The reason to call them "provisional species" is that all of them have been differentiated through molecular studies, but they have not yet been formally described.

In the past, *Hyalella azteca* (De Saussure, 1858) was considered as one species, widely distributed in the American continent but not as a complex of species. This was due to the absence of evident morphological variability, as well as to the lack of carefully detailed morphological studies (González and Watling 2002). In Mexico, *H. azteca* was the only epicontinental, epigeous species of amphipod recorded, with a wide distribution in the whole country. However, we now know that this species is, in fact, a complex of several species, taxonomically close, but that their ecological and morphological characteristics have not been sufficiently studied to separate them accurately (González and Watling, 2002; Brito et al., 2014; Soucek and Lazo-Wasem, et al.,2015).

De Saussure (1858) described *Hyalella azteca* as *Amphitoe aztecus* from material collected in Veracruz state and Lago de Chapultepec, Mexico City. However, the description, as well as the illustrations, are not detailed enough and the type locality was not specified. That is why González and Watling (2002) redescribed it, making a morphologically-detailed diagnosis based on the syntypes, to try and clarify its taxonomic status.

Currently, two species of *Hyalella* (Fig. 1) are known in Mexico: *H. cenotensis,* with no eyes, from a cenote in Tulum, Quintana Roo, and *H. azteca,* with well-developed eyes and with a distribution probably limited to the state of Veracruz, Mexico (González and Watling, 2002; Graening et al., 2012).

The objective of this study is to describe a new species of *Hyalella,* collected in a sinkhole in the Yucatan Peninsula, to compare it to the other species of the genus in the area (*H. cenotensis* and *H. azteca*) and to other species from North America and the Caribbean. In addition to contributing to the knowledge of this complex of species, we wish to demonstrate that more studies, focused on this genus of amphipods, are needed in these fragile, endangered environments.

[1]Universidad Nacional Autónoma de México, Posgrado en Ciencias del Mar y Limnología, Av. Universidad 3000, Delegación Coyoacán, 04510, Ciudad de México.
[2]CONABIO, Comisión Nacional para el Conocimiento y Uso de la Biodiversidad, Liga Periférico – Insurgentes Sur, Núm. 4903, Col. Parques del Pedregal, Delegación Tlalpan, 14010, Ciudad de México.
[3]Universidad Nacional Autónoma de México, Instituto de Ciencias del Mar y Limnología, Unidad Académica Sistemas Arrecifales, Q. Roo 77580 México.
[C]Corresponding autor: solisw@cmarl.unam.mx

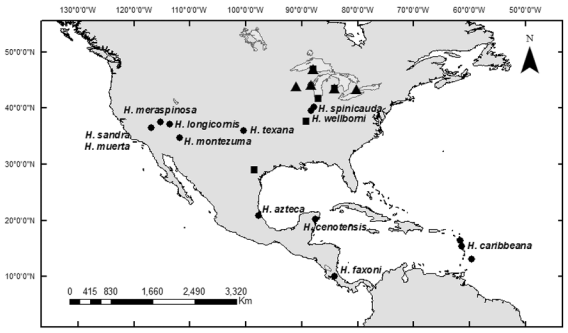

Figure 1. Map with the location of the species of *Hyalella* in North America, Central America and the Caribbean region. Circles indicate the type locality of each species. Triangles indicate the localities of *H. spinicauda*. Squares indicate the localities of *H. wellborni*.

Method

Samples were collected manually at a depth of 1-2 m, while snorkeling at Cenote Aktun-Ha, Quintana Roo, Mexico (20°16.48´N, 87°29.20´W), in April 2008 on dense algal mats. The upper level taxon was identified following Lowry and Myers (2013). The specimens collected are deposited in the National Collection of Crustaceans, Instituto de Biología of the Universidad Nacional Autónoma de México (UNAM). Specimens were dissected and body parts were mounted on permanent slides. The total length was measured from the tip of the head to the base of the telson, using an optical microscope with a micrometric scale on the objective lens. The terminology for the setae follows Zimmer et al. (2009). Characters for the key were taken from Soucek et al. (2015).

Scanning electron photographs were taken from paratypes (one female and one male) with a Hitachi SU1510 scanning electron microscope (SEM) from the Laboratory of Microscopy and Photography of Biodiversity I, at the Instituto de Biología, UNAM.

The number of articles in the flagellum of antennae 1 and 2 were compared between males' and females' paratypes using a linear regression of the total body length and the number of articles of at least 10 organisms of each sex.

Table 1. *Hyalella* species recorded in North America, Central America and the Caribbean in chronological order.

Species	Distribution	Country	Habitat	References
H. azteca (De Saussure, 1858)	Veracruz	Mexico	freshwater, epigean, benthic	De Saussure (1858); González and Watling (2002)
H. faxoni Stebbing, 1903	Reventado Volcano and Barva Volcano	Costa Rica	freshwater, epigean, littoral	Stebbing (1903)
H. texana Stevenson and Peden, 1973	Clear Creek Spring, Texas	USA	freshwater, epigean, benthic	Stevenson and Peden (1973)
H. montezuma Cole and Watkins, 1977	Montezuma Well, Yavapai, Arizona	USA	freshwater, epigean, planktonic	Cole and Watkins, (1977)
H. caribbeana Bousfield, 1996	Pond and lakes in Grand Terre islands, Guadeloupe, Dominica, Barbados and probably in other lesser Antilles windward islands.	Guadeloupe, Dominica and Barbados	freshwater, epigean, benthic	Bousfield (1996)
H. longicornis Bousfield, 1996	Utah	USA	freshwater, epigean, benthic	Bousfield (1996)
H. muerta Baldinger, Shepard and Threloff, 2000	Texas Springs and Travertine Springs, Death Valley National Park, Inyo, California	USA	freshwater, hypogean, benthic	Baldinger et al. (2000)
H. sandra Baldinger, Shepard and Threloff, 2000	Texas Springs and Travertine Springs, Death Valley National Park, Inyo, California	USA	freshwater, epigean, benthic	Baldinger et al. (2000)
H. meraspinosa Baldinger, 2004	Ash Springs, Lincoln, Nevada	USA	freshwater, epigean, benthic	Baldinger (2004)
H. cenotensis Marrón-Becerra, Hermoso-Salazar and Solis-Weiss, 2014	Cenote Aktún-Ha, Tulum, Quintana Roo	Mexico	freshwater, hypogean, benthic	Marrón-Becerra et al. (2014)
H. spinicauda Soucek and Lazo-Wasem, 2015	Ponds, lakes and rivers in Illinois, Indiana, Michigan, Wisconsin and Texas, USA and Ontario, Canada	USA and Canada	freshwater, epigean, benthic	Soucek et al. (2015)
H. wellborni Soucek and Lazo-Wasem, 2015	Ponds, lakes and rivers in Illinois, Indiana, Michigan, Wisconsin and Texas, USA and Ontario, Canada	USA and Canada	freshwater, epigean, benthic	Soucek et al. (2015)
H. maya n. sp.	Cenote Aktún-Ha, Tulum, Quintana Roo	Mexico	freshwater, epigean, benthic	In this study

Results

Order AMPHIPODA Latreille, 1816
Suborder Senticaudata Lowry and Myers, 2013
Infraorder Talitrida Rafinesque, 1815

Parvorder Talitridira Rafinesque, 1815
Superfamily Talitroidea Rafinesque, 1815
Family Hyalellidae Bulycheva, 1957
Genus *Hyalella* S. I. Smith, 1874

***Hyalella maya* n. sp.**

Material examined: Holotype male, size 3.85 mm (Cat. No. CNCR 31502), from algae in the outer area of Cenote Aktun-Ha, Quintana Roo, Mexico (20°16.48´N, 87°29.20´W) in April 2008. Paratypes: male, size 4.10 mm, 1 ovigerous female, size 4.15 mm (Cat. No. CNCR 31503), locality was the same as holotype. Collectors: Vivianne Solis-Weiss and Sarita Frontana Uribe.

Type locality: Cenote Aktun-Ha, Quintana Roo, México (20°16.48´N, 87°29.20´W).

Etymology: The name is derived from the Mayan civilization that ruled the area in the past.

Habitat: In algae, freshwater (pH 7.2, water temperature 24.85°C, dissolved oxygen 1.93 mg/l).

Diagnosis: Eyes present. Tergites of pleon 1 and 2 with dorsoposterior carina. Head length: slightly shorter than the length of pereonites 1 and 2 combined, reaching more than half the length of pereonite 2. Antenna 1 is shorter than antenna 2; flagellum with nine articles. Antenna 2 is almost 1.3 times longer than antenna 1, longer than half body length; flagellum with 10 articles. Maxilla 1, vestigial palp, uni-articulated, short, rounded with an apical seta; inner plate with three strong, pappose apical setae. Lower lip, distal lobes rounded. Gnathopod 2 (males), carpus posterior lobe is approximately 1.5 times the width of merus, palm oblique without an evident, truncated process or distinct notch; length of palm is similar to the posterior margin of gnathopod 2. Pereiopod 7 basis with up to 12 short, fine setae. Telson is wider than long; distal margin is rounded with two long, separated, simple setae, with three short, sub-marginal setae on both left and right sides.

Male description (Figs. 2-3): Size 3.85 mm (holotype). Coxae 1-4 are sub-rectangular, longer than wide, inferior margin is rounded with small setules, coxa 4 with a posterior excavation. Coxae 5-7 are shorter than coxae 1-4; coxa 5 with two subequal lobes, coxa 6 with two unequal lobes, and coxa 7 with a single lobe.

Pleon (Fig. 2A): pleonites 1 and 2 with dorsoposterior carina, ventral margin of epimeral plates 2 and 3 slightly pointed.

Head (Figs. 2A, 5C): typically, gammaridean, smooth surface; length is less than pereionites 1 and 2 combined, reaching half of pereionite 2; eyes are present and rostrum is absent.

Antenna 1 (Figs. 2A, 3H, 5C): shorter than antenna 2, length reaching beyond two-thirds of the fourth pereionite; peduncle is longer than head, reaching more than half the length of first pereionite. Peduncle articles become gradually smaller in length and width toward their distal portion; close to the middle length of the ventral margin for the first peduncle article, a short cuspidate seta and one at the distal end; flagellum with nine articles, longer than peduncle, basal article of flagellum not elongate; no accessory flagellum.

Antenna 2 (Figs. 2A, 3I, 5C): almost 1.3 times longer than antenna 1, length is slightly longer than half the total body length, reaching half the length of the sixth pereionite. Peduncle articles increase gradually in length and decrease in width toward their distal end; flagellum with 10 articles, length 1.16 times the peduncle length.

Buccal parts (Fig. 3): upper lip (Fig. 3C), distal margin is rounded with numerous setules, longer and more distant toward the lateral ends; distal surface of the outer surface has two rows of short setules, very close toward the middle of the row. Lower lip (Fig. 3B): distal lobes are rounded distally; apices are relatively separated from one another with numerous setules; no inner lobes; mandibular lobes are rounded with distal ends slightly directed outward.

Mandibles (Figs. 3E-F): incisor with six teeth, distal tooth stronger than the proximal five; strong and triturative molar (Figs. 9E-F); left lacinia mobilis (Fig. 3E) is more developed than right, with five teeth; length of the external tooth is subequal to the distal tooth of the incisive process; right lacinia mobilis has two teeth, each with inner margin denticulate (Figs. 3F, 9G); left mandible ranker row has three longer and two shorter pappose setae, and a large accessory pappose seta at the end of the molar process in both mandibles; palp is lacking.

Maxilla 1 (Fig. 3A): outer plate of maxilla 1 is slightly longer than 2.5 times the width of the inner plate, distal margin with nine serrate setae; vestigial palp is uni-articulated, longer than wide, with rounded apex and a simple seta; palp length is slightly shorter than a third of the distance of the palp base, to the end of the longest seta of the outer plate; inner plate is slender and shorter than outer one, almost reaching the palp base, distal margin with two to three pappose setae.

Maxilla 2 (Fig. 3D): plates are subequal in length and shape; inner plate is almost half the length of the inner margin with two plumose setae; distal margin of both plates has simple setae.

Maxilliped (Fig. 3G): inner plate is shorter than outer; distal margin has three cuspidate setae of equal size with plumose setae; inner margin has plumose setae; outer plate is elongate; distal and inner margins have numerous simple setae; palp, longer than inner plate, is composed by four articles. The first article has three simple setae at the far-

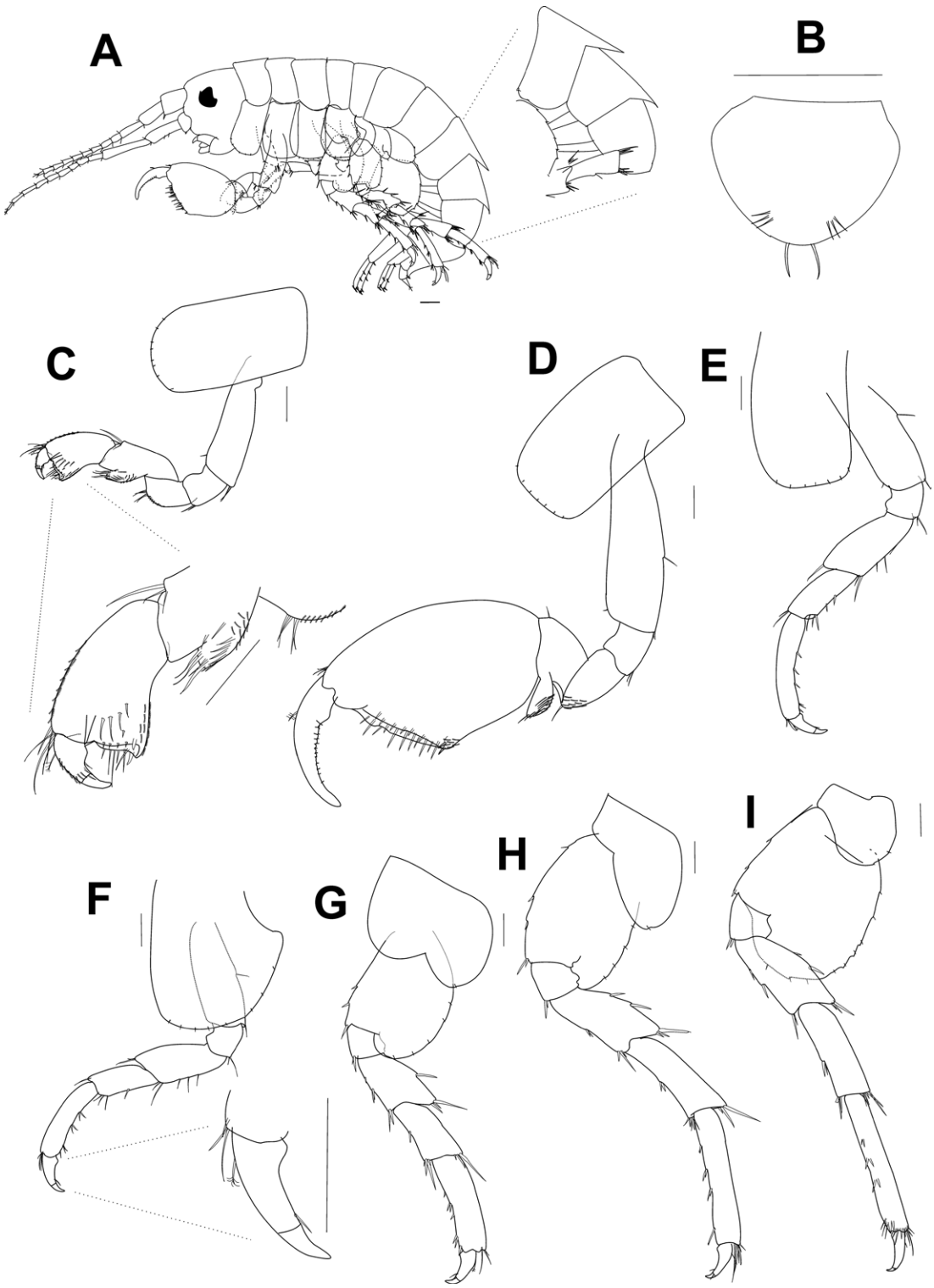

Figure 2. *Hyalella maya* n. sp., paratype, male (3.85 mm). A) complete body and mucronations on pereionites 1-2; B) telson; C) gnathopod 1; D) gnathopod 2; E-I) Pereiopods 3-7. Scale bars = 100 microns.

ther, anterior end of the inner margin; the second article has numerous simple setae in the inner margin and two in the outer margin; the third article has five simple setae at the distal, inner margin and eight simple setae at the apicolateral margin; the fourth article unguiform, distal end with three simple setae, shorter than the nail; nail reaches approximately half as long as the fourth article.

Gnathopod 1 (Figs. 2C, 6B): sub-chelate, hammer-shaped, and shorter than gnathopod 2; basis is elongate, approximately 3.5 times longer than wide; posterior margin is without setae; ischium is short, with maximum width and length subequal to the length of the merus, distal posterior end, and with two simple setae; merus is longer than wide, shorter

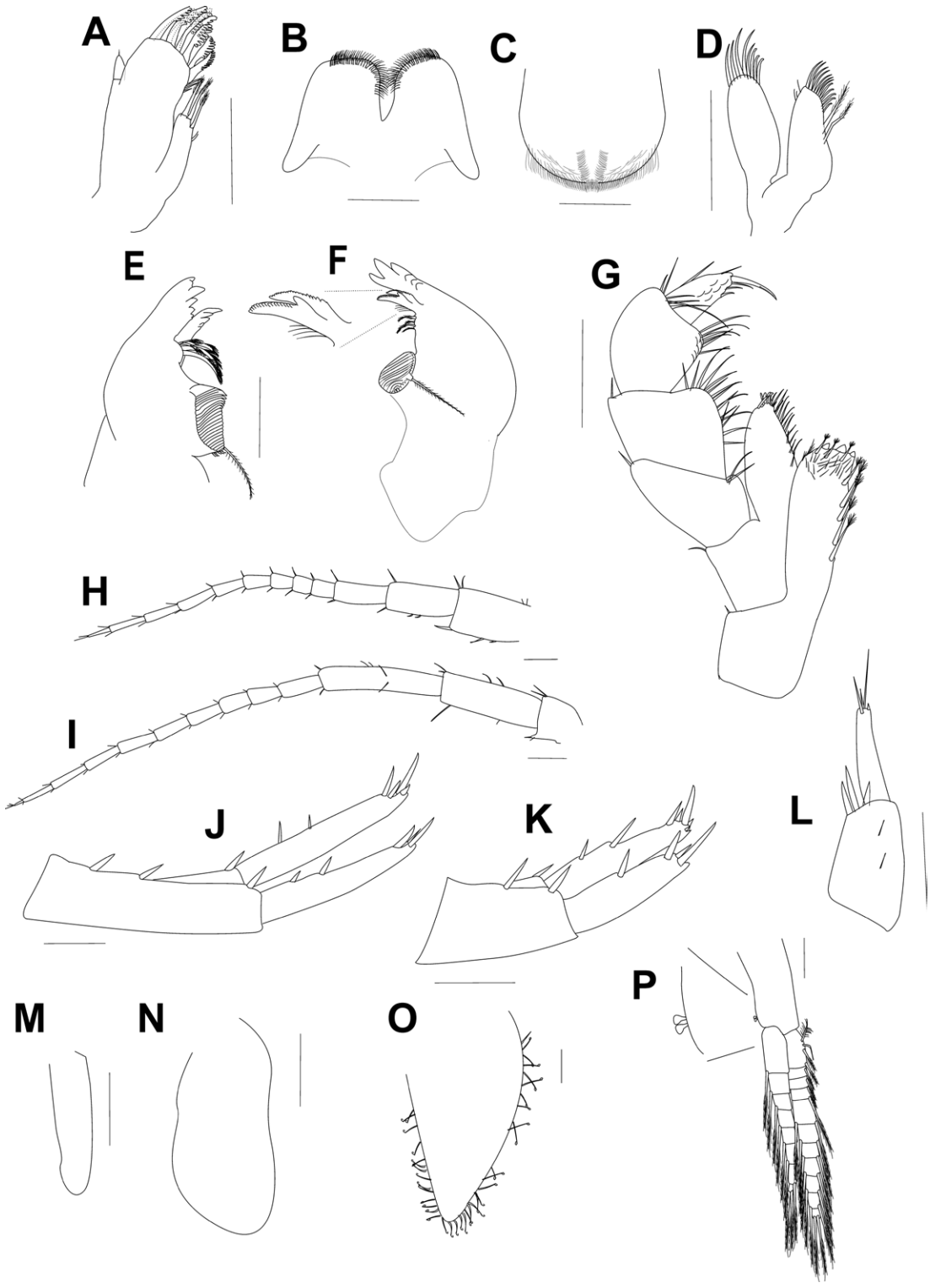

Figure 3. *Hyalella maya* n. sp., paratype, male (3.85 mm). A) maxilla 1; B) lower lip; C) upper lip; D) maxilla 2; E) left mandible; F) right mandible; G) maxilliped; H) antenna 1; I) antenna 2; J-L) uropods 1-3; M) sternal gills; N) coxal gills; O) oosteguites; P) pleopods showing the retinacula. Scale bars = 100 microns.

than the carpus, distal posterior, margin end with simple setae, and comb scales on mid-posterior surface (Figs. 2C, 7B-C); carpus is longer than wide, almost as long as the propodus, posterior margin of lobe, with several simple setae, and two simple setae on the medial surface; lobe, posterior surface of both sides has comb scales near the margin (Figs. 7B-C), distal anterior margin has two simple setae; propodus is 1.76 times longer than wide, distal end of anterior margin, with four simple setae, anterodistal and posterodistal margin, with comb scales; inner surface has four stout, simple setae in a row, and below it, a simple, short seta; palm transverse has long setae, posterior end with a robust seta and cup for dactyl, and with a robust seta in the inner face, near the cup of dactyl; dactyl, claw-like, nail is present, anterior end has a plumose seta, posterior margin has simple seta, and apex has comb scales.

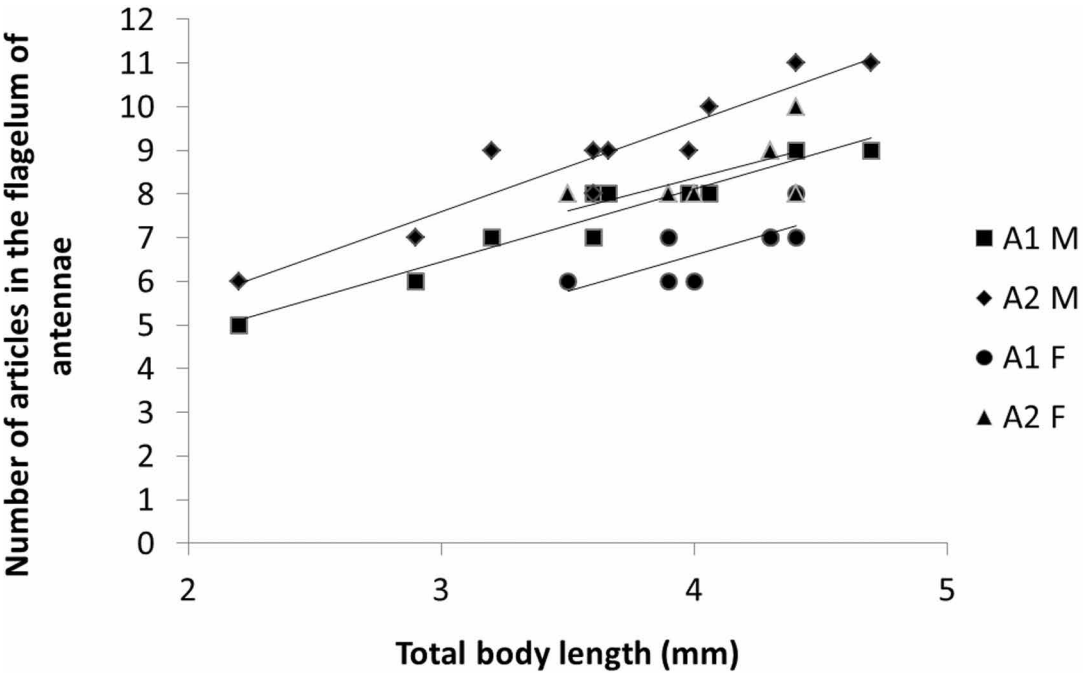

Figure 4. Linear regression between body length and number of articles in the flagellum of the antennae. The males (A1 M and A2 M) have more articles than the females (A1 F and A2 F). The number of articles increases with size of body.

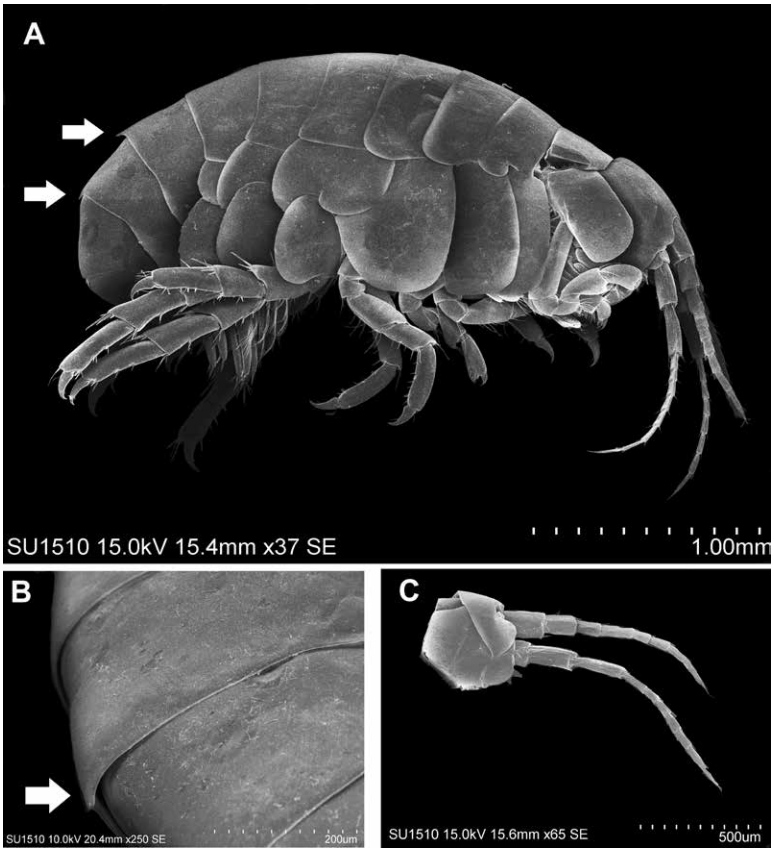

Figure 5. Paratype, ovigerous female (4.15 mm). A) complete body, arrows show the mucronations; B) pleon mucronations, arrow shows the mucronation. Paratype, male (4.10 mm). C) head.

Gnathopod 2 (Figs. 2D, 6E-F, 7A): sub-chelate, palm is slightly oblique; basis is elongate; posterior margin is almost half its length with a simple seta, anterodistal end with one short simple seta, and distal end of posterior margin with two simple setae; ischium is short, sub-quadrate, shorter than merus, posterodistal end with three simple setae; merus is short, distal end of the posterior margin with three simple setae, distal half of the posterior surface of the inner and outer surfaces with comb scales; carpus is shorter than propodus, distal end of the anterior margin with two simple setae; posterior lobe is elongate, almost 1.5 times the width of merus, with several sub-marginal, pappose setae; both the inner and outer surfaces of lobe have comb scales; propodus is rectangular and palm is subequal to the posterior margin; slope is slightly oblique, irregular, with several long, simple setae; anterior edge is without any evident, truncated process and without any evident notch at the base (Fig. 7A); posterior distal corner has strong setae and cup for dactyl; dactyl are claw-like, congruent with palm, and without comb scales.

Pereopods (Figs. 2E-I): simple, gradually longer posteriorly, and pereopod 5 is shorter than fourth and sixth. Pereopod 3, basis is elongate with a simple seta at half the length of the posterior margin, anterior distal end with a short simple seta, and distal posterior end has two simple setae; ischium is sub-quadrate, and distal end of posterior margin has two simple setae; merus is longer than ischium, posterior margin has three simple setae, anterodistal edge has two simple setae, and posterodistal edge has three simple setae; carpus is shorter than merus and longer than ischium; posterior margin of the carpus has two simple setae, anterodistal edge has three simple setae, and posterodistal edge has four simple setae; propodus, posterior margin has two cuspidate setae with an accessory

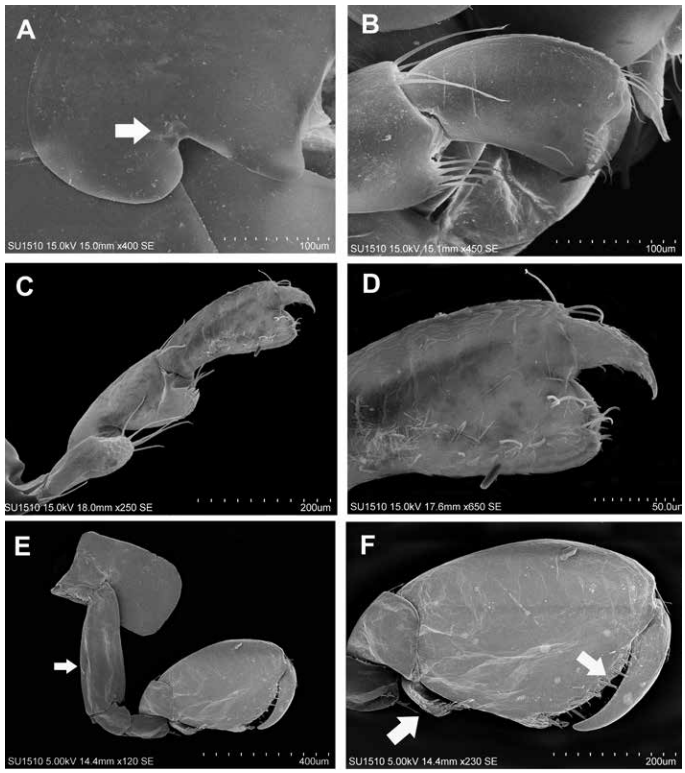

Figure 6. Paratype, ovigerous female (4.15 mm). A) arrow shows the copulatory notch on pereonite 2; B) gnathopod 1 (female); C) gnathopod 2 (female); D) propodous and dactyl, gnathopod 2 (female). Paratype, male (4.10 mm). E) gnathopod 2 (male), arrow shows the posterior setae on the basis; F) propodus and dactyl, gnathopod 2 (male), arrow shows carpus posterior lobe with comb setae and the lack of an evident notch in the palm.

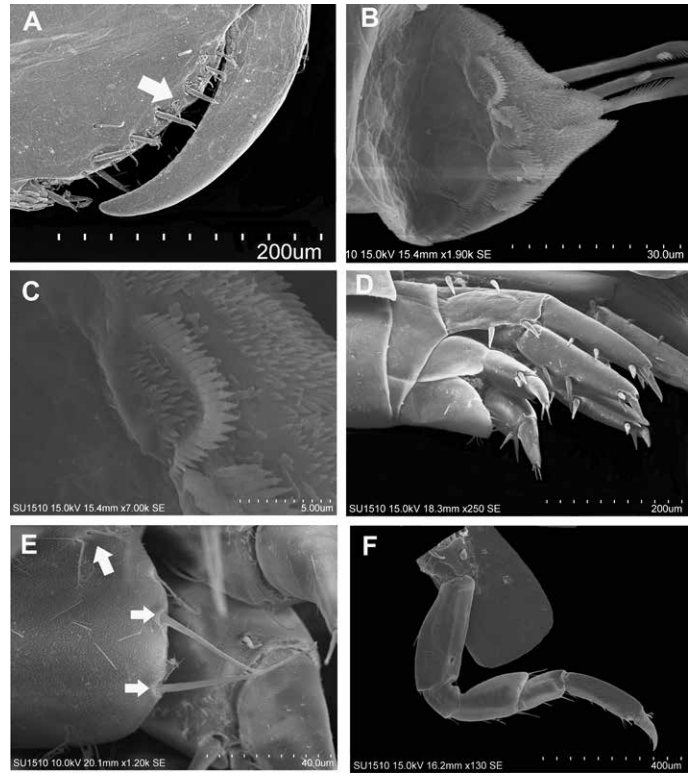

Figure 7. Paratype, male (4.10 mm). A) palm, arrow shows the absence of an evident notch; B) ventral face, carpus posterior lobe with comb scales; C) comb scales on the carpus posterior lobe; D) uropods 2-3. Paratype, ovigerous female (4.15 mm). E) telson, arrows show the two distal separated setae and the submarginal setae; F) pleopod 3.

seta, and anterodistal and posterodistal end with three simple setae; dactylus has a claw-like, nail present, at the first, proximal third of the anterior margin with a plumose seta; posterior margin has a simple seta close to the nail (Figs. 2F, 8F). Pereopod 4 is similar in shape to pereopod 3, but longer; coxa is wider than coxa 3 with a posterior excavation; basis is almost at half-length of the posterior margin, with one seta. Pereopods 5-7 are similar in shape; coxa of pereopod 5 is wider than long with two unequal lobes and posterior lobe is slightly longer; coxa of pereopod 6 has no anterior lobe and posterior lobe reaches half as long as the basis; coxa of pereopod 7 is short, with no anterior lobe. Basis of pereopods 5-7 have a rounded and denticulate posterior lobe; lobe of pereopod 7 basis is widely expanded and posterior margin has nine setae.

Pleopods (Fig. 3P): 1-3 are not modified, biramous and elongate, with numerous long plumose setae; peduncle's inner margin has two short retinacula (coupling hooks).

Uropods (Figs. 3J-L): uropod 1 is longer than uropod 2; length of peduncle is longer than rami, proximal half of dorsal margin has two stout, simple setae; ramus has two dorsal setae, three simple ones and one connate distal seta; inner ramus is scarcely longer than outer ramus, without curved seta. Uropod 2 has a sub-rectangular peduncle; length is longer than rami, dorsal margin is almost at distal half with a stout, simple seta and distal end with an apical, simple seta; inner ramus is slightly longer than outer one; dorsal margin has two stout setae and four distal, stout setae; outer ramus has dorsal margin with a simple, stout seta and distal end with three simple, stout setae. Uropod 3's total length is subequal to the peduncle length of uropod 2; peduncle is slightly longer than ramus with distal end having three robust setae; ramus styliform its apex truncate with three apical, simple setae and one connate seta.

Telson (Fig. 2B): slightly wider than long, entire, fleshy, and smooth dorsal surface with three short, sub-marginal plumose setae on both sides (left and right), reaching the distal margin; distal margin is rounded with two separated, apical setae.

Gills. Coxal gills are small, simple, and saclike, on segments 2-7 (Fig. 3N).

Sternal gills are tubular, on pereonites 3-7 (Fig. 3M).

Female (Figs. 5-9) differences: Size is 4.15 mm; Antennae 1 and 2 have flagellum with fewer articles (Figs. 4, 5A). Gnathopod 1 has similar size and shape to gnathopod 2; gnathopod 2, propodus is smaller and more slender than the

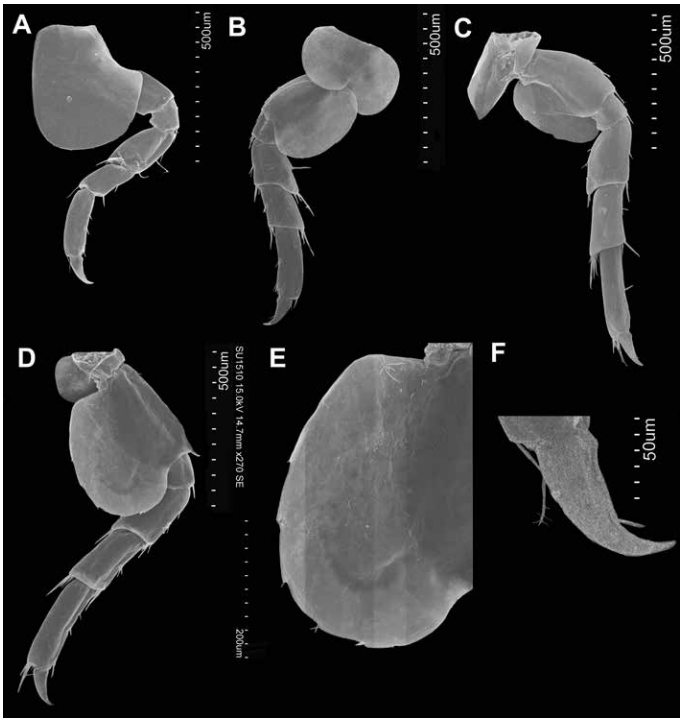

Figure 8. Paratype, ovigerous female (4.15 mm). A) pereopod 4; B) pereopod 5; C) pereopod 6; D) pereopod 7; E) posterior lobe, pereopod 7; E) dactylus and nail close up, pereopod 4.

García-Schroeder and Araujo (2009), said that the number of articles in the flagellum of the antennae increases with the size of the animal. In the redescription of González and Watling (2002), *H. azteca* is larger than the species described herein, but *H. maya* n. sp. had a larger number of articles in the flagellum; likewise, in the two pairs of antennae, the number of segments increases with the size of the specimen and differs between males and females (Fig. 4). Antenna 2 in *H. azteca* is less than half the length of the total length of body, while in *H. maya* n. sp. it is longer than half the total length of body (Fig. 2A). Other important differences are: the shape of the palp of maxilla 1, in *H. azteca* it is rounded and in *H. maya* n. sp. it is shorter and rounded with a distal seta (Figs. 3A; 9D); *H. maya* n. sp. has one seta on the posterior margin of the basis of gnathopod 2 (Fig. 6E), while *H. azteca* has two. The relationship between the length of the palm and the length of the posterior margin is another character that distinguishes *H. maya* n. sp.: the first length is similar to the second, while in *H. azteca,* the length of the palm is shorter than the posterior margin; in *H. maya* n. sp. the telson is described as being wider than long, with a rounded apex and a pair of apical setae widely separated (Fig. 7E), while in *H. azteca*, the width is equal to the length, the apical setae are apposed, and the margin is pointed (Table 2); finally, in *H. maya* n. sp. a smaller number of setae are present in the basis of the lobe of pereopods 5-7 (Figs. 8B-E), compared to *H. azteca*.

male, length to the dactyl is almost twice the maximum width, parachelated, and palm reverse oblique (Figs. 6C-D). Pereonite 2 has an anterior excavation or notch for the amplexus (Fig. 6A).

Oostegites foliaceous, setae end in a curl on the margin of pereonites 2-7 (Fig. 3O).

Remarks: The lack of clear morphological characters that could help distinguish the different species in the *H. azteca* complex make it difficult to identify them accurately. That is why it is considered a complex with cryptic phenotypes by González and Watling (2002), who declared that the characters that help distinguish the species of this complex are: the relative length of the antenna, the number of setae in the internal plate of maxilla 1, the setation in the palp of the maxilliped, the number and organization of the setae of the propodus of gnathopod 1, the setation of the posterior margin of the basis, the propodus shape and the irregular shape of the palm in gnathopod 2 of the males, the shape of the epimeral plates, the setation and proportions of the ramus and the peduncle of uropod 3, and, finally, the shape and setation of the telson.

Hyalella maya n.sp. is morphologically close to *H. azteca.* However, important differences are present. Geisler (1944), Stevenson and Peden (1973) and

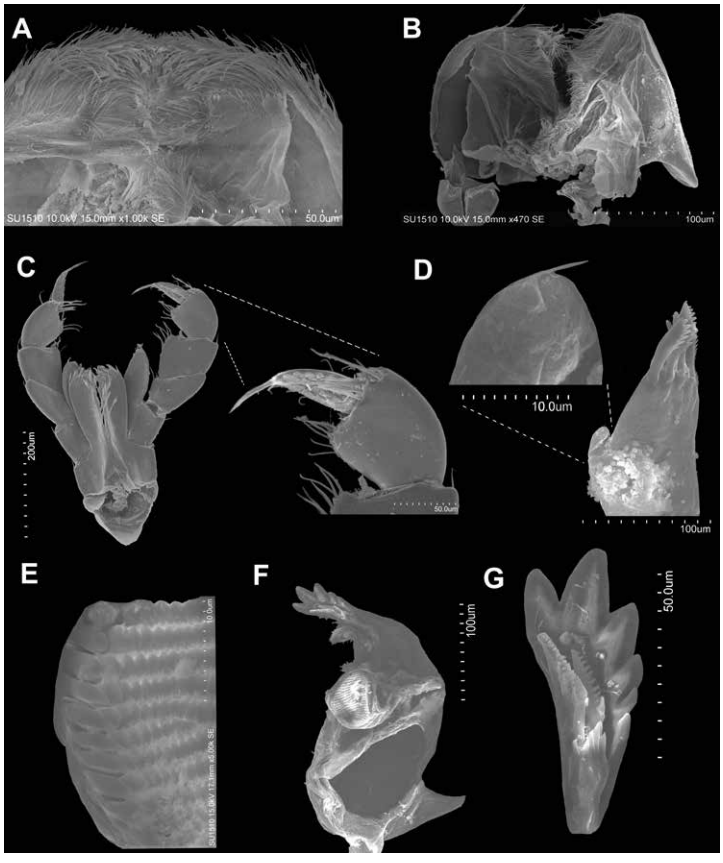

Figure 9. Paratype, ovigerous female (4.15 mm). A) upper lip; B) lower lip; C) maxilliped with a close-up of the third and fourth article and the nail of the peduncle; D) maxilla 1, close-up to the palp with an apical seta; E) molar process; F) right mandible; G) close-up to the incisor process and lacinia mobilis.

Table 2. Morphological comparison between ***Hyalella maya*** n. sp.***, H. spinicauda***, ***H. wellborni and H. azteca*** redescription (HBL = half body length, FTTS = First two thoracic segments, PM = Posterior margin, W = width, L = length).

Morphological Characteristics	*H. azteca* (redescription of González and Watling, 2002)	*H. spinicauda* Soucek and Lazo-Wasem, 2015	*H. wellborni* Soucek and Lazo-Wasem, 2015	*Hyalella maya* n. sp.
Size (mm)	7.8	5.76	4.28	3.85
Length of antenna 2	A2 < HBL	A2 < HBL (30%)	A2 < HBL (40%)	A2 ≥ HBL (>40%)
No. articles flagellum antenna 1	7	···	···	<9
No. articles flagellum antenna 2	8	···	···	<10
Relation between length of head and two first thoracic segments	H<FTTS	H<FFTS	H<FFTS	H<FFTS
Maxilla 1 outer plate, number of pappose setae	3	2	2	3
G1 carpus, inner face, pappose setae	4	3	4	3−4
G2 comb scales	present			present
G2 basis, posterior margin, setae	2	···	2	1
G2 propodus; relation between palm length and posterior margin	P < PM	P < PM	P = PM	PPM = PM
G2 propodus palm	notch	Angled step	No distinct step/ notch	No distinct step/notch
Telson, relation between width and length	W = L	W < L	W = L	W > L
Telson, setae	Apposed, larger and slender	Separated, short, stout	Apposed, larger, slender	Separated, larger slender
Telson margin	pointed	rounded	rounded	rounded

Soucek et al. (2015) examined the lectotype from the type material of De Saussure (1858) and described two new species from Canada and the U.S.A., *H. wellborni* and *H. spinicauda.* In this study, we analyzed useful morphological characters for the identification of the species of the complex *H. azteca,* such as: the number of setae in maxilla 1, the shapes of gnathopod 2, pereopod 7, uropod 3 and telson, in accordance with Soucek et al. (2015). *Hyalella maya* n. sp. can be distinguished from both species, *H. wellborni* and *H. spinicauda,* because of the presence of three setae in the internal plate of maxilla 1, while in *H. wellborni* and *H. spinicauda* only two are present. In their description, the authors mentioned that the male gnathopod 2 in *H. azteca* has a wide truncate process with a notch, an important difference between *H. wellborni, H. spinicauda* and *H. maya.* In *H. maya,* the notch is absent and the truncate process is not evident (Table 2).

In this locality, i.e. Cenote Aktun-Ha, another species of the same Genus: *Hyalella cenotensis* has already been described by Marrón-Becerra et al. (2014). The main differences between the two species are the absence of eyes and of distal setae in the telson in *H. cenotensis*, both present in *H. maya* n. sp. In addition, in *H. maya* n. sp.*,* the relative length of antenna 2, with respect to antenna 1, is bigger (more than 1.3 times), while in *H. cenotensis* it is less than 1.2 times. Another difference is that in the flagellum of antennae 1 and 2, *H. cenotensis* bears 7 and 9 articles, respectively, although the specimens are larger (5.3 mm) than *H. maya* n. sp. (4.15 mm), where a maximum of 9 and 10 articles are present. Finally, the relative length of the ramus in uropod 3 in *H. maya* n. sp. is longer than the peduncle, while in *H. cenotensis* it is slightly shorter, close to the length of the longest seta of the peduncle.

According to González and Watling (2002), due to the scarce variation in the characters of the *H. azteca* complex, the telson setation and the relative length of the antennae are important to distinguish among different species. In addition, Soucek et al. (2015) suggested to use the relative length of uropod 3 with respect to the peduncle and its longest seta to distinguish the species of the complex. This character, together with others, was useful to separate two species from the U.S. and Canada (*H. wellborni* and *H. spinicauda*), and those identifications were later confirmed with the analysis of the mitochondrial cytochrome oxidase gene, subunit I (COI).

The recent description of two species of epicontinental amphipods in the same sinkhole in Mexico could mean that we need more samplings to study adequately the amphipods in these environments.

Key to the species of *Hyalella* (*Hyalella*) in North America and the Caribbean region (Modified from Baldinger, 2004; Marrón-Becerra et al., 2014; Soucek et al., 2015).

1. Eyes absent 2
   – Pigmented eyes present 3
2. Antenna 1 is longer than antenna 2; sterna gills on pereonites 3-7; telson with four distal setae ..... *H. muerta*
   – Antenna 1 shorter than antenna 2; sterna gills on pereonites 2-7; telson without distal setae ..... *H. cenotensis*
3. Body with dorsal mucronations 8
   – Body without dorsal mucronations 4
4. Ramus of uropod 3 is vestigial or robust, subequal or shorter than peduncle 5
   – Ramus of uropod 3 slender, subequal or longer than peduncle 6
5. Ramus of male uropod 3 is robust with seven apical spines ..... *H. sandra*
   – Ramus of male uropod 3 vestigial with two to four spines ..... *H. meraspinosa*
6. Antenna 1 and 2 are subequal in length 7
   – Antenna 2 is nearly twice the length of antenna 1 ..... *H. longicornis*
7. Hind margin of merus of pereopods 3 and 4 has long setae, telson with two closely apical setae ..... *H. caribbeana*
   – Hind margin of article 4 of pereopods 3 and 4 with short setae, telson with two long, broadly-spaced, apical setae ..... *H. inermis*
8. Inner plate of maxilla 1 is narrow, with two to five apical plumose setae 9
   – Inner plate of maxilla 1 is broad, subtriangular with two or three apical plumose setae, followed closely by 22-30 similar medial setae ..... *H. montezuma*
9. Antenna 1 is longer than half the length of antenna 2, and only first, or first two abdominal segments bearing dorsal mucronations 10
   – Antenna 1 is less than half the length of antenna 2, with all three abdominal segments bearing dorsal mucronations ..... *H. texana*
10. Gnathopod 2 of males, carpus posterior lobe is about as long as width of merus; in pereopod 7, the distal/ bottom margin of basis posterior lobe, dentate or not, with one or two very small setae if any ... 11
    – Gnathopod 2 of males, carpus posterior lobe 1.5 times as long as width of merus; pereopod 7, distal/bottom margin of the basis posterior lobe is strongly dentate, and with two or more relatively long spines ..... *H. azteca*
11. Gnathopod 2 propodus (males), palm with a distinct angle step (visible under high power), tip of dactyl approximately aligns vertically with distal end of posterior lobe of carpus; telson distal setae is separated, short, and at least as stout as setae on uropod 3 ramus ..... *H. spinicauda*
    – Gnathopod 2 propodus (males), palm without a distinct angle step or notch, tip of dactyl aligning vertically well beyond (posteriorly) distal end of posterior lobe of carpus; telson terminal setae clearly finer and longer than setae on uropod 3 ramus 12
12. Telson with two long and slender apposed setae; uropod 3 ramus, approximately as long as or slightly longer than the longest seta on peduncle; pereopod 7, posterior lobe, ventral margin without stout spines; maxilla 1, inner plate with two pappose setae; maxilliped nail short (less than half the length of palp article 4) ..... *H. wellborni*
    – Telson with two long and slender setae widely separated; uropod 3 ramus longer than the longest setae on peduncle; pereopod 7, posterior lobe, ventral margin with one stout setae; maxilla 1, inner plate with three pappose setae; maxilliped nail is long (longer than half length of palp article 4) ..... *H. cenotensis* n. sp.

Acknowledgements

We wish to thank the “Laboratorio de Microscopía and Fotografía de la Biodiversidad I, of IBUNAM,” and Ma. Berenit Mendoza-Garfias for the SEM pictures, as well as Carlos Illescas Monterroso for his help and support and Fernanda Charqueño Celis for her help with the separation of the biological material. The first author is grateful for a scholarship granted by Consejo Nacional de Ciencia y Tecnología – Programa Nacional de Posgrados de Calidad (CONACYT-PNPC, number 406408), México.

References

Baldinger, A.J., 2004, A new species of *Hyalella* (Crustacea: Amphipoda: Hyalellidae) from Ash Springs, Lincoln County, Nevada, U.S.A., with a key to the species of the genus in North America and the Caribbean region: Journal of Natural History, v. 38, p. 1087−1096. http://dx.doi.org/10.1080/00222930310000753 67.

Baldinger, A.J., Shepard, W.D. and Threloff, D.L., 2000, Two new species of *Hyalella* (Crustacea: Amphipoda: Hyalellidae) from Death Valley National Park, California, U.S.A.: Proceedings of the Biological Society of Washington, v. 113, no. 2, p. 443−457.

Bousfield, E.L., 1996, A contribution to the reclassification of neotropical freshwater hyalellid amphipods (Crustacea: Gammaridea, Talitroidea): Bollettino del Museo Civico di Storia Naturale di Verona, v. 20, p. 175−224.

Brito, R.M., Francisco, F.O., Ho, S.Y.W. and Oldroyd, B.P., 2014, Genetic architecture of the *Tetragonula carbonaria* species complex of Australian stingless bees (Hymenoptera: Apidae: Meliponini): Biological Journal of the Linnean Society, v. 113, p. 149−161. http://dx.doi.org/10.1111/bij.12292.

Cole, G.A. and Watkins, R.L., 1977, *Hyalella montezuma*, a new species (Crustacea: Amphipoda) from Montezuma Well: Hydrobiologia, v. 52, no. 2-3, p. 175−184. https://doi.org/10.1007/BF00036441.

García-Schroeder, D.L. and Araujo, P.B., 2009, Post-marsupial development of *Hyalella pleoacuta* (Crustacea: Amphipoda): stages 1-4: Zoologia, v. 26, p. 391−406. http://dx.doi.org/10.1590/S1984-46702009005000010.

Geisler, F.S., 1944, Studies on the postembryonic development of *Hyalella azteca* (De Saussure): Biological Bulletin, v. 86, no. 1, p. 6−22. http://dx.doi.org/10.2307/1537947.

González, E.R. and Watling, L., 2001, Three new species of *Hyalella* from Chile (Crustacea: Amphipoda: Hyalellidae): Hydrobiologia, v. 464, p. 175−199. http://dx.doi.org/10.1023/A:1013961904370.

González, E.R. and Watling, L., 2002, Redescription of *Hyalella azteca* from its type locality, Vera-Cruz, Mexico (Amphipoda: Hyalellidae): Journal of Crustacean Biology, v. 22, no. 1, p. 173−183. https://doi.org/10.1651/0278-0372(2002)022[0173:ROHAFI]2.0.CO;2 https://doi.org/10.1163/20021975-99990220.

González, E. and Watling, L., 2003a, A new species of *Hyalella* from Patagonia, Chile, with redescription of *H. simplex* Schellenberg, 1943 (Crustacea: Amphipoda): Journal of Natural History, v. 37, no. 17, p. 2077−2094. http://dx.doi.org/10.1080/00222930210133246.

González, E. and Watling, L., 2003b, A new species of *Hyalella* from Colombia, and the redescription of *H. meinerti* Stebbing, 1899 from Venezuela (Crustacea: Amphipoda): Journal of Natural History, v. 37, no. 17, p. 2095−2111. http://dx.doi.org/10.1080/00222930210133255.

González, E. and Watling, L., 2003c, A new species of *Hyalella* from Brazil (Crustacea: Amphipoda: Hyalellidae), with redescriptions of three other species in the genus: Journal of Natural History, v. 37, no. 17, p. 2045−2076. http://dx.doi.org/10.1080/00222930210133237.

González, E. and Watling, L., 2003d, Two new species of *Hyalella* from Lake Titicaca, and redescriptions of four others in the genus (Crustacea: Amphipoda): Hydrobiologia, v. 497, p. 181−204. https://doi.org/10.1023/A:1025451813972.

Graening, G.O., Rogers, D.C., Holsinger, J.R., Barr, C. and Bottorff, R., 2012, Checklist of inland aquatic Amphipoda (Crustacea: Malacostraca) of California: Zootaxa, v. 3544, p. 1−27.

Hendrycks, E.A. and Bousfield, E.L., 2001, The amphipod genus *Allorchestes* in the North Pacific region: Systematics and distributional ecology: Amphipacifica, v. 3, no. 2, p. 3−38.

Hogg, I.D., Larose, C., de Lafontaine, Y. and Doe, K.G., 1998, Genetic evidence for a *Hyalella* species complex within the Great Lakes-St. Lawrence River drainage basin: implications for ecotoxicology and conservation biology: Canadian Journal of Zoology, v. 76, np. 6, p. 1134−1152. http://dx.doi.org/10.1139/z98-034.

Horton, T. and Lowry, J., 2013, *Hyalella* S. I. Smith, 1874, Horton, T., Lowry, J., De Broyer, C., Bellan-Santini, D., Coleman, C. O., Daneliya, M.; Dauvin, J-C.; Fišer, C.; Gasca, R.; Grabowski, M.; Guerra-García, J. M., Hendrycks, E., Holsinger, J., Hughes, L., Jaume, D., Jazdzewski, K., Just, J., Kamaltynov, R. M., Kim, Y.-H., King, R., Krapp-Schickel, T., LeCroy, S., Lörz, A.-N., Senna, A. R., Serejo, C., Sket, B., Tandberg, A.H., Thomas, J., Thurston, M., Vader, W., Väinölä, R., Vonk, R., White, K., Zeidler, W, World Amphipoda Database. Accessed through: World Register of Marine Species at http://www.marinespecies.org/aphia.php?p=taxdetails&id=158104 [accessed October 11, 2017].

Lowry, J.K. and Myers, A.A., 2013, A phylogeny and classification of the Senticaudata subord. nov. (Crustacea: Amphipoda): Zootaxa, v. 3610, no. 1, p. 001−080. http://dx.doi.org/10.11646/zootaxa.3610.1.1.

Marrón-Becerra, A., Hermoso-Salazar, M. and Solís-Weiss, V., 2014, *Hyalella cenotensis*, a new species of Hyalellidae (Crustacea: Amphipoda) from the Yucatan Peninsula, Mexico: Zootaxa, v. 3811, no. 2, p. 262−270. http://dx.doi.org/10.11646%2Fzootaxa.3811.2.7.

De Saussure, H., 1858, *Mémoires pour servir à l'Histoire Naturelle du Mexique, des Antilles et des États-Unis*: Genève, Paris, I Crustacés, 82 p.

Soucek, D.J., Lazo-Wasem, E.A., Taylor, C.A. and Major, K.M., 2015, Description of two new species of *Hyalella* (Amphipoda: Hyalellidae) from Eastern North America with a revised key to North American members of the genus: Journal of Crustacean Biology, v. 35, no. 6, p. 814−829. http://dx.doi.org/10.1163/1937240X-00002373.

Stebbing, T.R.R., 1903, Amphipoda from Costa Rica: Proceedings of the United States National Museum, v. 26, p. 925−931. https://doi.org/10.5479/si.00963801.26-1341.925.

Stevenson, M.M. and Peden, A.E., 1973, Description and ecology of *Hyalella texana* n. sp. (Crustacea: Amphipoda) from the Edwards Plateau of Texas: American Midland Naturalist, v. 89, no. 2, p. 426−436. http://dx.doi.org/10.2307/2424045.

Witt, J.D.S. and Hebert, P.N.D., 2000, Cryptic species diversity and evolution in the amphipod genus *Hyalella* within central glaciated North America: a molecular phylogenetic approach: Canadian Journal of Fisheries and Aquatic Sciences, v. 57, p. 687−698. http://dx.doi.org/10.1139/f99-285.

Witt, J.D.S., Threloff, D.L. and Hebert, P.D.N., 2006, DNA barcoding reveals extraordinary cryptic diversity in an amphipod genus: implications for desert spring conservation: Molecular Ecology, v. 15, p. 3073−3082. http://dx.doi.org/10.1111/j.1365-294X.2006.02999.x.

Zimmer, A., Araujo, P.B. and Bond-Buckup, G., 2009, Diversity and arrangement of the cuticular structures of *Hyalella* (Crustacea: Amphipoda: Dogielinotidae) and their use in taxonomy: Zoologia, v. 26, no. 1, p. 127−142. http://dx.doi.org/10.1590/S1984-46702009000100019.

N. Czaplewski, K. Rogers, and C. Russell. Late Pleistocene vertebrates from Three-Forks Cave, Adair County, Oklahoma Ozark Highland. *Journal of Cave and Karst Studies*, v. 80, no. 2, p. 1-16. DOI:10.4311/2017PA0118

LATE PLEISTOCENE VERTEBRATES FROM THREE-FORKS CAVE, ADAIR COUNTY, OKLAHOMA OZARK HIGHLAND

Nicholas J. Czaplewski[1,C], Kyler J. Rogers[1], and Clayton Russell[2]

Abstract

We report on an assemblage of vertebrate fossils from a limestone cave in the southwestern portion of the Ozark Highlands. The fauna includes several extinct, large-bodied mammalian taxa including *Megalonyx jeffersonii* (Jefferson's ground sloth), *Canis dirus* (dire wolf), *Arctodus simus* (short-faced bear; two individuals), and Equidae (extinct horses), which indicate a late Pleistocene age. In addition, there is a variety of extant vertebrates including a fish, *Aplodinotus* cf. *grunniens* (freshwater drum), unidentified Anura (frogs and toads) and Caudata (salamanders), *Terrapene* sp. (box turtles), cf. *Ophisaurus* (legless lizards), Colubroidea and Crotalidae (non-venomous snakes and pit vipers), *Bubo virginianus* (great horned owl), and at least 12 other mammals: *Sorex* sp. (long-tailed shrews), *Perimyotis subflavus* (tricolored bat), *Eptesicus fuscus* (big brown bat), *Myotis grisescens* (gray myotis), possibly other species of *Myotis*, Vulpini (foxes), several rodents, *Geomys* sp. (pocket gophers), *Chaetodipus* or *Perognathus* (pocket mice), Peromyscini (native mice), *Neotoma* cf. *floridana* (eastern wood rat), *Microtus* cf. *ochrogaster* (prairie vole), and, *Sylvilagus* sp. (cottontail rabbits). An earlier report provided a tentative age of one of the *Arctodus simus* of about 34,000 years ago (late Pleistocene, Rancholabrean). Among the 23 taxa in the Three-Forks Cave assemblage, two species are added to the Oklahoma Ozark Highland paleofauna: freshwater drum and great horned owl. One extralimital taxon, the pocket mouse *Chaetodipus* or *Perognathus*, is present in the assemblage. Numerous remains of juvenile bats of *Myotis grisescens* and *Eptesicus fuscus* provide evidence that these species used Three-Forks Cave as a maternity site. Large crater-like pits in the floor of Three-Forks Cave and other caves in the vicinity may represent ancient and modern beds of the short-faced bear and black bear, respectively.

Introduction

Late Pleistocene faunas are relatively well known from localities in the Ozark Highlands of central North America, especially those recovered from caves. In the online database for North American late Quaternary mammal localities, FAUNMAP II-NEOTOMA (FAUNMAP Working Group, 1994; http://www.ucmp.berkeley.edu/faunmap/about/index.html), 36 such vertebrate faunal assemblages are known in the Missouri Ozarks and four in the Arkansas Ozarks. No localities from the Oklahoma portion of the Ozark Highland are listed in FAUNMAP II-NEOTOMA, but three cave sites were overlooked. These are Gittin' Down Mountain Cave (an alternative name for Three-Forks Cave) with one species (Puckette, 1976; Smith and Cifelli, 2000), Sassafras Cave with nine taxa (Czaplewski et al., 2002); and CZ-9 Cave (aka Dressler Cave) with three taxa (Czaplewski and Puckette, 2015). Three-Forks Cave, with 23 taxa described herein, substantially adds to the Pleistocene fauna of the Ozark Highland in Oklahoma and bolsters knowledge of the Quaternary history of this physiographic region.

A single tooth of the short-faced bear, *Arctodus simus,* was reported from Gittin' Down Mountain Cave, Okla. by Puckette (1976). The specimen, a worn right m2, was deposited in the University of Arkansas Museum as UAM 75-839-1. We report additional remains of this same individual bear, as well as a second individual and an associated late Quaternary vertebrate assemblage from the same cave, aka Three-Forks Cave. The *Arctodus* molar from Three-Forks Cave was used by Schubert (2010) in his study of the chronology of late Quaternary *Arctodus* finds in North America. He provided a date of 34,063 ± 460 rcybp (NZA-27,734; 14C range at 2 sigma: 33,143 to 34,983 ybp) on the *Arctodus* m2 dentine, but noted that "The C:N ratio of 2.4 falls outside the range of well-preserved collagen…. Further, the percent C is particularly low, and these factors imply that the collagen from the sampled dentine is degraded. While this does not indicate a 'bad' date, it does mean that some degree of caution should be associated with it" (Schubert, 2010: p. 191). If the Three-Forks Cave *Arctodus* date is taken at face value, it is approximately equivalent to the oldest directly-dated *Arctodus simus* in North America from Island Ford Cave, Virginia (in which the collagen was well preserved; Schubert 2010). We, tentatively, use Schubert's (2010) 34 ka date as the approximate age for the Three-Forks Cave assemblage, while pointing out that fossils were collected from several different parts of the cave, and they are likely to be diachronous (Semken et al., 2010).

Three-Forks Cave is on private property adjacent to the Donald R. Russell Cave Preserve, in Adair County, Okla. (Fig. 1), and it is recorded as Oklahoma Museum of Natural History (OMNH) locality V1474. It developed within limestone

[1]Oklahoma Museum of Natural History, 2401 Chautauqua Avenue, and Department of Biology, University of Oklahoma, Norman, OK 73072, USA.
[2]Chair, Donald R. Russell Cave Preserve; Rt. 1 Box 1459, Stilwell, OK 74960, USA.
[C]Corresponding Author: nczaplewski@ou.edu

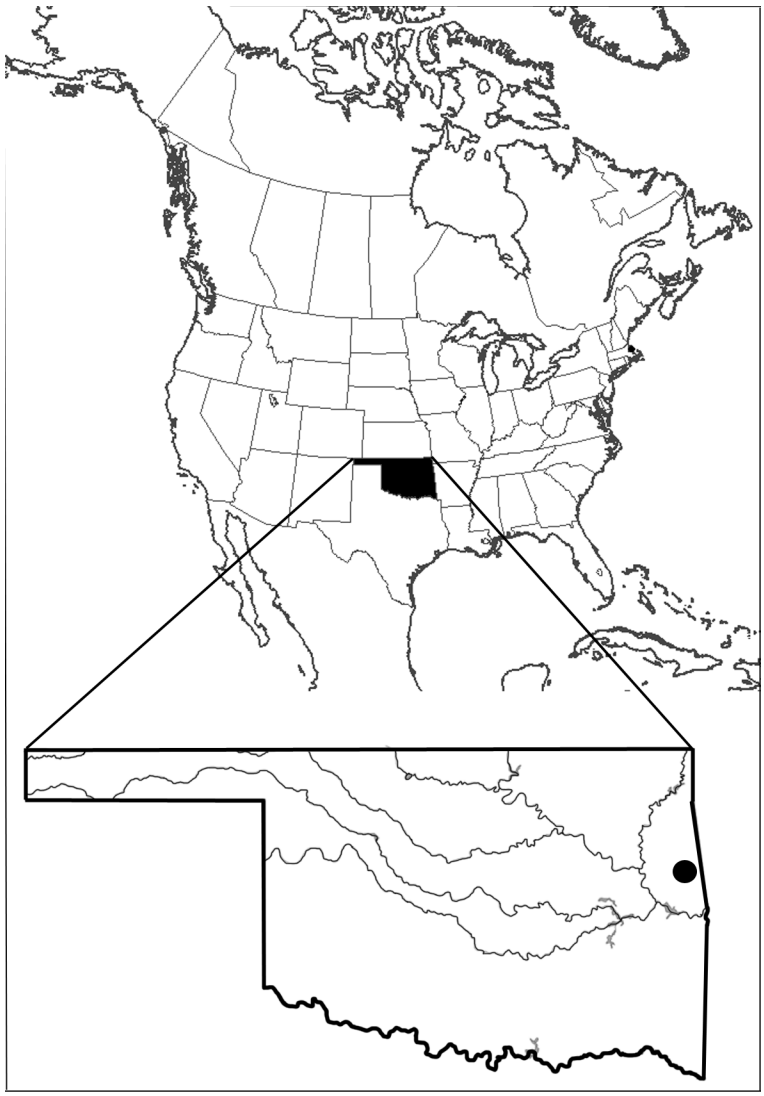

Figure 1. Locator map of central North America with state of Oklahoma in black, enlarged below, showing location of Three-Forks Cave (dot).

of the Pitkin Formation, late Mississippian age; the formation is about 18 m thick in this area. Within the cave there are two main bone accumulation areas, the Drain (Fig. 2A) and the Second Parachute Room (Fig. 2B), as well as a few additional isolated occurrences of fossils elsewhere (Fig. 2C, 2D). The Drain is an area in which the small stream running through this part of the cave drops through the floor downstream of several rimstone dams. Numerous small bones that had been cemented into the floor are exposed. From the dams, the stream drops into lower level passages too small to be entered. Many of the larger vertebrates, each of which was represented by an isolated bone, and most of the microvertebrate fossils came from the Drain area (Fig. 2A). The Second Parachute Room is named for a fringed canopy speleothem in the passage. The more complete fossils of two short-faced bears came from the Second Parachute Room (Fig. 2B), while the other bear bones came from a passage not far from the Drain (Fig. 2D). The provenience data for all cave fossils were recorded with individual, cataloged specimens and are also recorded below in the systematic accounts (under Materials). The preservation and condition of fossils in these distinctive areas of the cave differs somewhat, and even varies within one area (microvertebrates in the Drain). Although the temporal span during which fossils accumulated in these cave areas probably also differ, the assemblage is considered a single local fauna.

Some Three-Forks Cave fossils were collected by Clayton and Donald Russell in the mid-late 20th century. We did further collecting in April, 2003, May, 2004, and May, 2006, resulting in a total of 988 cataloged specimens. Most of the bones from the Drain are dark brown to reddish brown, and many are encrusted in yellowish-buff to brown carbonate with included pebbles and cobbles. In contrast, bones from the Second Parachute Room are mostly light in color with dark-tinted edges, where they had been partly exposed by foot traffic in a walking passage. These bones are more fragmentary and were found in mud on the cave floor. The isolated bones from other areas of the cave vary in color. The dissimilar preservation probably reflects varying conditions in different areas of the cave.

Methods

Specimens were collected on three trips during 2003, 2004, and 2006, using rock hammer, awls, trowels, and chisels. Fossils were selectively removed from carbonate and gravelly mud deposits in the wet crawlways and stream beneath the floor and a natural bridge at the Drain, and in the floor of the Second Parachute Room. They were also removed from rock and mud in the floor at a few other passages. Fossils were wrapped, bagged, and labeled for transport to the OMNH, where they underwent preparation and cleaning. Bulk samples of sedimentary deposits amounting to perhaps 100 kg from the Drain and Second Parachute Room were bagged for transport and processed to recover microvertebrate fossils by standard screenwashing methods using tandem screen boxes of 1.5 mm (coarse) and 0.6 mm (fine) mesh (Cifelli, 1996).

Measurements of larger specimens were made with dial calipers; smaller specimens were measured with an eyepiece reticle in an Olympus SZX9 stereomicroscope. All measurements are in millimeters. Standard measurements of teeth are abbreviated APL for greatest anteroposterior length of crown, and TW for greatest transverse width of crown. Other measurements are described in the text and tables. Of the total of 988 vertebrate specimens recovered from

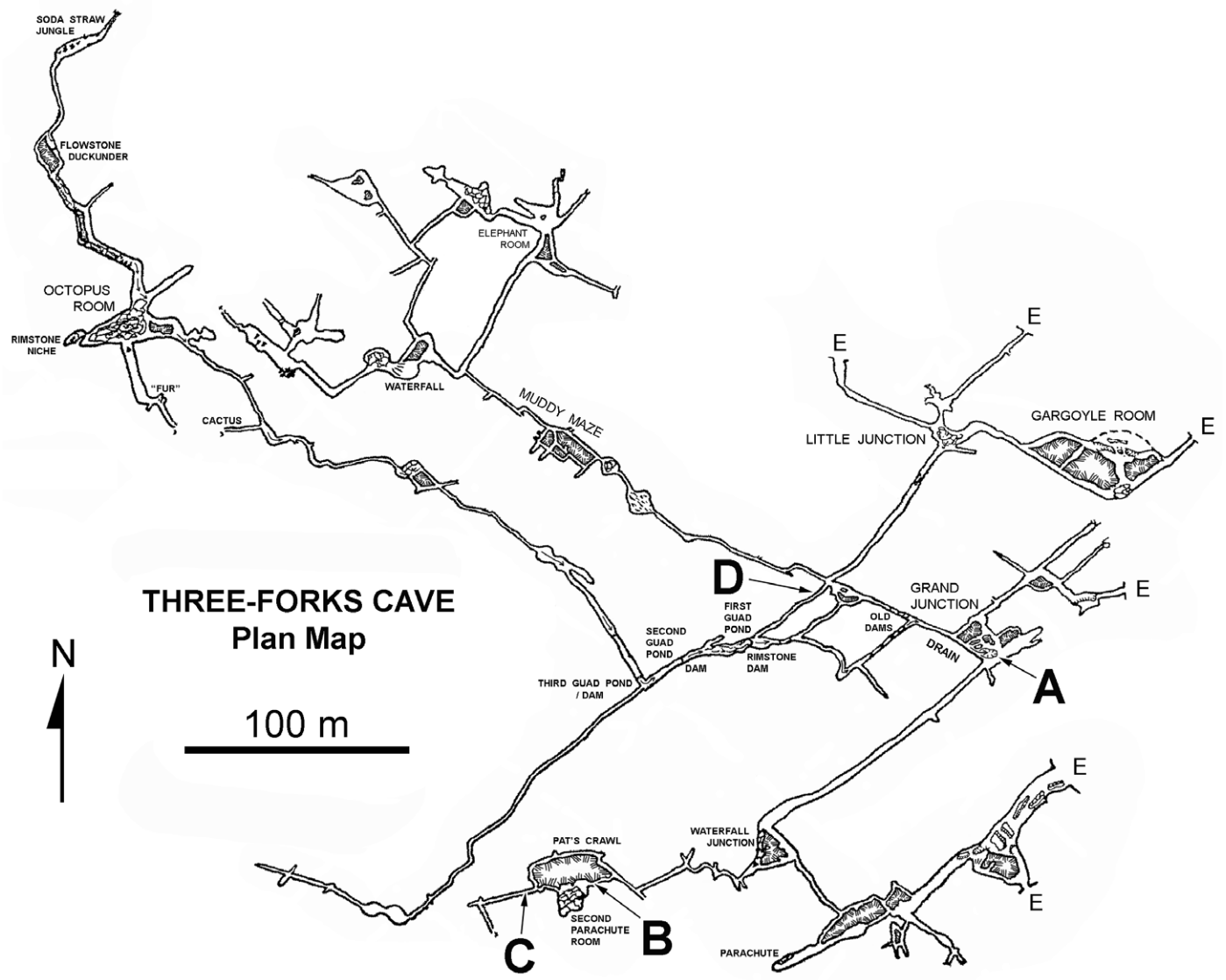

Figure 2. Plan map of Three-Forks Cave, Adair County, Oklahoma, by Donald Russell, 1976, indicating areas in which fossils in this report were recovered. Abbreviations: A, main concentration of fossils, including most microvertebrates, within the Drain; B, concentration of *Arctodus simus* bones and a few microvertebrates near Second Parachute Room; C, isolated horse bone; D, isolated *Arctodus* bones; E, entrances; Small Arrows within cave passages indicate present stream flow to the Drain.

Three-Forks Cave, about 840 are bats (85% of cataloged specimens) of which 700 were identified only to the family level. Herein we list the taxa recovered, with discussion of only those identifiable to lower-level categories (family, genus, or species) or with implications of paleontological significance. A complete inventory of cataloged and identified vertebrate skeletal elements recovered from Three-Forks Cave, Adair County, Okla., is available from the Department of Vertebrate Paleontology at the OMNH.

Systematic Paleontology

Osteichthyes

Sciaenidae

Aplodinotus cf. *grunniens* (freshwater drum)

Material: OMNH 78544, partial premaxilla (Fig. 3A) from the Drain.

The lateral branch of the bone and crowns of the teeth are broken away, but the remainder of the premaxilla, with cuplike tooth bases, is nicely preserved. A few other fish bones, all from the Drain, were recovered but were not identifiable to family. We did not have access to comparative osteological fish specimens. Morphology of the premaxilla resembles that of other sciaenids: having the ascending process rising at a right angle to the alveolar process, ascending process slender and straight and closely appressed to, but separated from, the articular process by a distinct notch, and

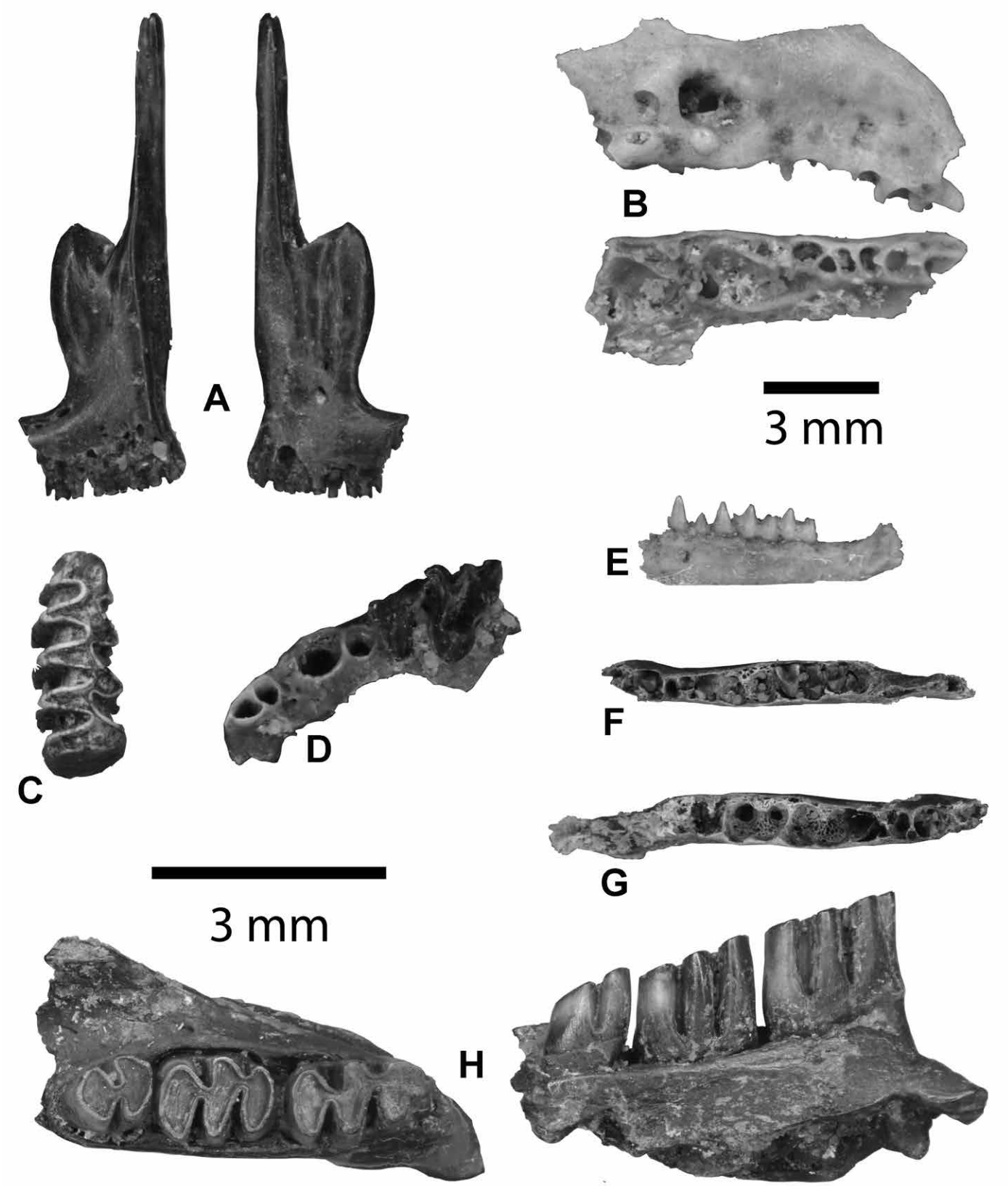

Figure 3. Selected microvertebrate fossils from Three-Forks Cave, Oklahoma. A, *Aplodinotus* cf. *grunniens* right premaxilla (OMNH 78544) in medial and lateral views. B, Sorex sp. rostrum fragment (OMNH 78524) in labial and occlusal views. C, *Microtus* cf. *ochrogaster* m1 from dentary fragment (OMNH 78353) in occlusal view. D, *Perimyotis subflavus* rostrum fragment with empty alveoli and P4-M1 (OMNH 77789) in occlusal view; E, *P. subflavus* dentary with c1-m2 (OMNH 77695) in labial view. F, *Myotis grisescens* juvenile dentary with deciduous and permanent tooth alveoli and developing teeth (OMNH 77728) in occlusal view. G, *Eptesicus fuscus* juvenile dentary showing deciduous tooth alveoli and developing permanent teeth (OMNH 77729) in occlusal view. H, *Neotoma* cf. *floridana* dentary fragment with m1-m3 (OMNH 77700) in occlusal and labial views. Scale bar at left pertains to A, C, D, and H; scale bar at right pertains to B, E, F, and G.

articular process about half the height of the ascending process. However, no autapomorphies of the premaxilla are recorded in *Aplodinotus* (Sasaki, 1989). The specimen from Three-Forks Cave matches the premaxilla of the freshwater drum illustrated by Green (1941: plate I fig. 10), Sasaki (1989: fig. 34A), and Qadri and McAllister (1967: plate II fig. 11c). The freshwater drum is distinct among the Sciaenidae as the only member of this large family to inhabit freshwater (Sasaki, 1989); all other Sciaenidae are marine. The recent native distribution of *A. grunniens* includes relatively large bodies of water in the Mississippi River drainage and Great Lakes regions over much of the eastern United States, including the entire Ozark Highlands and surrounding regions (Page and Burr, 1991). If the fossil actually represents the living species and not an unrecognized, extinct one, this is the first fossil record of *A. grunniens* from the Ozark Highlands. The species is relatively common as a Pleistocene fossil in the United States (Jacquemin et al., 2016) and is known as a fossil elsewhere in Oklahoma in the early Pleistocene (Irvingtonian land mammal age) Berends local fauna (Smith, 1954). However, because of our inability to find autapomorphic characters in the fossil, its paleogeographic significance is dubious.

Amphibia

Anura

Sixteen skeletal elements, including several ilia, from an undetermined number of individual frogs or toads were recovered from the Drain but lacked morphological characters by which they could be further identified.

Caudata

A total of 45 salamander skeletal elements including several vertebrae were recovered from the Drain. The vertebrae of salamanders are considered taxonomically useful (Holman, 1995). They are identifiable as salamanders, based on the hourglass-shaped centrum and two elongated rib-bearing processes on either side, and on being amphicoelous or with ossified caps on some cotyles as in Plethodontidae. The specimens from Three-Forks Cave could not be identified to family level, but both simple and complex forms noted by Holman (1995) are represented. They are important in providing a basis for inclusion of Caudata in the faunal list.

Reptilia

Chelonia

Emydidae

Terrapene sp. indet. (box turtle)

Material: OMNH 77923, costal bone from the Drain.

The costal is long and narrow, parallel-sided along the sutures with adjacent costals, and curved to indicate a high-domed carapace. It shows grooves proximally for parts of two overlying neural scutes, but no groove for the pleural scutes. Probably, it represents a left fifth costal. These characteristics agree with those of box turtles and differ from costals of other Quaternary genera of North American turtles (Sobolik and Steele, 1996).

Squamata

Anguidae

cf. *Ophisaurus sp.* (glass lizards)

Material: OMNH 78540, osteoderm from the Drain.

The osteoderm is quadrate in outline, unkeeled, thin, with a rugose surface and fairly matches the mid-trunk, dorsal osteoderms of various anguids (Mead et al., 1999). Given the intra- and interindividual morphological variation in osteoderms of these lizards, we can only tentatively refer the isolated specimen to cf. Ophisaurus.

Serpentes

Colubroidea indet. (non-venomous snakes)

Material: OMNH 73029-73030, two partial trunk vertebrae from the Drain.

These vertebrae are diagnostic of snakes in possessing zygosphenes and zygantra. They resemble certain North American colubroids in lacking a long, stout hypapophysis; instead they bear low, flattened, spatulate to gladiate, hemal keels (Holman, 2000).

Crotalidae (pit vipers)

Genus indet.

Material: OMNH 78545, trunk vertebra from the Drain.

This vertebra is identifiable as that of a crotalid based on the stout, long hypapophysis (Holman, 2000). The morphological variability of crotalid vertebrae is such that individual vertebrae are not reliably identifiable beyond the family level (Bell et al., 2004). The element could feasibly represent a member of either *Agkistrodon or Crotalus,* but is too large (neural arch width, 7.8 mm; width across post-zygapophyses, 11.5 mm) to represent a member of *Sistrurus.*

Aves
Strigiformes
Strigidae
Bubo virginianus (great horned owl)
Material: OMNH 77903, complete right humerus from the Drain.

Measurements (mm) of the specimen are: length, 132.1; width of shaft, 9.3; width of proximal end, 22.6; width of distal end, 10.9. These measurements are well within the ranges of the same measurements for the species provided in Avian Osteology — Bird Bone Identification Guide (https://royalbcmuseum.bc.ca/Natural_History/Bones/Species-Pages/GHOW.htm).

There is some damage proximally to the medial crest and internal tuberosity (tuberculum ventrale). OMNH 77903 is smaller than the humerus of the snowy owl, *Bubo scandiaca*, and great gray owl, *Strix nebulosa*, and larger than that of the barred owl, *Strix varia* and other small North American owls. Morphologically, the humerus differs from that of *Strix* owls in that the ectepicondylar prominence is papilla-shaped and is distinct from the shaft and ectepicondyle (epicondylus dorsalis) (Howard, 1929). It differs from the humerus of the related *B. scandiaca* in having the ectepicondylar prominence shorter relative to its length (Howard, 1929).

This is the first fossil record of the great horned owl in the Ozark Highlands and in Oklahoma. As a late Pleistocene fossil in North America, the species *B. virginianus* is widespread and recorded from sites in the Mexican states of Chihuahua and Nuevo León, and in Arizona, California, Florida, Nevada, New Mexico, Texas, Utah, and Wyoming in the United States (Miller and DeMay, 1942; Miller, 1943; Howard, 1952; Emslie, 1985; Emslie and Heaton, 1987; Hulbert, 2001; Brasso and Emslie, 2006; Harris, 2014).

Mammalia
Xenarthra
Megalonychidae
Megalonyx jeffersonii (Jefferson's ground sloth)
Material: OMNH 77904, either manual digit IV phalanx 2 or manual digit III phalanx 2, lacking the proximal epiphysis, indicating a subadult individual (Fig. 4D−H). From the Drain. Measurements (mm) are greatest depth of distal condyles, 28.7; distal width, 19.4

Because the specimen lacks the proximal epiphysis, the proximal articular surface is absent and cannot be characterized. Adjacent to the growth plate, the dorsoventral height of the bone shaft is less deep than the distal condyles and quickly shallows to a height of 17.1 mm before reaching the distal condyles. The distal articulation is extensive, with the condyles sweeping through an arc of more than 180°, with a deep groove between the condyles. A prominent dorsal pit and more modest ventral pit at either end of the groove receive the projecting processes of the ungual phalanx (Fig 4D−H). These characteristics are unique to xenarthran manual phalanges and the large size indicates a ground sloth. However, the incomplete nature of the bone and the similarity in certain manual phalanges of late Pleistocene North American ground sloths obscures the identification of the element. Of North American late Pleistocene ground sloths, the manual phalanx 2 of digit IV in *M. jeffersonii* is quite similar to the manual phalanx 2 of digit III in *N. shastensis.*

If OMNH 77904 is a manual digit IV phalanx 2, that element in *Paramylodon harlani* (Harlan's ground sloth) is rudimentary (Stock, 1925). The same element in *Nothrotheriops shastensis* (Shasta ground sloth) is greatly foreshortened with hardly any shaft between the proximal and distal articulations (Stock, 1925). Thus, OMNH 77904 is unlike that of these two sloths and instead resembles the bone of *M. jeffersonii*. On the other hand, if OMNH 77904 is a manual digit III phalanx 2, that element in *P. harlani* is foreshortened with hardly any shaft (Stock, 1925). The same phalanx of *M. jeffersonii* is far more robust with a mediolaterally, much wider shaft (McDonald, 1977). Thus, OMNH 77904 is unlike both of these taxa, and instead it resembles the element in *N. shastensis* (Paula Couto, 1976). Perhaps future ancient DNA analysis could help identify this incomplete bone.

Nothrotheriops shastensis has no late Pleistocene (Rancholabrean) records in the Ozark Highlands and no fossil record in Oklahoma (McDonald and Jefferson, 2008; a previous record of the species in western Oklahoma (Akersten and McDonald, 1991; Smith and Cifelli, 2000) is Irvingtonian, early Pleistocene, and was re-identified as *Nothrotheriops texanus* [McDonald and Jefferson, 2008]). If the Three-Forks Cave sloth were *N. shastensis*, it would represent a huge 980 to 1190 km northeastward or northward extension in its late Pleistocene range from the nearest known localities in New Mexico, USA, and Nuevo León, Mexico (McDonald and Jefferson, 2008). The numerous North American records of Wisconsin glacial age of *M. jeffersonii* were summarized by Hoganson and McDonald (2007). These records included several from the northern Ozark Highland in Missouri but none in the Arkansas or Oklahoma portions of the Ozarks. Thus, the Three-Forks Cave record represents the first occurrence of Jefferson's ground sloth in the southern Ozark Highlands. We assert that the record in Three-Forks Cave is inconsistent and unparsimonious as *N. shastensis*. This assertion is based on the known paleogeographic distribution of that species and its absence in other Ozark Highland late Pleistocene assemblages and caves, and that the fossil instead represents *M. jeffersonii*.

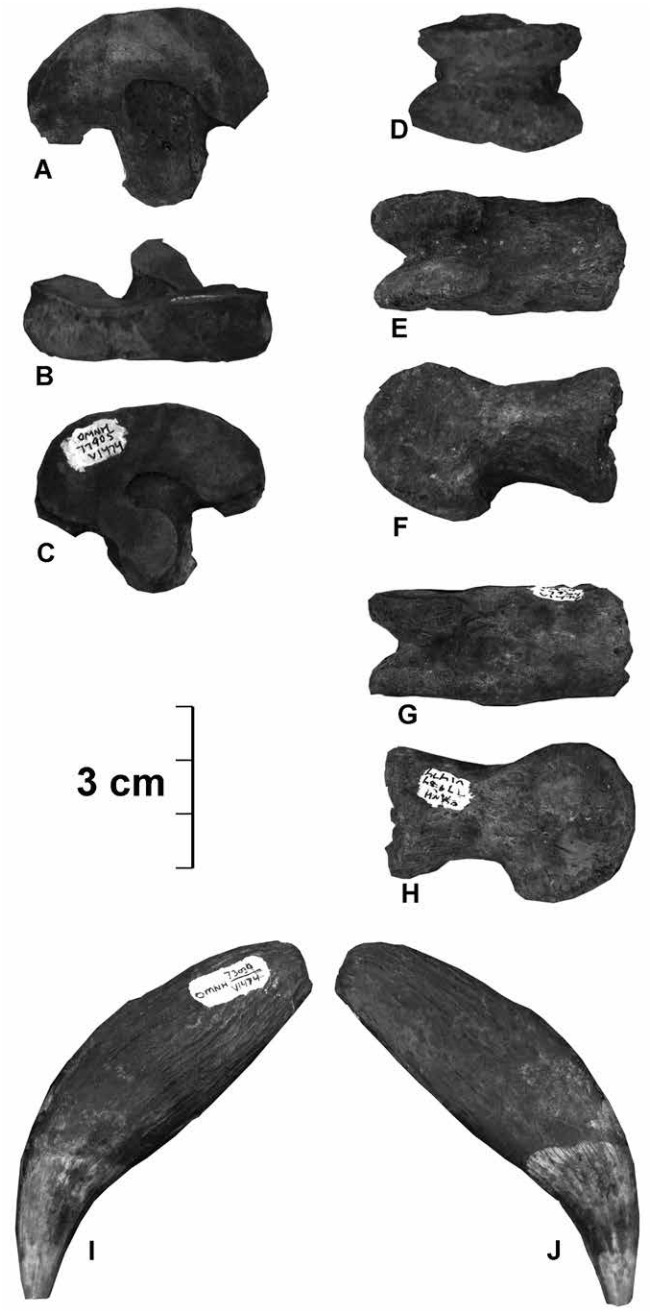

Figure 4. Fossils of large mammals from Three-Forks Cave, Oklahoma. Equidae left lateral ectocuneiform (OMNH 77905) in A, distal view; B, anterior view; C, proximal view. *Megalonyx jeffersonii* phalanx lacking proximal epiphysis (OMNH 77904) in D, distal view; E, palmar view; F, lateral view; G, dorsal view; H, lateral view. *Canis dirus* right upper canine (OMNH 73039) in I, labial view and J, lingual view.

Soricomorpha

Soricidae

Sorex sp. indet. (long-tailed shrews)

Material: OMNH 78524, edentulous right rostrum fragment with alveoli for the entire upper tooth row except for those of the M3 (Fig. 3B), from the Drain.

The alveoli in this skull fragment indicate five unicuspids decreasing in size slightly from front to back, and with the last being distinctly smaller than the others. This condition is seen in several species, including *Sorex arizonae, S. cinereus, S. haydeni, S. lyelli, S. merriami, S. nanus,* and *S. preblei*; thus, we are unable to assign the specimen to a species.

Chiroptera

Skeletal elements of bats are by far the most common fossils in the Three-Forks Cave deposits, represented by over 840 bones and isolated teeth. All pertain to Vespertilionidae, and most probably belong to *Myotis*, with a few pertaining to other genera. Those elements most diagnostic to the species level are discussed in detail below.

Vespertilionidae

Perimyotis subflavus (tricolored bat)

Material: OMNH 77789, left premaxilla-maxilla fragment with P4-M1 (Fig. 3D); 78214, left P4; 77851, left P4; 78516, edentulous left half rostrum; 78321, left M1 or M2; 78324, right M1 or M2; 77712, left dentary fragment with p4-m1; 77765, right maxilla with C1, P4-M1; all from the Drain. OMNH 77695, left dentary with c1-m2 (Fig. 3E) from the Second Parachute Room.

All specimens include teeth showing very little wear and thus represent young adults. We observed living tricolored bats in Three-Forks Cave, but females of this species typically give birth and raise their young outside caves in summers in tree foliage, lichen-bedecked trees, bromeliads, and rock crevices (Carter et al., 1999; Veilleux et al., 2003, 2004; Perry and Thill, 2007; Farrow and Broders, 2011). As a result, the remains of juveniles are not normally found in caves.

Eptesicus fuscus (big brown bat)

Material: OMNH 78038, left dentary fragment with m1-m2; 77705, left half rostrum with I2-M3; 78337, right M1 or M2; 77729, right dentary with erupting p4 and m3; all from the Drain.

The dentary with erupting teeth (OMNH 77729; Fig. 3G) indicates that *E. fuscus* was using the cave as a nursery roost in the late Pleistocene. The species still utilizes the cave today, but in our paleontological work we noticed no evidence of their use of it as a nursery.

Myotis grisescens (gray myotis)

Material: OMNH 72965, nearly complete cranium in a small piece of carbonate matrix, with left and right P4-M3, missing petrosals (Fig. 5); 72954, rostrum with left M2 and right M2-M3; 72955, rostrum with left P4-M3; 72958, rostrum with both P4-M3; 72960, edentulous rostrum; 77703, right half rostrum with P4-M3; 77704, rostrum with right P4 and M2; 77733, rostrum with left P4; 77734, rostrum with left C1-M3 and right P2-M3; 77735, rostrum with both P4-M3; 77736, rostrum with left P4, M2-M3 and right M2; 77737, rostrum with left P4-M3 and right P4, M2-M3; 77832, left P4; 72956-72957, right dentaries with p4-m3; 78109, left dentary with i2-m2 in a small chunk of matrix; OMNH 72969−72972,

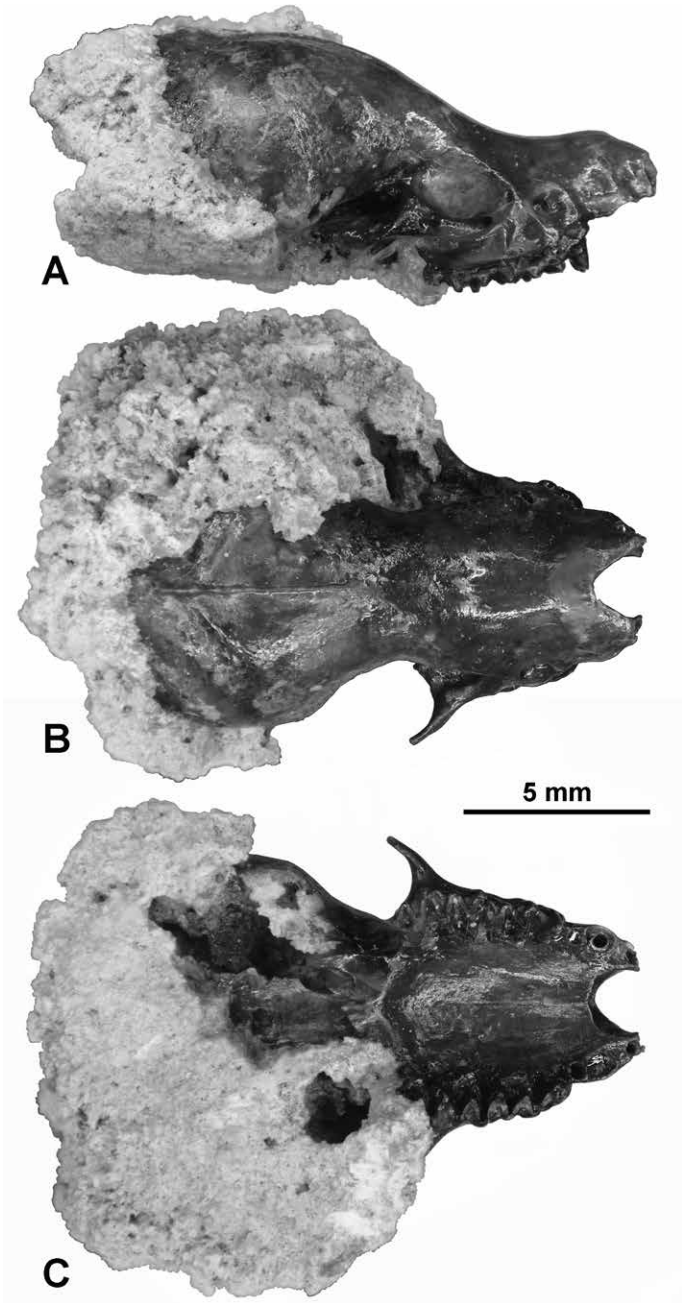

Figure 5. *Myotis grisescens* cranium with adhering matrix (OMNH 72965) in A, lateral view; B, dorsal view; C, palatal view.

77747−77748, 77848−77850, complete humeri; OMNH not separately listed by number, numerous elements including juveniles with deciduous and unerupted or erupting permanent teeth (e.g., OMNH 77728, Fig. 3F). All of the specimens, complete enough to be identified as this species, came from the Drain.

We used the key provided by Gaudin et al. (2011) for partial help identifying dentaries of *Myotis* from Three-Forks Cave. *Myotis grisescens* was largest of their Tennessee species of *Myotis* among modern specimens measured. This species has a mandibular length greater than or equal to 11.5 mm whereas *Myotis septentrionalis* and other eastern species have the mandibular length less than 11.4 mm (Gaudin et al., 2011). Of these, their smallest species *Myotis leibii* had an alveolar length (c1-m3) less than or equal to 5.0 mm. Between these size extremes, "No current method can be used to unambiguously identify skeletal remains of the other southeastern US species of *Myotis* to the species level (*M. sodalis*…*M. austroriparius*…and *M. lucifugus*…. Therefore, we were unable to distinguish these species in this study" (Gaudin et al., 2011: p. 612).

Of our specimens from Three-Forks Cave referred to the genus *Myotis*, 41 dentaries were measured for species identification using the criteria provided by Gaudin et al. (2011). Summary measurements of this sample were as follows: mandibular length, n = 18, observed range = 10.5−14.0, mean = 12.50; mandibular alveolar toothrow length, n = 41, observed range = 5.0−8.1, mean = 6.82. The largest of these measurements are consistent with those of Gaudin et al. (2011) to diagnose *Myotis grisescens* and inconsistent with *M. septentrionalis*, while the smallest are equivalent to *M. leibii*. However, some Three-Forks Cave specimens overlap with *M. septentrionalis* and other species. Nine of the large humeri of *Myotis* were complete enough for measurements (Table 1) and all are assigned to *M. grisescens*. Thus, *M. grisescens* is probably present, and additional species of *Myotis* are also likely represented in the sample from Three-Forks Cave, but we cannot identify them with current methods.

Myotis grisescens is the most abundant bat in the Three-Forks Cave sample. Many specimens with erupting permanent teeth indicate use of the cave as a maternity roost in the late Pleistocene. Other specimens exhibit heavy tooth wear and indicate aged individuals, whereas relatively few show light to moderate wear. The most complete cranium (OMNH 72965; Fig. 5) and numerous rostra agree closely with modern specimens of *M. grisescens* in morphology and size. The cranium bears a sagittal crest. One rostrum, OMNH 77733, has a less abruptly rising forehead profile than the others, and also has somewhat deeper facial concavities anterior to the orbits and above the infraorbital foramina. It is included here with *M. grisescens* because of a lack of other distinguishing features, but possibly represents a second large species of Myotis. Numerous isolated upper molars of bats document a range of sizes, suggesting that more than one species of *Myotis* is present in the assemblage but not represented by any of the more complete specimens. Evidence for this is the relatively small size of several M1s and M2s with transverse widths of 1.5−1.7 mm (e.g., OMNH 77920, 78178, 78179, 78200) compared to those identified as *M. grisescens* with transverse widths of 1.7−2.3 mm. We assigned only our largest specimens to *M. grisescens*, whereas isolated teeth and other elements are assigned to *Myotis* sp. indeterminate.

Table 1. Measurements (mm) of adult, complete fossil humeri referred to the species *Myotis grisescens* from Three-Forks Cave, Oklahoma.

Specimen/OMNH No.	Greatest Length	Proximal Width	Distal Width
72969	24.9	3.7	3.5
72970	24.85	3.45	3.25
72971	24.2	3.5	3.35
72972	25.15	3.45	3.2
77747	26.5	3.65	3.45
77748	24.95	3.5	3.5
77848	24.8	3.7	3.75
77849	25.6	3.55	3.5
77850	24.8	3.5	3.3
77863	26.65	3.75	3.5
77864	26.6	3.8	...
77865	27.05	3.8	3.55
77868	23.75	3.3	3.05
77870	25.3	3.7	3.55
78014	24.9	3.3	3.0
78412	27.85	3.55	3.5
78413	26.5	3.55	3.35
78414	24.5	3.45	3.15
78415	25.4	3.5	2.95
Total number of samples Mean of samples	N = 19, Mean = 25.487	N = 19, Mean = 3.566	N = 18, Mean = 3.356

Although we did not notice *M. grisescens* using Three-Forks Cave during our paleontological work and no systematic search for them has been done there, the species forms a large maternity colony in another nearby cave on Gittin' Down Mountain (Sasse et al., 2007). They almost certainly also utilize Three-Forks Cave and other caves in the vicinity at times, although we are unaware of their recent use of Three-Forks Cave as a nursery. These bats form part of the historical "Southern Sub-population" of the Ozark population of this endangered species (Sasse et al., 2007).

Carnivora

Canidae

Canis dirus (dire wolf)

Material: OMNH 73039, right upper canine (Fig. 4I, J), from the Drain.

The tooth shows light wear on the tip and a slight wear facet from contact with the lower canine on its anterior face; there are modest longitudinal ridges running down the mesial and distal surfaces. The complete root is preserved and the pulp cavity is closed, indicating an adult. The crown of the canine measures (APL × TW) 19.7 × 14.1. By comparison, two other C1s of *C. dirus* from localities of Pleistocene age in Oklahoma (at Burnham and Marlow; Cifelli et al., 2002; Czaplewski, 2003) measure 17.1 × 12.1 and 18.7 × 12.1, and a C1 from Pul-103 Cave, Pulaski Co., Missouri measured 17.7 x 12.7 (Hawksley et al., 1963). Upper canines of modern *Canis lupus* are about 2−4 mm smaller in each of these dimensions. Elsewhere in the Ozark Highlands, *C. dirus* is known as a late Pleistocene fossil at 10 localities in Missouri and two in Arkansas (Dundas, 1999).

Vulpini (foxes)

Genus indet.

Material: OMNH 77902, right humerus missing distal end, from the Drain. Measurements of the specimen are proximal articular width, 16.6 mm; midshaft diameter medial-lateral, 7.0 mm; midshaft diameter, anterior-posterior, 9.4 mm.

The humerus is identified as that of a canid based on the lack of an entepicondylar foramen and the presence of a supratrochlear foramen. Its small size further distinguishes it from *Canis* spp. (coyotes and wolves) as one of the foxes (*Vulpes* or *Urocyon*).

Ursidae

Arctodus simus (short-faced bear)

Material: OMNH 73334, partial skeleton from the Second Parachute Room (consisting of small cranial fragments, partial dentary: left c1, lower incisor, right P4, right M1, right maxillary fragment with alveoli for P1 and P2, P2 or P3; portions of ilium, ischium, head of humerus, right humerus distal fragment, portions of femur, cervical vertebrae, thoracic vertebrae, rib fragments, costal ribs and sternebrae, lumbar vertebra, caudal vertebrae). Nine elements are referred to as a second individual because they were collected from a passage west of the Drain (Fig. 2D). These remains are cataloged separately as OMNH 78515, unworn small P/p2 or P/p3; 73040, thoracic vertebra; 73041, partial ulna; 77897, left proximal radius shaft fragment; 77898, navicular; 77896, right proximal tibia with partial articular surface; 77899, metatarsal III; 77900, proximal phalanx; 73042, phalanx.

Measurements of teeth associated with the partial skeleton from the Second Parachute Room are: c1 APL 28.6, TW 19.3; P4 APL 21.6, TW 14.9; M1 APL 24.9, TW 23.1; m2 (from Puckette 1976) APL 29.5, TW 19.5. Measurements of the metatarsal III from the Drain are: greatest length 79.4, greatest proximal width 18.0, greatest proximal depth 24.7,

greatest distal width 18.1. The measurements of the metatarsal III from Three-Forks Cave are smaller than those for two third metatarsals, reported by Merriam and Stock (1925). By comparison with other published measurements, the bears from Three-Forks Cave were both small individuals of A. simus.

This species is recognizable by the presence of a deep pre-masseteric fossa in the dentary (Fig. 6G), large size, and cheek teeth morphologically distinct from those of ursine bears. Two individuals of the giant short-faced bear are represented in the faunal assemblage from Three-Forks Cave; parts of each were found in separate rooms (Figs. 2B and 2D) within the cave and show different preservation. One individual, found in a passageway adjacent to the Second Parachute Room (Fig. 2B), is represented by greatly worn teeth and numerous postcranial bones and fragments (OMNH 73334; Figs. 6, 7). The second individual, from a passage near the Drain, comprised a cluster of scattered bones and a little-worn P/p2 or P/p3 (Fig. 8). The former specimen represents associated parts of a senescent individual bear, while the latter cluster of isolated elements represents a younger adult. The former specimen includes a tooth collected years ago and prior to our work in the cave that was previously published by Puckette (1976), conserved in the University of Arkansas Museum (UAM) collection. The specimen from the University of Arkansas consists of a heavily worn m2, UAM catalog number 75-839-1, and was the first record of *A. simus* in Oklahoma. This m2 is almost certainly associated with the elements collected by us from the same, aged individual, because it shows a similar advanced stage of tooth wear and identical preservation. Thus, parts of this individual are preserved in two different collections, in the University of Arkansas and the Oklahoma Museum of Natural History. In general, preservation of the bones and teeth of the first bear was poorer, with the bones being light in color, much broken and abraded, and with extensive rodent-gnawing on some pieces (Fig. 7D, L). Bones of the second bear were dark brown and some pieces had originally been concreted with calcite (visible on the centrum of the thoracic vertebra, Fig. 8E). Because direct association of the several scattered elements of the second individual of *A. simus* could not be demonstrated, these elements were cataloged separately.

Short-faced bears are hypothesized to have been sexually dimorphic, with males larger than females (Kurtén, 1967; Churcher et al., 1993). The two individuals of *A. simus* in Three-Forks Cave are relatively small and, therefore, likely to represent females; this is consistent with the conclusions of Schubert and Kaufmann (2003) that only females denned in caves. We cannot determine whether the bears used the cave for hibernation, birthing young, or denning. Adjacent to Three-Forks Cave is a small, separate cave that was probably once a part of the same cave complex. It contains a crater-like feature about 2 m in diameter that represents a possible short-faced bear bed, and other caves in the area may contain them as well (personal observations). By comparison, recent black bear beds in Three-Forks Cave are

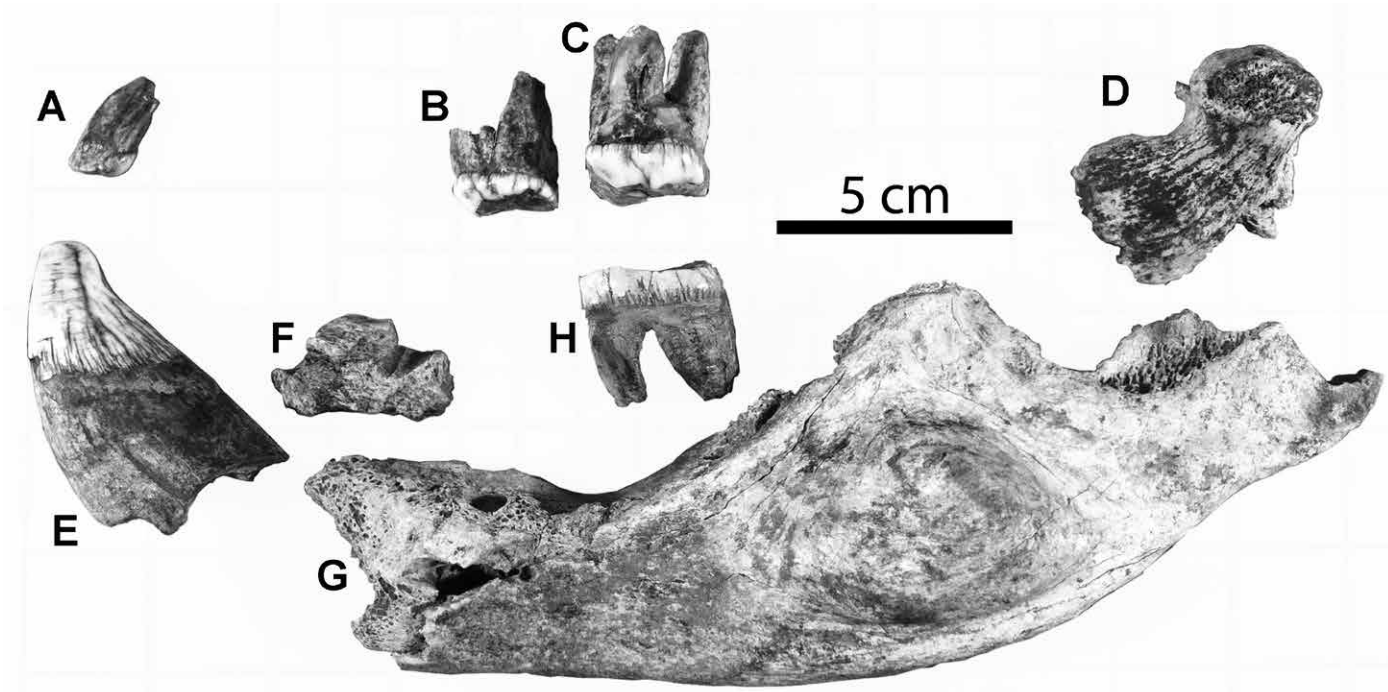

Figure 6. Teeth and dentary fragments of *Arctodus simus* found near the Second Parachute Room in Three-Forks Cave, Oklahoma. All are cataloged as parts of OMNH 73334 except H. A, upper(?) incisor in lateral view; B, right P4 in lingual view; C, left M1 in lingual view; D, medial end of right condyloid process of dentary in medial view; E, left lower(?) canine in labial view; F, small fragment of right dentary with alveoli for p3 and p4; G, broken and abraded left partial dentary with deep ends of some alveoli forward to the canine alveolus, in lateral view; H, right m2 (UAM 75-839-1) in labial view.

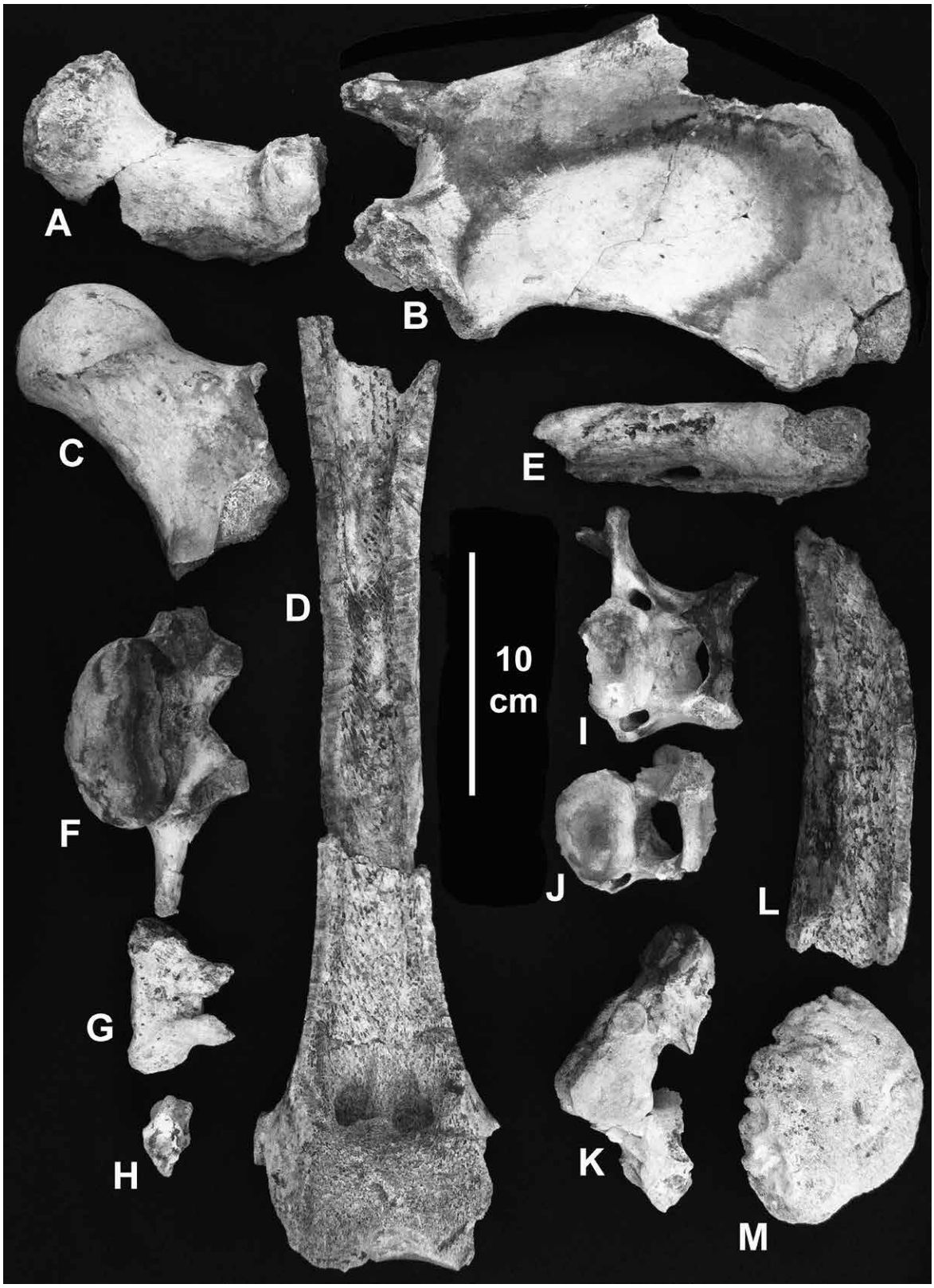

Figure 7. Selected postcranial skeletal elements of *Arctodus simus* (OMNH 73334) found near the Second Parachute Room in Three-Forks Cave, Oklahoma. A, right ischium in lateral view; B, right ilium in lateral view; C, head of femur in anterior view; D, longitudinally split, posterior and distal portion of the left femur in anterior view, with broken edges of shaft extensively gnawed by rodents and distal portion abraded; E, distal fragment of humerus showing entepicondylar foramen in posteromedial view; F, partial lumbar vertebra in posterior view; G, proximal caudal vertebra in dorsal view; H, mid-caudal vertebra in anterior view; I, J, portions of two cervical vertebrae in posterior view; K, partial thoracic vertebra in anterior view; L, shaft fragment of femur showing extensive rodent gnawing; M, right partial head of humerus in proximal view.

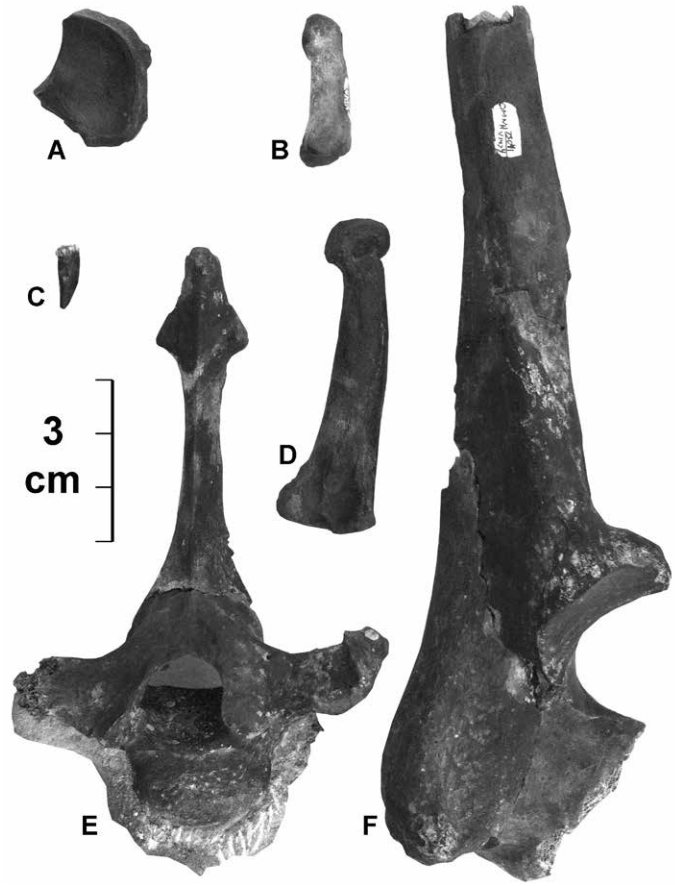

Figure 8. Skeletal elements of *Arctodus simus* found west of the Drain in Three-Forks Cave, Oklahoma. A, left navicular (OMNH 77898) in proximal view; B, phalanx (OMNH 77900) in lateral view; C, little worn P/p2 or P/p3 (OMNH 78515) in lateral view; D, left metatarsal III (OMNH 77899) in lateral view; E, thoracic vertebra (OMNH 73040) in anterior view, with adhering calcite on ventral surfaces; F, right partial proximal ulna (OMNH 73041) in medial view.

about 1−1.5 m across (personal observation). The potential short-faced bear beds deserve further investigation.

As noted in the Introduction, the *A. simus* tooth UAM 75-839-1 from Three-Forks Cave was included by Schubert (2010) in his review of North American records of giant short-faced bears, and he also provided a tentative radiometric date of 33,143 to 34,983 ybp for the specimen. This remains the only available age estimate for the vertebrate faunal assemblage of Three-Forks Cave. Elsewhere in the Ozark Highlands, *A. simus* has been found in seven other localities in Missouri (Richards et al., 1996; Schubert and Kaufmann, 2003).

Perissodactyla

Equidae

Equus or *Haringtonhippus* sp. indet. (extinct horse)

Material: OMNH 77905, left ectocuneiform (Fig. 4A−C), from a passage near the Second Parachute Room.

This ankle element is the only identifiable horse bone recovered from the cave. It is not diagnostic to the generic level because late Pleistocene North American horses were recently separated into two genera, *Equus* and *Haringtonhippus* (stout-legged and stilt-legged horses, respectively), that are morphologically distinguishable only by their proximal foot bones (metacarpals and metatarsals) (Heintzman et al., 2017), which were not found in Three-Forks Cave. Measurements of the ectocuneiform from Three-Forks Cave are: greatest medial-to-lateral width, 43.6 mm; least anterior depth, 8.9 mm. Horses were widespread throughout the Ozark Highlands in the late Pleistocene, as evidenced by their occurrence in at least nine localities (FAUNMAP Working Group, 1994; http://www.ucmp.berkeley.edu/faunmap/about/index.html).

Rodentia

Geomyidae

Geomys sp. indet. (plains pocket gopher)

Material: OMNH 78523, p4, from the Drain.

The p4 is abraded and polished with all edges rounded, probably from water-wear. Nevertheless, it can be identified as that of *Geomys* in being hypselodont and bilophodont with wide dentine tracts on either side extending the full height of the crown, a narrow connection between the protolophid and metalophid, and V-shaped re-entrant angles (Hall and Kelson, 1959).

Heteromyidae

Chaetodipus or *Perognathus* sp. indet. (pocket mouse)

Material: OMNH 78522, right m1 or m2, from the Drain.

Measurements of the molar are APL, 0.95; TW, 1.35. The cheek tooth is rooted, low-crowned, and bunolophodont with two lophs. It bears three well-developed roots, and its occlusal surface is worn such that the protostylid is confluent with metalophid-protoconid. Its measurements are slightly smaller than m1s and m2s in *Chaetodipus hispidus*, the species of pocket mouse with a modern distribution nearest to the Ozark Highland in Oklahoma (Caire et al. 1989; Kays and Wilson, 2002). A worn, isolated molar such as this lacks apomorphic morphological characteristics to distinguish between the genera *Chaetodipus* and *Perognathus*.

Nevertheless, the pocket mouse specimen, potentially, is biogeographically significant. If it represents a true occurrence in a habitat near the cave, it indicates the extralimital presence of a perognathine in the late Pleistocene of the southwestern Ozark Highlands, where none has occurred in historic times. In modern times, the mouse *Chaetodipus hispidus* has only been found west of the Neosho-Arkansas Rivers that delimit the western edge of the Ozark Highland in Oklahoma. The species has been recorded as near as 70−90 km west of Three-Forks Cave just west of the Ozark

Highland (Caire et al., 1989). The species' modern habitat preference suggests an extension of relatively dry, grassy or open plains habitat into the Ozarks during the late Pleistocene. However, the pocket mouse fossil might represent the remains of a prey species brought into the cave from a more distant habitat by a predator such as an owl. Owls can transport prey animals they have ingested for some distance until later egesting a pellet. This phenomenon and the distance involved appears to have received little attention in taphonomic studies of owl pellet accumulations (Andrews, 1990; Walton, 1990; Terry, 2004; Czaplewski, 2011). If an owl moves a great distance in between ingestion and egestion, such as during a migration or a less distant hunting bout, it could potentially accumulate prey from habitats far from the locality where it casts a pellet containing the prey remains. The presence of a great horned owl fossil bone in Three-Forks Cave heightens the possibility, but the owl bone does not demonstrate, that the pocket mouse fossil is an intrusive member of the paleo assemblage of the cave (Andrews, 1990). The species *Chaetodipus* cf. *hispidus* was previously recorded in the Ozark Highlands at Crankshaft Cave, Missouri, in the Wisconsinan glacial period (Parmalee et al., 1969; FAUNMAP Working Group, 1994).

Cricetidae
Peromyscini
Peromyscus, *Ochrotomys*, or *Podomys* sp. indet. (mouse)
Material: OMNH 77861, left m1; 78525−78526, left M1s; 78527, right M3; 77701−77702, right dentaries with i1; 73038, edentulous maxilla; all from the Drain. OMNH 77699, dentary with i1, from the Second Parachute Room.

Measurements of the molars (APL × TW) are: 77861, 1.50 × 0.95; 78525, 1.85 × 1.10; 78526, 1.80 × 1.10; 78527, 0.95× x 0.90.

The specimens have small, rooted, cuspate, bunodont teeth typical of deer mice and their relatives (Osgood, 1909; Bradley et al., 2007). Based on the paucity of material and the possibility that several different, but morphologically similar, species of *Peromyscus* and closely-related genera occurred in the vicinity of Three-Forks Cave, it is not possible to refer these few specimens to a genus.

Neotoma cf. *floridana* (eastern woodrat)
Material: OMNH 77700, left dentary fragment with m1-m3; 78550, left calcaneum; 73019, proximal ulna; 77922, femur; all from the Drain.

The molar teeth are rooted, hypsodont, lophodont and semi-prismatic, which are typical of woodrats that commonly utilize caves and rock shelters across North America (Vaughan et al., 2015). The bilophate m3 is characteristic of species in the subgenus *Neotoma* and the m1 has essentially no anterior lateral dentine tract, consistent with *N. floridana* (Harris, 2014). The teeth and bones represent a large woodrat the size of recent *N. floridana* (Fig. 3H). In addition to the body fossils, several coprolites (OMNH 78551, 78546) from the Drain are similar to scats of *Neotoma* and probably are attributable to woodrats dwelling in and near the cave in the late Pleistocene. The original scat contents have been replaced by sediment grains, but the contents retain the shape of *Neotoma* scat pellets as are seen in numerous caves throughout North America.

Arvicolinae
Microtus cf. *ochrogaster* (prairie vole)
Material: OMNH 78353, right dentary fragment with m1 (Fig. 3C), from the Drain.

The m1 is hypselodont, with prismatic crown pattern, and bears cementum in the re-entrant angles, characteristic of voles of the genus *Microtus* (Semken and Wallace, 2002). The crown pattern shows three closed triangles, an anteriorly-rounded anterior loop, and low dentine tracts, typical of the subgenera *Pitymys* and *Pedomys*. Enamel is thicker on the forward edges of triangles relative to the rearward edges; the medial portions of the re-entrant angles curve forward or not at all; and the sixth re-entrant angle is shallow. These features are characteristic of *Microtus (Pedomys) ochrogaster*, but the specimen is only tentatively referred to that species because of variability and overlap of some characteristics with *M. (Pitymys) pinetorum* (Semken and Wallace, 2002).

Lagomorpha
Leporidae
Sylvilagus sp. indet. (cottontail rabbit)
Material: OMNH 77732, left p3; 78552, right fifth metatarsal V; 78554, phalanx; from the Drain.

The p3 measures 2.8 mm APL × 2.7 mm TW, is hypselodont, heavily invested with cementum anteriorly, labially, and within the re-entrant angles, and has enamel that varies greatly in thickness across the occlusal surface. It shares with *Sylvilagus* the normal anterior, anteroexternal, and posteroexternal re-entrant angles, as well as weak crenulations of the enamel, including that on the walls of the posteroexternal re-entrant (Hibbard, 1963), but the material lacks species-level diagnostic characters.

Discussion

Other than four extinct large mammals, none of the vertebrates from Three-Forks Cave became extinct at the end of the Pleistocene. In Three-Forks Cave, these extinct megafaunal members include the ground sloth *Megalonyx jeffersonii,* the short-faced bear *Arctodus simu*s, the dire wolf *Canis dirus*, and a horse, family Equidae; indicating a Rancholabrean age for the assemblage. All other taxa, as far as they are identifiable, still occur in the Ozark Highlands today except for one, a pocket mouse of the subfamily Perognathinae, genus *Chaetodipus* or *Perognathus*. The pocket mouse suggests either the extralimital occurrence of this mouse in the southwestern Ozark Highlands during the late Pleistocene--and thus a potential extension of relatively dry, grassy or open habitat into the Ozarks--or else it represents the remains of a prey species brought into the cave from a more distant habitat by a predator such as an owl, and, thus, is intrusive. In historic times, the mouse *Chaetodipus hispidus* has been found as near to Three-Forks Cave in several of the Oklahoma counties immediately west of the edge of the Ozark Highland (Caire et al., 1989). The total of 23 vertebrate taxa in the fauna from Three-Forks Cave makes it the largest known vertebrate assemblage from a cave in the Ozark Highland of Oklahoma, exceeding nearby Sassafras Cave with an assemblage of nine taxa (Czaplewski et al., 2002). Two of the taxa provide the first records of their respective species in the late Pleistocene of Oklahoma, the freshwater drum (*Aplodinotus cf. grunniens*) and great horned owl (*Bubo virginianus*).

Among the bat bones, numerous specimens, especially of *Myotis grisescens*, consisting of jaws and jaw fragments with deciduous teeth, erupting teeth, and enamel caps of upper and lower molars from juveniles (Fig. 3F, G) were recovered. Similarly, less common remains of *Eptesicus fuscus*, with erupting permanent teeth, occurred in the cave deposits. The fossils of immature individuals indicate the use of Three-Forks Cave as a maternity roost for these two species. Other than the juveniles, specimens of *M. grisescens* include fossils showing stages of tooth wear from slight to heavy, indicating at least some aged adult bats. Of the few bat specimens that could be identified as *Perimyotis subflavus*, all pertained to young adults with little-worn teeth. All three species of bats found as fossils still occur in Three-Forks Cave today; we also observed *Corynorhinus townsendii ingens*, the endangered Ozark big-eared bat, in the cave, However, we found no fossils of that species. The fossils indicate that environmental conditions of temperature and humidity, suitable for birthing young bats within Three-Forks Cave in the late Pleistocene, were not so different from today.

Two individuals of the short-faced bear, *Arctodus simus*, occurred in Three-Forks Cave, as determined by their discovery in two separate parts of the cave, different bone preservation, and different stages of tooth wear, with one having greatly worn teeth and the other preserving a single, lightly worn tooth. Both individuals are relatively small, possibly indicating they were females of this potentially sexually-dimorphic species (Schubert and Kaufmann, 2003). As noted above, several of the bone fragments of *A. simus* are extensively rodent-gnawed, possibly by woodrats living in the cave; their scats were also preserved. Woodrats might also have been responsible for collecting some of the bones in the cave deposits. The owl *Bubo virginianus* probably contributed to the accumulation of small vertebrate remains. Short-faced bears are thought to have been carnivorous-omnivorous and are implicated as scavengers of large mammal carcasses (Matheus, 1995, 2003; Sorkin, 2006; Figueirido et al., 2010, 2017). Short-faced bears and dire wolves using the cave are additional potential sources of the remains of large mammals (horse, ground sloth), and possibly also of smaller mammals like the fox (Vulpini), brought in as prey remains or scavenged body parts. Large depressions in Three-Forks Cave and other nearby caves resemble beds of denning black bears, except for the much larger size of some, suggesting they could be beds of short-faced bears.

Acknowledgments

Thanks to Linda DeBerry for her cheerful enthusiasm and help in collecting the fossils in the cave. Thanks to Clayton and Sylvia Russell for access to and help in the cave, for logistical support during this work, and for donating the fossils from the cave to the OMNH. We greatly appreciate Donald R. Russell for all the efforts he made to protect and conserve caves of the Cherokee Nation (Russell, 1971). We extend our sincere thanks to Bill May for picking microfossils from screened concentrate, to Tamaki Yuri for use of the OMNH bird osteology collection, to Jen Larsen for compiling lists of specimens, and to Steve Westrop and Roger Burkhalter for use of their bellows camera. We express our appreciation to Chris Bell, two anonymous reviewers, and Associate Editor Greg McDonald for their time and effort in providing helpful, critical reviews that improved the manuscript from an earlier version.

References

Akersten, W.A., and McDonald, H.G., 1991, Nothrotheriops from the Pleistocene of Oklahoma and paleogeography of the genus: Southwestern Naturalist, v. 36, p. 178−185. https://doi.org/10.2307/3671918.

Andrews, P., 1990, Owls, Caves, and Fossils: Chicago, University of Chicago Press, 231 p.

Bell, C.J., Head, J.J., and Mead, J.I., 2004, Synopsis of the herpetofauna from Porcupine Cave, *in* Barnosky, A.D., ed., Biodiversity Response to Climate Change in the Middle Pleistocene: The Porcupine Cave Fauna from Colorado: Berkeley, University of California Press, p. 117−126. https://doi.org/10.1525/california/9780520240827.003.0019; https://doi.org/10.1525/california/9780520240827.003.0011.

Bradley, R.D., Durish, N.D., Rogers, D.S., Miller, J.R., Engstrom, M.D., and Kilpatrick, C.W., 2007, Toward a molecular phylogeny for *Peromyscus*: evidence from mitochondrial cytochrome-b sequences: Journal of Mammalogy, v. 88, p. 1146−1159. https://doi.org/10.1644/06-MAMM-A-342R.1.

Brasso, R.L., and Emslie, S.D., 2006, Two new late Pleistocene avifaunas from New Mexico: The Condor, v. 108, p. 721−730. https://doi.org/10.1650/0010-5422(2006)108[721: TNLPAF]2.0.CO;2.

Caire, W., Tyler, J.W., Glass, B.P., and Mares, M.A., 1989, Mammals of Oklahoma: Norman, University of Oklahoma Press, 567 p.

Carter, T., Menzel, M., Chapman, B., and Miller, K., 1999, Summer foraging and roosting behaviour of an eastern pipistrelle, *Pipistrellus subflavus*: Bat Research News, v. 40, p. 5−6.

Churcher, C.S., Morgan, A.V., Carter, L.D., 1993, *Arctodus simus* from the Alaskan Arctic Slope: Canadian Journal of Earth Sciences, v. 30, p. 1007−1013. https://doi.org/10.1139/e93-084.

Cifelli, R.L., 1996, Techniques for recovery and preparation of microvertebrate fossils: Norman, Oklahoma Geological Survey Special Publication 96-4, p. 1−36.

Cifelli, R.L., Smith, K.S., and Grady, F.V., 2002, Dire wolf in the Pleistocene of Oklahoma: Norman, Oklahoma Geological Survey Notes, v. 62, p. 92−96.

Czaplewski, N.J., 2003, A dire wolf from the Burnham site, in Wyckoff, D.G., Theler, J.L., and Carter, B.J., eds., The Burnham Site in northwestern Oklahoma: glimpses beyond Clovis?: Norman, Oklahoma Museum of Natural History and Oklahoma Anthropological Society Memoir no. 9, p. 161−167.

Czaplewski, N.J., 2011, An owl-pellet accumulation of small Pliocene vertebrates from the Verde Formation, Arizona, USA: Palaeontologia Electronica v. 14, p. 1−33.

Czaplewski, N.J., and Puckette, W.L., 2015, Late Pleistocene remains of an American black bear (*Ursus americanus*) and two small vertebrates from an Oklahoma Ozark cave: Norman, Proceedings of the Oklahoma Academy of Science, v. 94, p. 10−27.

Czaplewski, N.J., Puckette, W.L., and Russell, C., 2002, A Pleistocene tapir and associated mammals from the southwestern Ozark Highland: Journal of Cave and Karst Studies, v. 64, p. 97−107.

Dundas, R.G., 1999, Quaternary records of the dire wolf, *Canis dirus*, in North and South America: Boreas, v. 28, p. 375−385. https://doi.org/10.1111/j.1502-3885.1999.tb00227.x; https://doi.org/10.1080/030094899422109.

Emslie, S.D., 1985, The late Pleistocene (Rancholabrean) avifauna of Little Box Elder Cave, Wyoming: Contributions to Geology, University of Wyoming, v. 23, p. 63−82.

Emslie, S.D., and Heaton, T.H., 1987, The late Pleistocene avifauna of Crystal Ball Cave, Utah: Journal of the Arizona-Nevada Academy of Science, v. 21, p. 53−60.

Farrow, L.J., and Broders, H.G., 2011, Loss of forest cover impacts the distribution of the forest-dwelling tri-colored bat (*Perimyotis subflavus*): Mammalian Biology, v. 76, p. 172−179. https://doi.org/10.1016/j.mambio.2010.04.004.

FAUNMAP Working Group, 1994, Faunmap: A Database Documenting Late Quaternary Distributions of Mammal Species in the United States: Springfield, Illinois State Museum, Scientific Papers, v. 25, nos. 1 & 2, p. 1−690. http://www.ucmp.berkeley.edu/faunmap/, http://www.ucmp.berkeley.edu/faunmap/about/index.html

Figueirido, B., J.A. Pérez-Claros, V. Torregrosa, A. Martín-Serra, and P. Palmqvist. 2010. Demythologizing *Arctodus simus*, the 'short-faced' long-legged and predaceous bear that never was: Journal of Vertebrate Paleontology, v. 30, p. 262−275. https://doi.org/10.1080/02724630903416027.

Figueirido, B., Pérez-Ramos, A., Schubert, B.W., Serrano, F., Farrell, A.B., Pastor, F.J., Neves, A.A., and Romero, A., 2017, Dental caries in the fossil record: a window to the evolution of dietary plasticity in an extinct bear: Scientific Reports, v. 7:17813, p. 1−7. https://doi.org/10.1038/s41598-017-18116-0.

Gaudin, T.J., Miller, A.N., Bramblett, J.L., and Wilson, T.P., 2011, Holocene and late Pleistocene bat fossils (Mammalia: Chiroptera) from Hamilton County, TN, and their ecological implications: Southeastern Naturalist, v. 10, p. 609−628. https://doi.org/10.1656/058.010.0403.

Green, M., 1941, The cranial and appendicular osteology of *Aplodinotus grunniens* Rafinesque: Lawrence, Transactions of the Kansas Academy of Science, v. 44, p. 400−414. https://doi.org/10.2307/3624913.

Guilday, J.E., Parmalee, P.W., and Hamilton, H.W., 1977, The Clark's Cave bone deposit and the late Pleistocene paleoecology of the Central Appalachian Mountains of Virginia: Pittsburgh, Bulletin of Carnegie Museum of Natural History, v. 2, p. 48−51.

Hall, E.R., and Kelson, K.R., 1959, The Mammals of North America. Volume 1: New York, Roland Press, 546 p.

Harris, A.H., 2014, Pleistocene Vertebrates of Southwestern USA and Northwestern Mexico: El Paso, University of Texas at El Paso, Digital book downloaded at http://digitalcommons.utep.edu/bio_papers/120/ [accessed May 3, 2017]

Hawksley, O., Reynolds, J., and McGowan, J., 1963, The dire wolf in Missouri: Missouri Speleology, v. 5, p. 63−72.

Heintzman, P.D., Zazula, G.D., MacPhee, R. D. E., Scott, E., Cahill, J.A., McHorse, B.K., Kapp, J.D., Stiller, M., Wooler, M.J., Orlando, L., Southon, J., Froese, D.G., and Shapiro, B., 2017, A new genus of horse from Pleistocene North America: eLife 2017, v. 6:e29944, p. 1−43.

Hibbard, C.W., 1963, The origin of the p3 pattern of *Sylvilagus, Caprolagus, Oryctolagus,* and *Lepus*: Journal of Mammalogy, v. 44, p. 1−15. https://doi.org/10.2307/1377162.

Hoganson, J W., and McDonald, H.G., 2007, First report of Jefferson's ground sloth (*Megalonyx jeffersonii*) in North Dakota: paleobiogeographical and paleoecological significance: Journal of Mammalogy, v. 88, p. 73−80. https://doi.org/10.1644/06-MAMM-A-132R1.1.

Holman, J.A., 1995, Pleistocene Amphibians and Reptiles in North America: New York, Oxford University Press, 243 p.

Holman, J.A., 2000, Fossil Snakes of North America: Origin, Evolution, Distribution, Paleoecology: Bloomington and Indianapolis, Indiana University Press, 357 p.

Howard, H., 1929, The avifauna of Emeryville Shellmound: University of California Publications in Zoology, v. 32, p. 301−394.

Howard, H., 1952, The prehistoric avifauna of Smith Creek Cave, Nevada, with a description of a new gigantic raptor: Los Angeles, Bulletin of the Southern California Academy of Sciences, v. 51, p. 50−54.

Hulbert, R.C., Jr., 2001, The Fossil Vertebrates of Florida: Gainesville, Florida, University Press of Florida, 351 p.

Jacquemin, S.J., Ebersole, J.A., Dockinson, W.C., and Ciampaglio, C.N., 2016, Late Pleistocene fishes of the Tennessee River Basin: An analysis of a late Pleistocene freshwater fish fauna from Bell Cave (site ACb-2) in Colbert County, Alabama, USA: Peer J, v. 4, e1648. https://doi.org/10.7717/peerj.1648.

Kays, R.W., and Wilson, D.E., 2002, Mammals of North America: Princeton, Princeton University Press, 240 p.

King, J.E., 1973, Late Pleistocene palynology and biogeography of the western Missouri Ozarks: Ecological Monographs, v. 43, p. 539−565. https://doi.org/10.2307/1942305.

Kurtén, B., 1967, Pleistocene bears of North America. 2. Genus *Arctodus*, short-faced bears: Acta Zoologica Fennica, v. 117, p. 1−58.

Matheus, P.E., 1995, Diet and co-ecology of Pleistocene short-faced bears and brown bears in Eastern Beringia: Quaternary Research, v. 44, p. 447–453. https://doi.org/10.1006/qres.1995.1090.

Matheus, P.E., 2003, Locomotor adaptations and ecomorphology of short-faced bears (*Arctodus simus*) in eastern Beringia: Whitehorse, Palaeontology Program, Government of the Yukon, Occasional Papers in Earth Sciences, no. 7, p. 1−126.

McDonald, H.G., 1977, Osteology of the extinct gravigrade edentate *Megalonyx* with observations on its taxonomy, ontogeny, phylogeny and functional anatomy. [M.S. thesis]: Gainesville, University of Florida, p. 1−329.

McDonald, H.G., and Jefferson, G.T., 2008, Distribution of Pleistocene *Nothrotheriops* (Xenarthra, Nothrotheriidae) in North America: Los Angeles, Natural History Museum of Los Angeles County, Science Series no. 41, p. 313−331.

Mead, J.I., Arroyo-Cabrales, J., and Johnson, E., 1999, Pleistocene lizards (Reptilia: Squamata) from San Josecito Cave, Nuevo León, Mexico: Copeia, v. 1999, p. 163−173. https://doi.org/10.2307/1447397.

Merriam, J.C., and Stock, C., 1925, Relationships and structure of the short-faced bear, *Arctotherium*, from the Pleistocene of California: Washington, Carnegie Institution of Washington, Publication no. 347, p. 1−36.

Miller, L., 1943, The Pleistocene birds of San Josecito Cavern, Mexico: Berkeley, University of California Publications in Zoology, v. 47, p. 143−167.

Miller, L., and DeMay, I., 1942, The fossil birds of California: an avifauna and bibliography with annotations: Berkeley, University of California Publications in Zoology, v. 47, p. 47−142.

Osgood, W.H., 1909, Revision of mice of the American genus *Peromyscus*: North American Fauna, v. 28, p. 1−285. https://doi.org/10.3996/nafa.30.0001; https://doi.org/10.3996/nafa.28.0001.

Page, L.M., and Burr, B.M., 1991, A Field Guide to Freshwater Fishes North America North of Mexico: Boston, Houghton Mifflin Company, 432 p.

Parmalee, P.W., Oesch, R. D., and Guilday, J.E., 1969, Pleistocene and recent vertebrate faunas from Crankshaft Cave, Missouri: Springfield, Illinois State Museum, Reports of Investigations, no. 14, p. 1−37.

Paula Couto, C. de, 1976, The manus of *Nothrotheriops shastense* (Sinclair, 1905): Anais do XXVIII Congresso Brasileiro de Geologia, no. 2, p. 165−176.

Perry, R.W., and Thill, R., 2007, Tree roosting by male and female eastern pipistrelles in a forested landscape: Journal of Mammalogy, v. 88, p. 974−981. https://doi.org/10.1644/06-MAMM-A-215R.1.

Puckette, W.L., 1976, Notes on the occurrence of the short-faced bear (*Arctodus*) in Oklahoma: Norman, Proceedings of the Oklahoma Academy of Science, v. 56, p. 67−68.

Qadri, S.U., and McAllister, D.E., 1967, Fish remains from a 700-year-old southern Ontario archaeological site: Ottawa, National Museum of Canada, Natural History Papers, no. 34, p. 1−6.

Richards, R.L., Churcher, C.S., and Turnbull, W.D., 1996, Distribution and size variation in North American short-faced bears, *Arctodus simus*, in Stewart, K. M., and Seymour, K. L., eds., Palaeoecology and Palaeoenvironments of Late Cenozoic Mammals: Tributes to the Career of C.S. (Rufus) Churcher: Toronto, University of Toronto Press, p. 191−-246.

Russell, D.R., 1971, An Essay on the Caves of the Cherokee Nation: Stilwell, Oklahoma, privately published, 50 p.

Sasaki, K., 1989, Phylogeny of the family Sciaenidae, with notes on its zoogeography (Teleostei, Perciformes): Hokkaido, Japan, Memoirs of the Faculty of Fisheries, Hokkaido University, v. 36, p. 1−137.

Sasse, D.B., Clawson, R.L., Harvey, M.J., and Hensley, S.L., 2007, Status of populations of the endangered gray bat in the western portion of its range: Southeastern Naturalist, v. 6, p. 165−172. https://doi.org/10.1656/1528-7092(2007)6[165:SOPOTE]2.0.CO;2.

Schubert, B.W., 2010, Late Quaternary chronology and extinction of North American giant short-faced bears (*Arctodus simus*): Quaternary International, v. 217, p. 188−194. https://doi.org/10.1016/j.quaint.2009.11.010.

Schubert, B.W., and Kaufmann, J.E., 2003, A partial short-faced bear skeleton from an Ozark cave with comments on the paleobiology of the species: Journal of Cave and Karst Studies, v. 65, p. 101−110.

Semken, H.A., Jr., Graham, R.W., and Stafford, T.W., Jr., 2010, AMS ^{14}C analysis of late Pleistocene non-analog faunal components from 21 cave deposits in southeastern North America: Quaternary International, v. 217, p. 240−255. https://doi.org/10.1016/j.quaint.2009.11.031.

Semken, H.A., Jr., and Wallace, S C., 2002, Key to arvicoline (“microtine” rodents) and arvicoline-like lower first molars recovered from late Wisconsinan and Holocene archaeological and palaeontological sites in eastern North America: Journal of Archaeological Science, v. 29, p. 23−-31. https://doi.org/10.1006/jasc.2001.0680.

Smith, C.L., 1954, Pleistocene fishes of the Berends fauna of Beaver County, Oklahoma: Copeia, v. 1954, p. 282−289. https://doi.org/10.2307/1440043.

Smith, K.S., and Cifelli, R.L., 2000, A synopsis of the Pleistocene vertebrates of Oklahoma: Norman, Oklahoma Geological Survey Bulletin, v. 147, p. 1−36.

Sobolik, K.D., and Steele, D.G., 1996, A Turtle Atlas to Facilitate Archaeological Identifications: Rapid City, South Dakota, Mammoth Site of Hot Springs, p. 1−117.

Sorkin, B., 2006, Ecomorphology of the giant short-faced bears *Agriotherium and Arctodus*: Historical Biology, v. 18, p. 1–20. https://doi.org/10.1080/08912960500476366.

Stock, C., 1925, Cenozoic gravigrade edentates of western North America with special reference to the Pleistocene Megalonychinae and Myslodontidae of Rancho La Brea: Washington, Carnegie Institution of Washington, Publication no. 331, p. 1−206 + 47 plates.

Terry, R., 2004, Owl pellet taphonomy: a preliminary study of the post-regurgitation taphonomic history of pellets in a temperate forest: Palaios, v. 19, p. 497−506. https://doi.org/10.1669/0883-1351(2004)019%3C0497:OPTAPS%3E2.0.CO;2.

Vaughan, T.A., Ryan, J.M., and Czaplewski, N.J., 2015, Mammalogy, sixth edition: Burlington, Massachusetts, Jones and Bartlett Learning, p. 1−755.

Veilleux, J.P., Whitaker, J.O., and Veilleux, S.L., 2003, Tree-roosting ecology of reproductive female eastern pipistrelles, *Pipistrellus subflavus*, in Indiana: Journal of Mammalogy, v. 84, p. 1068−1075. https://doi.org/10.1644/BEM-021.

Veilleux, J.P., Whitaker, J.O., and Veilleux, S.L., 2004, Reproductive stage influences roost use by tree roosting female eastern pipistrelles, *Pipistrellus subflavus*: Ecoscience, v. 11, p. 249−256. https://doi.org/10.1080/11956860.2004.11682830.

Walton, A.H., 1990, Owl pellets and the fossil record, in Boucot, A.J., ed., Evolutionary Paleobiology of Behavior and Coevolution: Amsterdam, Elsevier, p. 233−241.

GUIDE TO AUTHORS

The *Journal of Cave and Karst Studies* is a multidisciplinary journal devoted to cave and karst research. The *Journal* is seeking original, unpublished manuscripts concerning the scientific study of caves or other karst features. Authors do not need to be members of the National Speleological Society, but preference is given to manuscripts of importance to North American speleology.

LANGUAGES: The *Journal of Cave and Karst Studies* uses American-style English as its standard language and spelling style, with the exception of allowing a second abstract in another language when room allows. In the case of proper names, the *Journal* tries to accommodate other spellings and punctuation styles. In cases where the Editor-in-Chief finds it appropriate to use non-English words outside of proper names (generally where no equivalent English word exist), the *Journal* italicizes them. However, the common abbreviations i.e., e.g., et al., and etc. should appear in roman text. Authors are encouraged to write for our combined professional and amateur readerships

CONTENT: Each paper will contain a title with the authors' names and addresses, an abstract, and the text of the paper, including a summary or conclusions section. Acknowledgments and references follow the text. Manuscripts should be limited to 6,000 words and no more than 10 figures and 5 tables. Larger manuscripts may be considered, but the *Journal* reserves the right to charge processing fees for larger submissions.

ABSTRACTS: An abstract stating the essential points and results must accompany all articles. An abstract is a summary, not a promise of what topics are covered in the paper.

STYLE: The *Journal* consults The Chicago Manual of Style on most general style issues.

REFERENCES: In the text, references to previously published work should be followed by the relevant author's name and date (and page number, when appropriate) in brackets. All cited references are alphabetical at the end of the manuscript with senior author's last name first, followed by date of publication, title, publisher, volume, and page numbers. Geological Society of America format should be used (see http://www.geosociety.org/documents/gsa/pubs/GSA_RefGuide_Examples.pdf). Please do not abbreviate periodical titles. Web references are acceptable when deemed appropriate. The references should follow the style of: Author (or publisher), year, Webpage title: Publisher (if a specific author is available), full URL (e.g., http://www.usgs.gov/citguide.html), and the date the website was accessed in brackets. If there are specific authors given, use their name and list the responsible organization as publisher. Because of the ephemeral nature of websites, please provide the specific date. Citations within the text should read: (Author, Year).

SUBMISSION: Manuscripts are to be submitted via the PeerTrack submission system at http://www.edmgr.com/jcks/. Instructions are provided at that address. At your first visit, you will be prompted to establish a login and password, after which you will enter information about your manuscript and upload your manuscript, tables, and figure files. Manuscript files can be uploaded as DOC, WPD, RTF, TXT, or LaTeX. Note: LaTeX files should not use any unusual style files; a LaTeX template and BiBTeX file may be obtained from the Editor-in-Chief. Table files can be uploaded as DOC, WPD, RTF, TXT, or LaTeX files and figure files can be uploaded as TIFF, AI, EPS, or CDR files. Extensive supporting data may be placed on the Journal's website as supplemental material at the discretion of the Editor-in-Chief. The data that are used within a paper must be made available upon request. Authors may be required to provide supporting data in a fundamental format, such as ASCII for text data or comma-delimited ASCII for tabular data.

DISCUSSIONS: Critical discussions of papers previously published in the *Journal* are welcome. Authors will be given an opportunity to reply. Discussions and replies must be limited to a maximum of 1000 words and discussions will be subject to review before publication. Discussions must be within 6 months after the original article appears.

MEASUREMENTS: All measurements will be in Systeme Internationale (metric) except when quoting historical references. Other units will be allowed where necessary if placed in parentheses and following the SI units.

FIGURES: Figures and lettering must be neat and legible. Figure captions should be on a separate sheet of paper and not within the figure. Figures should be numbered in sequence and referred to in the text by inserting (Fig. x). Most figures will be reduced, hence the lettering should be large. Photographs must be sharp and high contrast. Figures must have a minimum resolution of 300 dpi for acceptance. Please do not submit JPEG images.

TABLES: See http://caves.org/pub/journal/PDF/Tables.pdf to get guidelines for table layout.

COPYRIGHT AND AUTHOR'S RESPONSIBILITIES: It is the author's responsibility to clear any copyright or acknowledgement matters concerning text, tables, or figures used. Authors should also ensure adequate attention to sensitive or legal issues such as land owner and land manager concerns or policies and cave location disclosures.

PROCESS: All submitted manuscripts are sent out to at least two experts in the field. Reviewed manuscripts are then returned to the author for consideration of the referees' remarks and revision, where appropriate. Revised manuscripts are returned to the appropriate Associate Editor who then recommends acceptance or rejection. The Editor-in-Chief makes final decisions regarding publication. Upon acceptance, the senior author will be sent one set of PDF proofs for review. Examine the current issue for more information about the format used.

Journal of Cave and Karst Studies

Volume 80 Number 2 June 2018

CONTENTS

Article 49
Mineralogical and Organic Study of Bat and Chough Guano: Implications for Guano Identification in Ancient Context
Alain Queffelec, Pascal Bertran, Teddy Bos, and Laurent Lemée

Article 66
Speleogenesis of Caves in a Cretaceous Shale: Bighorn Basin, Wyoming
Douglas M. Medville

Article 81
Hyalella Maya, a New Hyalellidae Species (Crustacea: Amphipoda) from a Cenote in the Yucatan Peninsula, Mexico
Aurora Marrón-Becerra, Margarita Hermoso-Salazar and Vivianne Solís-Weiss

Article 92
Late Pleistocene Vertebrates from Three-Forks Cave, Adair County, Oklahoma Ozark Highland
Nicholas J. Czaplewski, Kyler J. Rogers, and Clayton Russell